Stability of mixed gas hydrates and mass transfer during formation, accumulation and destabilization: laboratory experiment and modeling

DISSERTATION
Zur Erlangung des Doktorgrades
der Mathematisch-Naturwissenschaftlichen Fakultät
der Christian-Albrechts-Universität zu Kiel

Ludovic LEGOIX
Kiel, 2019

PhD Committee

Prof. Dr. Klaus Wallmann [Referent]	GEOMAR - FB 2 FE Marine Geosysteme
Dr. habil. Mark Schmidt [Koreferent]	GEOMAR - FB 2 FE Marine Geosysteme
Prof. Dr. Christian Berndt	GEOMAR - FB 4 FE Marine Geodynamik
Prof. Dr. Arne Körtzinger	GEOMAR - FB 2 FE Chemische Ozeanographie

Tag der mündlichen Prüfung 04.03.2019
Zum Druck genehmigt 04.03.2019

Der Dekan

Erklärung

Hiermit erkläre ich, dass die voliegende Doktorarbeit selbständig, abgesehen von der Beratung durch den Betreuer, erstellt wurde. Weder diese noch eine ähnliche Arbeit wurden an einer anderen Abteilung oder Hochschule im Rahmen eines Prüfungsverfahrens vorgelegt, veröffentlicht oder zur Veröffentlichung vorgelegt. Ferner versichere ich, dass die Arbeit unter Einhaltung der Regeln guter wissenschaftlicher Praxis der Deutschen Forschungsgemeinschaft entstanden ist.

Kiel, den 09. Dezember 2018

Ludovic Legoix

Acknowledgement

This PhD thesis was done in two oceanographic research institutes located in Brest (IFREMER) and Kiel (GEOMAR). I would like to thank Louis Géli and Klaus Wallmann for accepting me as a student in their research departments ''Géosciences Marines" and ''Marine Biogeochemie" during the time of this PhD. I thank the Committee for evaluating my work.

I want to express how grateful I am to my tutors, Livio Ruffine and Matthias Haeckel for their permanent support along this thesis. I always appreciated your human and professional qualities. This thesis needed a lot of work and personal investment. I thank you for the energy you spent to emphasize this work and develop my research skills.

I thank also everyone who helped me in the laboratories, especially Jean-Pierre and Christian. Thanks to you, I improved my competence to work in a lab, always in a good ambiance. I am also grateful to the intern students Morgane, Xavier, Mona, Mogens and Laurentz, who allowed me to share my experience and my pleasure of working in a science lab.

Furthermore, I thank all my colleagues from IFREMER and GEOMAR, for the friendly atmosphere and the good moments we spent in and outside work. I really enjoyed the MARSITE Cruise with the LGM team. Livio, I appreciate that you accepted me aboard and make me discover new horizons, and also that you gave me the opportunity to write a book chapter. I thank Claire who shared the PhD job offer and also taught me to do analyses on-board. I thank also Corinne, Kristin and Elke for your kindness and help in administrative or scientific tasks.

I am thankful to the DokTeam of GEOMAR for the warm get together. Deep-thank to the scuba diving group of IFREMER for the nice moments spent in cold waters. A big thank to Shubhangi for helping me on coding and typesetting, and for the friendly atmosphere in the office as well.

Thanks to my best comrade Gérard for your help and all the fun we had and still have together, despite these last years were very challenging. You often go against current and your capacity to achieve ambitious goals always impressed me. I want to thank all my family, my brother Léonard and Fanny for their support, I am still proud of you and of what you build together.

Je veux remercier mon père pour ses efforts, ses prises de risques et ses sacrifices afin que je puisse mener la vie que je souhaite. Tu m'as appris à apprécier les choses simples et à être résilient. Je ne remercierai jamais assez ma mère pour son soutient spontané et sans faille.

Abstract

Gas hydrates are fascinating ice-like compounds made of water cages that retain various types of guest molecules. Natural gas hydrates on Earth form below the seafloor and permafrost and contain mainly methane (CH_4). Methane from hydrate deposits could be considered as an energy resource. One possible production scenario of CH_4 from hydrates is the injection of carbon dioxide (CO_2) or carbon dioxide-nitrogen (CO_2-N_2) mixed gas into the reservoir. Depending on the thermodynamic constraints, the composition of the gas hydrate guest molecules changes: the energy source CH_4 is released and the greenhouse gas CO_2 is trapped. The aim of the present work is to study the mixed gas hydrates that form in gas hydrate reservoirs after injection of CO_2 or CO_2-N_2 gas mixtures, using laboratory experiments and modeling.

Firstly, phase equilibria of CH_4-CO_2 in presence of a CO_2-rich liquid phase were measured using a high-pressure cell. With these data, a model based on the Soave-Redlich-Kwong equation of state was developed to reproduce the vapor-liquid equilibria (VLE) envelopes between 0 and 31 degC. The envelopes give an information about the presence and composition of liquid and vapor phases, that are found at a given pressure and temperature. Moreover, hydrate-liquid-liquid equilibria (HLLE) of mixed CH_4-CO_2 hydrate in the presence of a CO_2-rich liquid phase were measured with the same apparatus. The results show an increase of gas hydrate stability when CH_4 is added to the mixture outside the vapor phase stability zone, and a decrease of the CH_4 content in the CO_2-rich phase after hydrate formation.

Secondly, a gas exchange experiment between gaseous CO_2 and CH_4 hydrate was performed. The evolution of the pressure and composition in the vapor phase indicates a decoupling between two processes. The first one is the formation of CO_2 hydrate in the aqueous phase, and the second one a direct CO_2 exchange occurring within CH_4 hydrate grains. Thirdly, hydrate-vapor-liquid equilibria (HVLE) data were measured for gas hydrate formed from a (CH_4)-CO_2-N_2 mixed gas phase in a gas limited system. At a given temperature and initial gas composition, the gas hydrate dissociation pressure is shifted to higher values when the relative water amount in the system is increased. This lower stability of the gas hydrate is due to a higher solubility of CO_2 compared to N_2 in the aqueous phase.

Finally, gas exchange in gas hydrate-bearing sediment (GHBS) has been studied with a 1L-scale sample. The GHBS was composed of pure CH_4 hydrate distributed in a coarse sand matrix with synthetic seawater. (CH_4)-CO_2-N_2 gas mixtures were injected through a GHBS, the produced gas and water phases were analyzed, and a resulting mass balance was calculated. A favorable retention of CO_2 in the aqueous and hydrate phase and a limited gas exchange in the initial CH_4 hydrate during the experiments were observed.

Kurzfassung (Translated by Dr. Elke Kossel)

Gashydrate sind faszinierende eisähnliche Verbindungen: Wassermolekülen bilden eine Käfigstruktur, in der verschiedenen Arten von Gastmolekülen enthalten sein können. Natürliche Gashydrate auf der Erde kommen im Meeresboden und in Permafrostgebieten vor und enthalten überwiegend Methan (CH_4) als Gastmolekül. Methan aus Methanhydratlagerstätten kann als Energierohstoff betrachtet werden. Eine mögliche Förderstrategie für CH_4 aus Gashydraten ist die Injektion von Kohlenstoffdioxid (CO_2) oder einem aus Kohlenstoffdioxid-Stickstoff (CO_2-N_2) bestehenden Mischgas in die Lagerstätte. Die Zusammensetzung der Gastmoleküle ändert sich dann abhängig von den thermodynamischen Randbedingungen: der Energierohstoff Methan wird freigesetzt und das Klimagas CO_2 eingefangen. Die Zielsetzung der vorliegenden Arbeit ist die Untersuchung von Mischhydraten, welche sich unter Reservoirbedingungen nach Injektion von CO_2 oder CO_2-N_2 Mischgas bilden, mit Hilfe von Laborexperimenten und numerischen Modellen. Zuerst wurden Phasengleichgewichte von CH_4-CO_2 in der Gegenwart einer CO_2-reichen Flüssigphase in einer Hochdruckzelle gemessen. Mit diesen Daten wurde ein auf der Soave-Redlich-Kwong Zustandsgleichung basierendes Modell entwickelt, mit dem die Einhüllenden des Dampf-Flüssigkeit Gleichgewichts (VLE) zwischen 0 und 31 degC beschrieben werden können. Aus dem Verlauf der Einhüllenden können Informationen über das Vorhandensein und die Zusammensetzung der Flüssig- und Gasphase bei gegebenem Druck und Temperatur gewonnen werden. Zusätzlich wurden Gashydrat-Flüssigkeit-Flüssigkeits-Gleichgewichte (HLLE) von CH_4-CO_2 Mischhydraten in Gegenwart einer CO_2-reichen Flüssigphase gemessen. Dabei zeigt sich eine Erhöhung der Gashydratstabilität, wenn dem System CH_4 außerhalb des Gasphasenstabilitätsbereichs hinzugefügt wird, und eine Verringerung des CH_4 Gehalts in der CO_2-reichen Phase nach Gashydratbildung. Als nächstes wurden Experimente zum Molekülaustausch zwischen einer CO_2 Gasphase und CH_4-Hydrat durchgeführt. Die Änderung des Drucks und der Zusammensetzung der Gasphase weisen auf zwei entkoppelte Prozesse hin: Der Erste ist die Bildung von CO_2-Hydrat in der wässrigen Phase, der Zweite ein direkte Austausch von CO_2 mit dem CH_4 in den Gashydraten. Weiterhin wurden Gashydrat-Dampf-Flüssigkeits-Gleichgewichte (HVLE) für Gashydrate, die in einem gaslimitiertem System aus einem (CH_4)-CO_2-N_2 Mischgas gebildet wurden, gemessen. Bei gegebener Temperatur und initialer Gaszusammensetzung wird der Dissoziationsdruck der Gashydrate zu höheren Werten verschoben, wenn der relative Wasseranteil im System erhöht wird. Diese geringere Stabilität der Gashydrate wird durch die höhere Löslichkeit von CO_2 gegenüber N_2 in der wässrigen Phase verursacht. Abschließend wurde der Gastmolekülaustausch in Gashydrat-haltigen Sedimenten (GHBS) untersucht. Die GHBS bestanden aus einer grobkörnigen Sandmatrix mit künstlichem Seewasser und reinem CH_4 Hydrat. (CH_4)-CO_2-N_2 Mischgase wurden durch eine GHBS injiziert und aus der Auswertung der Zusammensetzung der produzierten Gas- und Flüssigphase eine Massenbilanz erstellt. Beobachtet wurden eine vorteilhafte Zurückhaltung von CO_2 in der wässrigen und der Hydratphase und ein begrenzter Gasaustausch mit den ursprünglichen CH_4 Hydraten.

Résumé

Les hydrates de gaz sont des composés fascinants constitués par des cages d'eau enfermant différents type de molécules hôtes. Les hydrates de gaz naturel présent sur Terre contiennent beaucoup de méthane (CH_4) et se forment sous les fonds marins et sous le permafrost. Le méthane contenu dans les sédiments peuvent être considérés comme une source d'énergie. Un des scénario possible pour effectuer la production de CH_4 est d'injecter du dioxyde de carbone (CO_2) ou un mélange dioxyde de carbone - azote (CO_2-N_2) dans le reservoir. En fonction des contraintes thermodynamiques, la composition de l'hydrate change: le CH_4, source d'energie est produite pendant que le CO_2 contribuant à l'effet de serre est piégé. L'objectif de ce travail est d'étudier les hydrates de gaz mixte qui se forment dans les reservoirs à hydrates, après injection de CO_2 ou d'un mélange CO_2-N_2, en employant des expériences en laboratoire et de la modélisation.

En premier lieu, les equilibres de phase du mélange CH_4-CO_2 en présence d'une phase CO_2 liquide sont mesurés dans une cellule haute-pression. A partir de ces données, un modèle basé sur l'équation d'état Soave-Redlich-Kwong a été développé pour reproduire les enveloppes de phase liquide-vapeur (VLE) entre 0 et 31 degC. Ces enveloppes donnent des informations sur la présence et la composition de phases liquide et vapeur, à une pression et une température donnée. De plus, des équilibres hydrate-liquide-liquide (HLLE) des hydrates mixtes de CH_4-CO_2 en présence de CO_2 liquide ont été mesurés avec le même dispositif expérimental. Les resultats montrent qu'une augmentation du CH_4 dans ce milieu augmente la stabilité des hydrates mixte en absence de vapeur, et une diminution du CH_4 présent dans le CO_2 liquide se produit après formation d'hydrates.

Deuxièmement, une experience d'échange de gaz entre une phase CO_2 vapeur et une phase d'hydrate de CH_4 a été effectué. L'évolution de la pression et des composition dans la phase vapeur mettent en évidence un découplage entre deux phénomènes. Le premier est la formation d'hydrate de CO_2 dans la phase aqueuse, et le second est un échange direct du CO_2 dans les grains d'hydrate de CH_4. En troisième lieu, des équilibres hydrate-liquide-vapeur (HVLE) ont été mesurés pour des hydrates formés à partir d'un mélange (CH_4)-CO_2-N_2 avec une phase vapeur restreinte. A une température et une composition de gaz initiale donnée, la pression de dissociation des hydrates augemente lorsque la quantité de phase aqueuse est plus importante dans le système. Cette stabilitée plus faible des hydrates est due à l'écart important entre la solubilité du CO_2 et celle du N_2 dans la phase aqueuse.

Finalement, un échange de gaz dans des sédiments contenant des hydrates (GHBS) ont été effectué avec des échantillons synthétique d'un litre. Le GHBS est constitué d'hydrate de méthane pur distribué dans une matrice de sable avec de l'eau de mer synthétique. Des mélanges de gaz (CH_4)-CO_2-N_2 ont été injectés à travers le GHBS, le gaz et l'eau produit ont été analysés, et un bilan de matière a été réalisé. Une rétention favorable du CO_2 dans les phases aqueuse et hydrates, et un échange de gaz limité dans l'hydrate de méthane initial ont été observés.

Contents

1 Introduction **11**
- 1.1 Introduction to gas hydrates . . . 11
- 1.2 Natural gas hydrates . . . 13
  - 1.2.1 Occurence of gas hydrates . . . 13
  - 1.2.2 Geohazards and climate change . . . 14
  - 1.2.3 Carbon capture and storage . . . 16
  - 1.2.4 Energy resource . . . 16
- 1.3 Scope of work . . . 18

2 Phase equilibria of the CH_4-CO_2 binary and the CH_4-CO_2-H_2O ternary mixtures in the presence of a CO_2-rich liquid phase **29**
- 2.1 Introduction . . . 29
- 2.2 Experiments . . . 33
  - 2.2.1 Experimental apparatus . . . 33
  - 2.2.2 Materials . . . 34
  - 2.2.3 Experimental procedure . . . 34
- 2.3 Results and discussion . . . 35
  - 2.3.1 CH_4-CO_2 binary system . . . 35
  - 2.3.2 CH_4-CO_2-H_2O ternary system . . . 36
- 2.4 Conclusions . . . 38

3 Experimental study of mixed gas hydrates from gas feed containing CH_4, CO_2 and N_2: phase equilibrium in presence of excess water and gas exchange **47**
- 3.1 Introduction . . . 47
- 3.2 Experiments . . . 49
  - 3.2.1 Experimental setups . . . 49
  - 3.2.2 Materials . . . 50
  - 3.2.3 Experimental Procedures . . . 50
- 3.3 Results and discussion . . . 52
  - 3.3.1 Phase equilibrium of mixed gas hydrates . . . 52
  - 3.3.2 CH_4-CO_2 exchange between a vapor phase and a bulk gas hydrate phase . . . 54
- 3.4 Conclusion . . . 57
- 3.5 Appendix . . . 58

4 Flow-through experiments in gas hydrate bearing sediments with CH_4-CO_2-N_2 gas mixtures **65**
4.1 Introduction . . . 65
4.2 Experiment . . . 67
4.2.1 Apparatus . . . 67
4.2.2 Material . . . 68
4.2.3 Experimental Procedure . . . 68
4.3 Results and discussion . . . 72
4.3.1 Experimental results . . . 72
4.3.2 Insights on a field scale production scheme . . . 79
4.4 Conclusion . . . 80
4.5 Appendix . . . 81

5 Synthesis **93**

6 Additional work **95**
6.1 Physicochemical properties of gas hydrate-bearing sediments . . . 95
6.2 Multidisciplinary investigation on cold seeps with vigorous gas emissions in the Sea of Marmara (MarsiteCruise): Strategy for site detection and sampling and first scientific outcome . . . 96
6.3 Multiple gas reservoirs are responsible for the gas emissions along the Marmara fault network . . . 98

Chapter 1

Introduction

1.1 Introduction to gas hydrates

Gas hydrates were first discovered in the early 19th century, synthesized by Davy et al. [1811] with water and chlorine. Although Priestley [1778] made sulfur dioxide hydrate in his laboratory decades before, Faraday [1823] was the first to call this chemical component hydrate. After these discoveries in laboratories, gas hydrates were observed in an industrial context by Hammerschmidt during the 1930s [Hammerschmidt, 1934]. He realized that natural-gas pipeline may be plugged due to hydrate formation in cold regions; slowing down drastically the natural gas transport process and leading to important financial losses. Following that unpleasant discovery, several mitigation methods to prevent hydrate formation within pipelines have been investigated, triggering the era of gas hydrate research [Hammerschmidt, 1939, Kobayashi, 1951, Ng and Robinson, 1985, Dholabhai et al., 1991].

Gas hydrates, or clathrate hydrates, are ice-like crystals able to host organic or inorganic molecules. The water framework of gas hydrate is an assembly of several polyhedral-shaped cages. Different structures of gas hydrates have been discovered yet and three of them have been discovered in nature (Figure 1.1). These different structures are all made of small and large cages. The structure 1, i.e. sI, usually contains the smallest gas molecules and is a cubic crystallographic structure (Pm3n) made of 2 small cages (5^{12} water structures) for 6 larger cages ($5^{12}6^2$). The $5^{12}6^2$ notation means that the cage is made of 12 pentagons, and 2 hexagons, where the oxygen atom of each water molecule represents a node. The most common guest molecules trapped in sI hydrates are methane (CH_4), ethane (C_2H_8) and inorganic compounds like carbon dioxide (CO_2) and hydrogen sulfide (H_2S). The structure 2, i.e. sII, is also a cubic structure (Fd3m) containing larger molecules like propane, cyclohexane and other kind of inorganic gases such as nitrogen (N_2) and oxygen (O_2). Here, 16 small 5^{12} water polyhedra and 8 larger ones of the type $5^{12}6^4$ forms the sII crystal lattice. The third category of commonly found gas hydrates is the structure H, i.e. sH, hosting large guest molecules as cyclooctane and 3,3-dimethylpentane. This one is a hexagonal type crystallographic structure (P6/mmm), and its lattice is made of 3 small cage (5^{12}), 2 medium size cages ($4^3 5^6 6^3$) and one large cage ($5^{12}6^8$). Usually, this structure needs to contain also small guest molecules to help

for stability. Thus, the geometry of molecules and the strength induced by van der Waals forces [Platteeuw and Van der Waals, 1958] between the hosts and the guests determine the crystalline structure of the hydrate.

It is possible to identify the structure of a sample experimentally with solid state characterization techniques such as X-ray diffraction [Stackelberg and Müller, 1951], neutron diffraction of powders [Kuhs et al., 1997], nuclear magnetic resonance with magic angle spinning (MAS-NMR) [Ripmeester and Ratcliffe, 1988], derivative proton NMR [Davidson et al., 1977] and Raman spectroscopy [Seitz et al., 1993, Sum et al., 1997]. These technologies, among others, were also employed to further study the hydration number [Ripmeester and Ratcliffe, 1988, Uchida et al., 1999], the filling ratio of each cages [Ripmeester and Ratcliffe, 1988] and the growth kinetics of gas hydrates [Henning et al., 2000].

When formation conditions of hydrate are favorable, they are able to host a huge amount of gas. Using a mixture of water and gases, the formation usually takes place at low temperature and high pressure, and providing a saturation of the aqueous phase in the hydrate-former gases. For example, arround 172 STP-m^3 of methane could be released from 1 m^3 of hydrate exposed at standard pressure (0.1 MPa) and temperature (273.15 K) conditions. This intrinsic storage properties of hydrates led to the emergence of new potential applications in gas purification processes, hydrogen storage technologies, refrigeration and cold storage, as well as CO_2 capture and storage. These new fields of investigation are centered on synthetic hydrates made in laboratories, commonly called technogenic hydrates [Y.F Makogon, 1997].

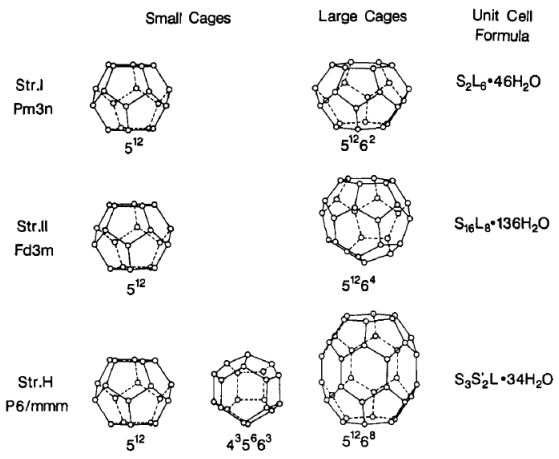

Figure 1.1: Structures of gas hydrates I, II and H with corresponding water cages [Ripmeester et al., 1994].

1.2 Natural gas hydrates

1.2.1 Occurence of gas hydrates

On Earth, considerable amounts of gas hydrates are found in permafrost regions and continental margins [Kvenvolden, 1988]. Initially Makogon [1966] assumed their presence in the Siberian permafrost and few years latter they were discovered using different geophysical, geochemical and thermodynamic methods by Sapir et al. [1973] in the Messoyakah Field (Russia), Bily and Dick [1974] using Well-Log detection in the MacKenzie Delta (Canada), Yefremova and Zhizhchenko [1974] from collection of samples in the Black Sea (Russia), Tucholke et al. [1977] with Bottom Simulating Reflector detection along the Blake Ridge (U.S.). They were discovered at many other places and are commonly called natural gas hydrates, and mainly contain methane as guest molecule. However, homologous hydrocarbons such as ethane, propane, isobutane as well as non-hydrocarbon molecules like hydrogen sulfide and carbon dioxide may also be enclathrated within the lattice [Davidson et al., 1986]. The total amount of these heavier hydrocarbon (C_2+) is generally lower than 0.5%-mol.

Guest hydrocarbons are supplied by two type of sources: microbial and thermogenic gases. The first one is produced by microbial processes within the sediments. In microbial gases, methane is by far the major constituent [Kvenvolden, 1993], and this gas supply represents the main source for most of the natural hydrate deposits discovered on continental margins. Thermogenic natural gases are generated at deep-seated sources from the thermal cracking of refractory organic matter and they are stored in deep hydrocarbon reservoirs. Hydrates made of thermogenic gases [Davidson et al., 1986, Sassen et al., 1999, Bourry et al., 2009], often mixed in different proportions with microbial gases, were inferred in several locations around the world: offshore in the Gulf of Mexico (South East U.S.) [Brooks et al., 1984, Davidson et al., 1986, Suess et al., 1999], Caspian Sea [Ginsburg and Soloviev, 1994], Cascadia margin [Chapman et al., 2004], Barrents Sea [Niemann et al., 2006], Baikal Lake (Russia) [Kida et al., 2006], offshore Taïwan [Oung et al., 2006], Sea of Marmara (Turkey) [Bourry et al., 2009], Niger Delta [Ruffine et al., 2013] and also onshore in the Prudhoe Bay (Alaska, U.S.) [Collett et al., 1990] and in the Quilian mountain permafrost [Lu et al., 2010, 2013]. With relatively high contents of molecules with large steric hindrance, structure II hydrate [Brooks et al., 1984] and structure H hydrate [Sassen and MacDonald, 1994] have been discovered in nature, and are more stable than structure I hydrate [Lu et al., 2007]. This is not a general case since nitrogen hydrate (structure II) that could be formed in laboratory [Van Cleeff and Diepen, 1960] is less stable than methane hydrate (structure I) for example. This higher stability of thermogenic hydrates allows them to tollerate higher temperature and/or lower pressure conditions where structure I microbial hydrates would be unstable. This explains the occurence of hydrates within the sediment of the Sea of Marmara (Figure 1.3), where hydrates formed from thermogenic gases were collected at temperature and pressure around 287.65 K and 6.68 MPa [Bourry et al., 2009]. At such a temperature, a pressure of at least 14.4 MPa is required to stabilize pure

CH_4 hydrates [Duan and Sun, 2006]). Then gas hydrates have been found at various depth (i.e. pressure conditions), natural gas hydrates have been located in the Quilian mountain [Lu et al., 2010] at small depth 130 m underground, but also very deep in continental margins where the water column in addition to the sediment depth can reach several thousands of meters [Milkov and Sassen, 2002].

Overall the Gas Hydrate Stability Zone (GHSZ) is defined as the sedimentary interval where hydrates can occur due to favorable temperature and pressure conditions for its formation. However it does not mean that hydrates would be effectively present in this interval because other parameters as significant gas flux allowing gas saturation of the aqueous medium is also required to sustain hydrate occurrence. Accordingly, the gas hydrate occurrence zone (GHOZ) represents the sedimentary interval where hydrates are really present [Xu and Ruppel, 1999]. Free gas are often encountered below the GHSZ. Such boundary between hydrates and free gas is characterized by a strong seismic response due to the density contrast between the two medium, and it is called the Bottom Simulating Reflector (BSR) [Markl et al., 1970, Tucholke et al., 1977, Shipley et al., 1979](Figure 1.2).

Thus, gas hydrate bearing-sediments (GHBS) are hydrates formed in nature within various porous media type made of coarse sand, silt, fine clay, and often mixtures of them, and formed where hydrate-forming molecules are supplied differently (e.g., dissolved methane and/or presence of gas phase). This results in different gas hydrate distribution within the sediments, affecting the mechanical properties of the GHBS and the fluid flow properties of the aqueous phase (plus eventually vapor). On macroscale, the hydrate could adopt different morphologies within the sediment. In coarse sand the hydrate is likely disseminated [Ruffine, 2015], and for fine-grained sediments in the vicinity of gas vents, the hydrate will more likely form fracture-filling, lenses or massive structures [Suess et al., 1999, Haeckel et al., 2004](Figure 1.3). On microscale, the hydrate can grow as pore-filling (likely with excess water), grain-coating or pore-throat clogging, affecting differently the load-bearing behaviour of the GHBS [Priest et al., 2009].

1.2.2 Geohazards and climate change

Research on identification, assessment and mitigation of geohazards are performed to prevent human casualties, economical damages and ecological disasters. These phenomenon, like earthquake and slope stability, may be involved together and occur onshore and offshore [Dawson et al., 1988, Zabel and Schulz, 2001]. One section of offshore geohazards deals with slope stability. Many processes could lead to slope failure (seafloor landslide) as seismic hazard, gas hydrate dissociation, fast accumulation of sediments, gas charging, glacial loading, volcanic processes, fluid seepage and human activities [Sultan et al., 2004b]. Any mechanical weakening could damage casings and well structures during drilling operations: over-pressured sands, shallow gas accumulations and gas hydrates represents common hazards of drilling [McConnell et al., 2012]. Concerning gas hydrates implications, many research activities are carried out to evaluate risks due to its destabilization.

Indeed, natural gas hydrates might represent a geohazard for the petroleum indus-

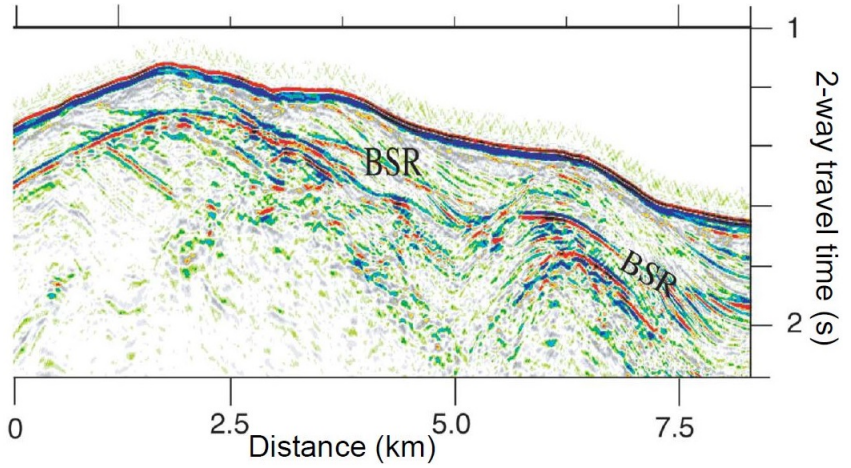

Figure 1.2: Example of BSR identified in seismic reflection images (offshore Oregon, U.S.), suggesting gas hydrate occurrence with two high amplitude envelopes (seafloor and BSR) (GEOMAR).

Figure 1.3: Left: combustion after ignition of muddy thermogenic gas hydrates sampled in the Sea of Marmara with a 12 m gravity core, at a depth around 658 m and a seafloor temperature of 287.15 K (L.N. Legoix, 2014). Right: Methane hydrate lens formed in laboratory with a clay/sand mixture (modified from Ruffine [2015]).

try which target offshore production fields. When the produced hot hydrocarbon fluid is transported through a hydrate-stability zone, heat exchange between both bodies (hot fluid and hydrate-bearing zone) may heat up enough the hydrate-bearing sediments and leads the system outside its stability domain. This can, in turn, provokes the destabilization of the sediment and jeopardizes both production and transport facilities [Sultan et al., 2004a]. The hydrates will undergo destabilization processes which leads to changes in the mechanical properties with potential failures. Thus, hazards on slope stability are seriously considered by the hydrocarbon industry during the assessment of the production and transportation facilities offshore [Austvik et al., 2000].

A dissociation of gas hydrates could also occur when the pressure decreases too

much (decrease of sealevel), when the global water temperature becomes greater than the stability temperature of the gas hydrate, or when the gas supply is not anymore sufficient. Depending on the $p-T$ stability of the gas hydrate the dissociation would occur from the top of the GHOZ, the bottom or both. When the temperature of the seafloor (and in the sediment) is increasing over the stability of the hydrate localized on the top of the GHOZ, the hydrate will dissociate first from the top and later (depending on the heat transfer within the sediment) from the bottom. When the temperature increase is not high enough to dissociate the top, the hydrate will dissociate only from the bottom. The impact on the top and bottom part of the GHOZ is similar for a pressure decrease.

Thus a possible dissociation could be caused by climate change (e.g., global warming, sealevel decrease due to a glaciation) that occurred in the past [Nisbet, 1990] or in the present period [Archer, 2007]. In this scenario, methane release could occur above deep-sea sediments producing ocean acidification due to the microbial oxidation of CH_4 [Biastoch et al., 2011]. In case CH_4 is released from the permafrost to the atmosphere, this could also provoke a positive retroaction on global warming due to the high greenhouse gas potent of this gas.

1.2.3 Carbon capture and storage

Carbon dioxide, followed by methane, are the most encountered greenhouse gases emitted in the atmosphere which needs to be mitigated to avoid global warming and ocean acidification. Thus, the IPCC compels to reduce their emissions [Pachauri et al., 2013]. Accordingly, there are a lot of investigations ongoing in order to capture and sequester anthropogenic CO_2. The storage of carbon dioxide in depleted hydrocarbon reservoirs is a mature technology which is carried out in several fields as Sleipner (North sea), Wayburn (Canada) and In Salah (Algeria) [Verdon et al., 2013]. However, the available storage volume is limited and there is a need to explore other storage possibilities. Another advanced technology is the storage of CO_2 in deep saline aquifers or porous rocks. However, some studies pointed out the possibility of correlations between earthquakes and carbon dioxide capture and storage due to geomechanical deformation [Cappa and Rutqvist, 2011, Zoback and Gorelick, 2012]. This motivates for the investigation on other storage methods and areas. Another option under consideration is the storage in the deep-sea sediments or within deep sedimentary strata covered by impermeable sediment or hydrate layer [Ohgaki et al., 1993, Lackner, 2003]. The deep-sea sediment seems to be a serious option as the storage capacity is greater [Lackner, 2003]. For instance, the U.S. would be able to store thouthands of years of carbon emitted within its economic exclusive zone (EEZ) [House et al., 2006]. However, many questions need to be answered to perform a sustainable storage, and this primarily resides on the integrity of the storage over time (e.g., [Tohidi et al., 2010]).

1.2.4 Energy resource

Natural gas hydrates is also related to the economical benefits this huge amount of methane bound into these accumulations can represent in term of energy resource.

Indeed the amount of methane within gas hydrate deposits is estimated to be larger than the total amount of hydrocarbons traps within conventional and unconventional exploitable reservoirs [Boswell and Collett, 2011].

Worldwide population has been keeping on growing since the last decades and the energy demand evolution follows the population increase. Emergent countries are developing in order to achieve the standard lifestyle of the western world, and therefore strongly contribute to the growth of energy demand. Moreover several studies have shown a decrease of hydrocarbon resources because of their natural limitation (e.g., [Bentley et al., 2007, Sorrell et al., 2010]). Each country needs to manage energy and sustainability to find a balance between energy independence and carbon emissions mitigation. The place of natural gas used among all energy sources will grow over next decades since this resource can provide chemical compounds and energy with low CO_2 emissions [Economides and Wood, 2009, Petroleum, 2018]. In order to meet the world energy demand, natural gas hydrate extraction is an option which deserves consideration. With an estimated amount between 100 and 2000 Gt [Archer et al., 2009, Burwicz et al., 2011, Wallmann et al., 2012, Pinero et al., 2013] of methane-bounded carbon in marine hydrates, gas hydrates could represent the largest source of methane on the earth. However, industrial methods to produce methane from natural gas hydrates in an economical viable way are not developed enough yet [Walsh et al., 2009, Kong et al., 2018].

Several methods for recovering methane from hydrate accumulations have been investigated with three main options of production: heating, depressurization and injection of chemicals [Y.F Makogon, 1997]. Indeed a shift of one of the parameters that governs hydrate stability, e.g., $p-T$ or gas composition, would allow the recovery of methane via dissociation or gas replacement.

Methane hydrate recovery by thermal stimulation of a deposit consists in heating the hydrate to extract the hydrocarbons. This thermal-stimulation technique has been tried to extract methane bellow the permafrost, using a hot fluid circulation on Mallik test site (MacKenzie Delta, Canada) in 2002 [Dallimore and Collett, 2002]. A volume of 470 m^3 of gas has been produced over 5 days with a conclusion that a thermal stimulation alone is not enough efficient for a long term production. This method is not efficient yet, since the total energy budget needed for recovery is important. However, this method is still under investigation, and derived processes has been proposed like a pilot-scale experimental reactor using the in situ combustion of a hydrate deposit [Schicks et al., 2011].

Several production tests applying the depressurization method followed the thermal stimulation test. The depressurization consists in recovering CH_4 by decreasing the pressure of the hydrate deposit to drive it outside its stability field. On Messoyakha Gas Field (Siberia, Russia) [Sapir et al., 1973] the pressure decrease occurring over decades was lower than expected, implying that the dissociation of hydrates was a source of natural gas during the production. Two depressurization tests have been done on the Mallik site in winter 2007 and winter 2008, from a well-head placed at the bottom of the GHOZ (c.a. 1100 m deep) by (JOGMEC/NRCan/Aurora) [Yamamoto and Dallimore, 2008]. The first test collected 830 m^3 of gas in half-day

production and the second test produced 13,000 m^3 over 6 days. Few years later, the first depressurization test from deep-water hydrate layers was performed by the JOGMEC in the Nankai Trough (offshore Japan) in 2013 [Yamamoto et al., 2014, Konno et al., 2017]. The production was aborted due to significant sand production but the drilling vessel collected 119,500 m^3 of gas over 6 days. However, the endothermic characteristics of the hydrate dissociation may be favorable for the formation of ice or even reformation of hydrates, which limits the methane recovery [Moridis et al., 2004]. More recently, a depressurization test has been done again two times in the eastern Nankai Trough in 2017 with 35,000 m^3 of gas collected over 12 days for the first production well and 200,000 for the second over 24 days (not clearly confirmed, [METI]). Finally, in the Shenhu Area (South China Sea, China) in 2017, 309,000 m^3 of gas were produced over 60 days [JWNenergy].

The third method is the injection of chemicals like thermodynamic or kinetic inhibitors, or CO_2 fluid for gas replacement. The injection of chemical inhibitors as alcohols is prohibited into the marine realm, and the cost of the post-treatment of methane stream is also a drawback, as the chemical inhibitor needs to be recycled. An other solution is the carbon dioxide sequestration into methane hydrate deposits coupled with methane recovery, as it both responds to the energy demand and favors greenhouse gas mitigation. It consists in exchanging the CH_4 guests molecules of the hydrates by CO_2 guests [Ohgaki et al., 1996]. This method has been tested in the Ignik Sikumi site (Alaska, U.S.) [Schoderbek et al., 2013, Boswell et al., 2016], where a CO_2-N_2 mixture was injected in hydrate layer located bellow the permafrost (c.a. 690 m deep), followed by CH_4 production using a depressurization method. All methods cost yet too much energy or chemicals, with secondary issues which need to be corrected in order to make them economically viable.

1.3 Scope of work

The aim of the present work is to study mixed gas hydrates that could be present in nature or encountered in processes developped for CH_4 hydrate production coupled with CO_2 sequestration. Such developments show a need to better describe and predict phase equilibrium thermodynamics of systems containing methane and carbon dioxide at different compositions. There is first a need to predict the influence of the presence or absence of different phases (liquid, vapor, excess water) on the stability of gas hydrates and also the influence of different components as CO_2 and N_2 when they are in contact with CH_4 hydrates. Here, several high-pressure laboratory experiments are conducted using three different apparatus (Figure 1.4).

Chapter 2 is a study of the behavior of CH_4-CO_2 bulk gas hydrates in equilibrium with only CO_2-rich liquid phase. The system contains bulk gas hydrates made artificially for defining the stability of mixed CH_4-CO_2 hydrates when no vapor phase is present. In many studies, it was proved that pure CO_2 hydrate needs a very high pressure to be stable at higher temperature (over 283.19 K) when only liquid CO_2 coexists with gas hydrates, compared to lower temperature where CO_2 hydrates could coexist with a vapor phase. However, formation conditions of a mixed CH_4-CO_2

hydrate are poorly known and more data on this system are required to establish which phases could forms when CO_2 is present in high-proportions together with CH_4 when CO_2 is injected below the seafloor. The apparatus employed here is a high pressure cell with a sapphire window with a variable volume of 21-65 cm^3 (Figure 1.4, Left). In this work, it was shown that the addition of CH_4 (low enough to prevent vapor phase formation) decreases the stability pressure of the resulting gas hydrates. In addition to that, a set of vapor-liquid equilibrium envelopes of CH_4-CO_2 were monitored with the same apparatus an modeled with an equation of state.

One of the most promising way to council natural gas production, geohazard mitigation and environment preservation is to inject CO_2 with N_2 into the CH_4 hydrate. Then there is a need to study the behavior of mixed gas hydrates containing CH_4-CO_2-N_2. Chapter 3 focuses on this problematic with the aim to study the stability of CH_4-CO_2-N_2 gas hydrate. Thus, a thermodynamic study of bulk gas hydrates containing CH_4, CO_2 and N_2 is presented, together with an exchange experiment between a bulk CH_4 hydrate and a gas phase containing CO_2. The evolution of the pressure and of the composition of the gas phase is monitored and employed to perform a mass balance, understand better the phenomenon occurring during a gas exchange and predict the time required to complete the conversion into rich-CO_2 hydrate. This work was done on the high-pressure view cell described in the first part for the exchange experiment (Figure 1.4, Left), and on a high-pressure titanium cell with a volume of 52 cm^3 for the thermodynamic study (Figure 1.4, Middle). Due to the solubility difference between different gases in water, especially the high solubility of CO_2, the present amount of H_2O affects considerably the stability of gas hydrates. It was experimentally shown that the gas hydrate produced by a CO_2-N_2 injected in excess water has a stability of formation shifted to higher pressures, compared to a system containing a small proportion of water.

In natural system, methane-rich hydrate may be found as disseminated inside a sediment matrix below the seafloor or the permafrost, coexisting with seawater. This makes the system more complex, the salinity changes the water activity and stability of gas hydrates. The presence of a porous media also affects fluid transports and gas hydrate formation, growth, distribution and dissociation. Chapter 4 presents then a study on a more realistic system. Indeed, the initial setup is prepared to mimic a typical gas hydrate deposit that can be found in nature, formed from CH_4 at low temperature and high-pressure, and distributed in the sand matrix with seawater. The experiments were carried out with a vertical reactor containing a volume of 1044 cm^3 of artificial hydrate-bearing sand (Figure 1.4, Right). This high-pressure flow-through reactor is then used to investigate the gas exchange of methane hydrate-bearing sediments with CH_4-CO_2-N_2 gas mixtures. The behaviour of the GHBS in term of gas retention and hydrate contents are then studied when a CH_4-CO_2-N_2 gas mixture is flushed through the gas hydrate-bearing sediment. The CH_4 content in the flushed gas is gradually increased over the experiments, in order to study the impact of the enrichment in CH_4 in the CO_2-N_2 stream initially injected.

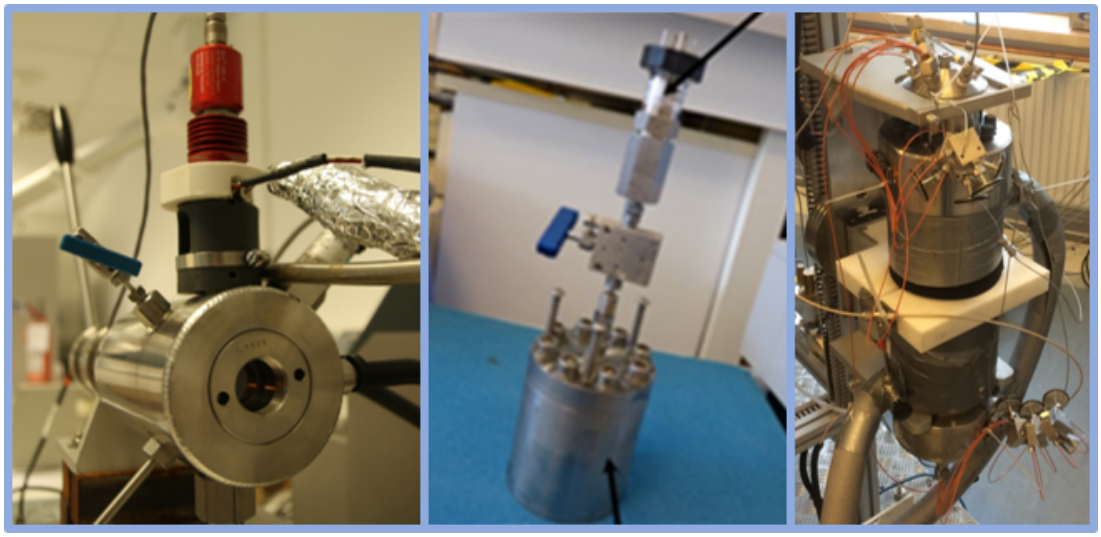

Figure 1.4: High-pressure cells employed to study gas hydrates (refer to corresponding chapters for complete sketches of each system). Left: Cell equipped with sapphire window (IFREMER-LCG). Middle: Titanium cell for phase equilibria measurements (IFREMER-LCG). Right: Vertical cell for flow-through experiments (GEOMAR-FB2).

Bibliography

D. Archer. Methane hydrate stability and anthropogenic climate change. *Biogeosciences Discussions*, 4(2):993–1057, 2007. doi: 10.5194/bgd-4-993-2007.

D. Archer, B. Buffett, and V. Brovkin. Ocean methane hydrates as a slow tipping point in the global carbon cycle. *Proceedings of the National Academy of Sciences*, 106(49):20596–20601, 2009. doi: 10.1073/pnas.0800885105.

T. Austvik, X. Li, and L. H. Gjertsen. Hydrate Plug Properties: Formation and Removal of Plugs. *Annals of the New York Academy of Sciences*, 912(1):294–303, 2000. doi: 10.1111/j.1749-6632.2000.tb06783.x.

R. W. Bentley, S. A. Mannan, and S. J. Wheeler. Assessing the date of the global oil peak: The need to use 2P reserves. *Energy Policy*, 35(12):6364–6382, 2007. doi: 10.1016/j.enpol.2007.08.001.

A. Biastoch, T. Treude, L. H. Rüpke, U. Riebesell, C. Roth, E. B. Burwicz, W. Park, M. Latif, C. W. Böning, G. Madec, et al. Rising arctic ocean temperatures cause gas hydrate destabilization and ocean acidification. *Geophysical Research Letters*, 38(8), 2011. doi: 10.1029/2011GL047222.

C. Bily and J. Dick. Naturally occurring gas hydrates in the mackenzie delta, nwt. *Bulletin of Canadian Petroleum Geology*, 22(3):340–352, 1974.

R. Boswell and T. S. Collett. Current perspectives on gas hydrate resources. *Energy Environ. Sci.*, 4(4):1206–1215, 2011. doi: 10.1039/C0EE00203H.

R. Boswell, D. Schoderbek, T. S. Collett, S. Ohtsuki, M. White, and B. J. Anderson. The Ignik Sikumi Field Experiment, Alaska North Slope: Design, Operations, and Implications for CO_2–CH_4 Exchange in Gas Hydrate Reservoirs. *Energy & Fuels*, 31(1):140–153, 2016. doi: 10.1021/acs.energyfuels.6b01909.

C. Bourry, B. Chazallon, J. L. Charlou, J. P. Donval, L. Ruffine, P. Henry, L. Geli, M. N. Çagatay, S. İnan, and M. Moreau. Free gas and gas hydrates from the sea of marmara, turkey: Chemical and structural characterization. *Chemical Geology*, 264(1-4):197–206, 2009. doi: 10.1016/j.chemgeo.2009.03.007.

J. Brooks, M. Kennicutt, R. Fay, T. McDonald, and R. Sassen. Thermogenic gas hydrates in the gulf of mexico. *Science*, 225(4660):409–411, 1984. doi: 10.1126/science.225.4660.409.

E. B. Burwicz, L. Rüpke, and K. Wallmann. Estimation of the global amount of submarine gas hydrates formed via microbial methane formation based on numerical reaction-transport modeling and a novel parameterization of holocene sedimentation. *Geochimica et Cosmochimica Acta*, 75(16):4562–4576, 2011. doi: 10.1016/j.gca.2011.05.029.

F. Cappa and J. Rutqvist. Impact of CO_2 geological sequestration on the nucleation of earthquakes. *Geophysical Research Letters*, 38(17):2–7, 2011. doi: 10.1029/2011GL048487.

R. Chapman, J. Pohlman, R. Coffin, J. Chanton, and L. Lapham. Thermogenic gas hydrates in the northern cascadia margin. *Eos, Transactions American Geophysical Union*, 85(38):361–365, 2004. doi: 10.1029/2004EO380001.

T. S. Collett, K. A. Kvenvolden, and L. B. Magoon. Characterization of hydrocarbon gas within the stratigraphic interval of gas-hydrate stability on the north slope of alaska, usa. *Applied Geochemistry*, 5(3):279–287, 1990. doi: 10.1016/0883-2927(90)90003-N.

S. Dallimore and T. Collett. Summary and implications of the mallik 2002 gas hydrate production research well program. *Scientific results from the Mallik*, pages 1–36, 2002.

D. Davidson, S. Garg, S. Gough, R. Hawkins, and J. Ripmeester. Characterization of natural gas hydrates by nuclear magnetic resonance and dielectric relaxation. *Canadian Journal of Chemistry*, 55(20):3641–3650, 1977. doi: 10.1139/v77-512.

D. Davidson, S. Garg, S. Gough, Y. Handa, C. Ratcliffe, J. Ripmeester, J. Tse, and W. Lawson. Laboratory analysis of a naturally occurring gas hydrate from sediment of the gulf of mexico. *Geochimica et Cosmochimica Acta*, 50(4):619–623, 1986. doi: 10.1016/0016-7037(86)90110-9.

H. Davy et al. I. the bakerian lecture. on some of the combinations of oxymuriatic gas and oxygene, and on the chemical relations of these principles, to inflammable bodies. *Philosophical Transactions of the Royal Society of London*, 101:1–35, 1811.

A. G. Dawson, D. Long, and D. E. Smith. The Storegga Slides: Evidence from eastern Scotland for a possible tsunami. *Marine Geology*, 82(3-4):271–276, 1988. doi: 10.1016/0025-3227(88)90146-6.

P. Dholabhai, P. Englezos, N. Kalogerakis, and P. Bishnoi. Equilibrium conditions for methane hydrate formation in aqueous mixed electrolyte solutions. *The Canadian journal of chemical engineering*, 69(3):800–805, 1991. doi: 10.1002/cjce.5450690324.

Z. Duan and R. Sun. A model to predict phase equilibrium of CH_4 and CO_2 clathrate hydrate in aqueous electrolyte solutions. *American Mineralogist*, 91(8-9):1346–1354, 2006. doi: 10.2138/am.2006.2017.

M. J. Economides and D. A. Wood. The state of natural gas. *Journal of Natural Gas Science and Engineering*, 1(1-2):1–13, 2009. doi: 10.1016/j.jngse.2009.03.005.

M. Faraday. Xiv. on fluid chlorine. *Philosophical Transactions of the Royal society of London*, 113:160–165, 1823.

G. Ginsburg and V. Soloviev. Mud volcano gas hydrates in the Caspian Sea. *Bulletin of the Geological Society of Denmark*, 41(95):100, 1994.

M. Haeckel, E. Suess, K. Wallmann, and D. Rickert. Rising methane gas bubbles form massive hydrate layers at the seafloor. *Geochimica et Cosmochimica Acta*, 68 (21):4335–4345, 2004. doi: 10.1016/j.gca.2004.01.018.

E. Hammerschmidt. Gas hydrate formations, a further study on their prevention and elimination from natural gas pipe lines. *Gas*, 15(5):30–34, 1939.

E. G. Hammerschmidt. Formation of Gas Hydrates in Natural Gas Transmission Lines. *Industrial & Engineering Chemistry*, 26(8):851–855, 1934. doi: 10.1021/ie50296a010.

R. W. Henning, A. J. Schultz, V. Thieu, and Y. Halpern. Neutron diffraction studies of CO_2 clathrate hydrate: Formation from deuterated ice. *The Journal of Physical Chemistry A*, 104(21):5066–5071, 2000. doi: 10.1021/jp0001642.

K. Z. House, D. P. Schrag, C. F. Harvey, and K. S. Lackner. Permanent carbon dioxide storage in deep-sea sediments. *Proceedings of the National Academy of Sciences*, 103(33):12291–12295, 2006. doi: 10.1073/pnas.0605318103.

JWNenergy. China successfully completes first gas hydrate trial. https://www.jwnenergy.com/article/2017/8/china-successfully-completes-first-gas-hydrate-trial/. Accessed: 26 sept. 2018.

M. Kida, O. Khlystov, T. Zemskaya, N. Takahashi, H. Minami, H. Sakagami, A. Krylov, A. Hachikubo, S. Yamashita, H. Shoji, et al. Coexistence of structure I and II gas hydrates in Lake Baikal suggesting gas sources from microbial and thermogenic origin. *Geophysical Research Letters*, 33(24), 2006. doi: 10.1029/2006GL028296.

R. Kobayashi. Gas hydrate formation with brine and ethanol solutions. In *Proc. 30th Ann. Convention Natural Gasoline Assoc. Amer*, pages 27–31, 1951.

Z. Kong, Q. Jiang, X. Dong, J. Wang, and X. Wan. Estimation of China's production efficiency of natural gas hydrates in the South China Sea. *Journal of Cleaner Production*, 203:1–12, 2018. doi: 10.1016/j.jclepro.2018.08.262.

Y. Konno, T. Fujii, A. Sato, K. Akamine, M. Naiki, Y. Masuda, K. Yamamoto, and J. Nagao. Key findings of the world's first offshore methane hydrate production test off the coast of japan: Toward future commercial production. *Energy & Fuels*, 31(3):2607–2616, 2017. doi: 10.1021/acs.energyfuels.6b03143.

W. Kuhs, B. Chazallon, P. Radaelli, and F. Pauer. Cage occupancy and compressibility of deuterated N_2-clathrate hydrate by neutron diffraction. *Journal of inclusion phenomena and molecular recognition in chemistry*, 29(1):65–77, 1997. doi: 10.1023/A:1007960217691.

K. A. Kvenvolden. Methane hydrate - A major reservoir of carbon in the shallow geosphere? *Chemical Geology*, 71(1-3):41–51, 1988. doi: 10.1016/0009-2541(88)90104-0.

K. A. Kvenvolden. Gas hydrates—geological perspective and global change, 1993.

K. S. Lackner. A guide to CO_2 sequestration. *Science*, 300(5626):1677–1678, 2003. doi: 10.1126/science.1079033.

H. Lu, Y. T. Seo, J. W. Lee, I. Moudrakovski, J. A. Ripmeester, N. R. Chapman, R. B. Coffin, G. Gardner, and J. Pohlman. Complex gas hydrate from the Cascadia margin. *Nature*, 445(7125):303–306, 2007. doi: 10.1038/nature05463.

Z. Lu, Y. Zhu, H. Liu, Y. Zhang, C. Jin, X. Huang, and P. Wang. Gas source for gas hydrate and its significance in the qilian mountain permafrost, qinghai. *Marine and Petroleum Geology*, 43:341–348, 2013. doi: 10.1016/j.marpetgeo.2013.01.003.

Z.-q. Lu, Y.-h. Zhu, Y.-q. Zhang, H.-j. Wen, Y.-h. Li, Z.-y. Jia, P.-k. Wang, and Q.-h. Li. Study on genesis of gases from gas hydrate in the qilian mountain permafrost, qinghai. *Geoscience*, 3:024, 2010.

Y. Makogon. Features of natural gas fields' exploitation in permafrost zone. *Gazovaya Promyshlennost*, 9:1–17, 1966.

R. Markl, G. Bryan, and J. Ewing. Structure of the blake-bahama outer ridge. *Journal of Geophysical Research*, 75(24):4539–4555, 1970. doi: 10.1029/JC075i024p04539.

D. R. McConnell, Z. Zhang, and R. Boswell. Review of progress in evaluating gas hydrate drilling hazards. *Marine and Petroleum Geology*, 34(1):209–223, 2012. doi: 10.1016/j.marpetgeo.2012.02.010.

METI. Second offshore methane hydrate production test finishes. http://www.meti.go.jp/english/press/2017/0629_001.html. Accessed: 26 sept. 2018.

A. V. Milkov and R. Sassen. Economic geology of offshore gas hydrate accumulations and provinces. *Marine and Petroleum Geology*, 19(1):1–11, 2002.

G. J. Moridis, T. S. Collett, S. R. Dallimore, T. Satoh, S. Hancock, and B. Weatherill. Numerical studies of gas production from several CH_4 hydrate zones at the Mallik site, Mackenzie Delta, Canada. *Journal of Petroleum Science and Engineering*, 43(3-4):219–238, 2004. doi: 10.1016/j.petrol.2004.02.015.

H.-J. Ng and D. B. Robinson. Hydrate formation in systems containing methane, ethane, propane, carbon dioxide or hydrogen sulfide in the presence of methanol. *Fluid Phase Equilibria*, 21(1-2):145–155, 1985. doi: 10.1016/0378-3812(85)90065-2.

H. Niemann, T. Lösekann, D. De Beer, M. Elvert, T. Nadalig, K. Knittel, R. Amann, E. J. Sauter, M. Schlüter, M. Klages, et al. Novel microbial communities of the haakon mosby mud volcano and their role as a methane sink. *Nature*, 443(7113): 854, 2006.

E. Nisbet. The end of the ice age. *Canadian Journal of Earth Sciences*, 27(1): 148–157, 1990.

K. Ohgaki, Y. Makihara, and K. Takano. Formation of CO_2 hydrate in pure and sea waters. *Journal of chemical engineering of Japan*, 26(5):558–564, 1993. doi: 10.1252/jcej.26.558.

K. Ohgaki, K. Takano, H. Sangawa, T. Matsubara, and S. Nakano. Methane Exploitation by Carbon Dioxide from Gas Hydrates—Phase Equilibria for CO_2-CH_4 Mixed Hydrate System—. *Journal of chemical engineering of Japan*, 29(3):478–483, 1996. doi: 10.1252/jcej.29.478.

J.-N. Oung, C.-Y. Lee, C.-S. Lee, and C.-L. Kuo. Geochemical study on hydrocarbon gases in seafloor sediments, southwestern offshore taiwan-implications in the potential occurrence of gas hydrates. *Terrestrial Atmospheric and Oceanic Sciences*, 17(4):921, 2006.

S. Pachauri, B. J. Van Ruijven, Y. Nagai, K. Riahi, D. P. Van Vuuren, A. Brew-Hammond, and N. Nakicenovic. Pathways to achieve universal household access to modern energy by 2030. *Environmental Research Letters*, 8(2), 2013. doi: 10.1088/1748-9326/8/2/024015.

B. Petroleum. Bp statistical review of world energy 2017. british petroleum (66), 2018.

E. Pinero, M. Marquardt, C. Hensen, M. Haeckel, and K. Wallmann. Estimation of the global inventory of methane hydrates in marine sediments using transfer functions. *Biogeosciences (BG)*, 10(2):959–975, 2013. doi: 10.5194/bg-10-959-2013.

J. Platteeuw and J. Van der Waals. Thermodynamic properties of gas hydrates. *Molecular Physics*, 1(1):91–96, 1958.

J. A. Priest, E. V. Rees, and C. R. Clayton. Influence of gas hydrate morphology on the seismic velocities of sands. *Journal of geophysical research: solid earth*, 114 (B11), 2009. doi: 10.1029/2009JB006284.

J. Priestley. Experiments and observations on different kinds of air. *London: W. Bowyer and J. Nichols/London: Printed for J. Johnson*, 1778.

J. Ripmeester and C. Ratcliffe. Low-temperature cross-polarization/magic angle spinning carbon-13 NMR of solid methane hydrates: structure, cage occupancy, and hydration number. *The Journal of Physical Chemistry*, 92(2):337–339, 1988.

J. A. Ripmeester, C. I. Ratcliffe, D. D. Klug, and J. S. Tse. Molecular Perspectives on Structure and Dynamics in Clathrate Hydrates. *Annals of the New York Academy of Sciences*, 715(1):161–176, 1994. doi: 10.1111/j.1749-6632.1994.tb38832.x.

L. Ruffine. Exploring methane-hydrate formation and dissociation in geologic materials through laboratory experiments: Kinetic behavior and morphology. *Fuel*, 141:173–184, 2015. doi: 10.1016/j.fuel.2014.10.041.

L. Ruffine, J. C. Caprais, G. Bayon, V. Riboulot, J. P. Donval, J. Etoubleau, D. Birot, P. Pignet, E. Rongemaille, B. Chazallon, S. Grimaud, J. Adamy, J. L. Charlou, and M. Voisset. Investigation on the geochemical dynamics of a hydrate-bearing pockmark in the Niger Delta. *Marine and Petroleum Geology*, 43:297–309, 2013. doi: 10.1016/j.marpetgeo.2013.01.008.

M. Sapir, E. Khramenkov, I. Yefremov, G. Ginzburg, A. Beniaminovich, S. Lenda, and V. Kislova. Geologicheskie i promislovo—geofizicheskie osobennosti gazogidratnoi zalezhi messoiakhskogo gazovogo mestorozhdenia (geologic and geophysical features of the gas hydrate deposits in the messoiakh field). *Geologiia Nefti i Gaza*, 6:26–34, 1973.

R. Sassen and I. R. MacDonald. Evidence of structure H hydrate, Gulf of Mexico continental slope. *Organic Geochemistry*, 22(6):1029–1032, 1994. doi: 10.1016/0146-6380(94)90036-1.

R. Sassen, S. Joye, S. T. Sweet, D. A. DeFreitas, A. V. Milkov, and I. R. MacDonald. Thermogenic gas hydrates and hydrocarbon gases in complex chemosynthetic communities, Gulf of Mexico continental slope. *Organic Geochemistry*, 30(7):485–497, 1999. doi: 10.1016/S0146-6380(99)00050-9.

J. M. Schicks, E. Spangenberg, R. Giese, B. Steinhauer, J. Klump, and M. Luzi. New approaches for the production of hydrocarbons from hydrate bearing sediments. *Energies*, 4(1):151–172, 2011. doi: 10.3390/en4010151.

D. Schoderbek, H. Farrell, J. Howard, K. Raterman, S. Silpngarmlert, K. Martin, B. Smith, and P. Klein. Conocophillips gas hydrate production test. Technical report, ConocoPhillips Co., Houston, TX (United States), 2013.

J. C. Seitz, J. D. Pasteris, and I.-M. Chou. Raman spectroscopic characterization of gas mixtures; I, Quantitative composition and pressure determination of CH_4, N_2 and their mixtures. *American Journal of Science*, 293(4):297–321, 1993.

T. H. Shipley, M. H. Houston, R. T. Buffler, F. J. Shaub, K. J. McMillen, J. W. Ladd, and J. L. Worzel. Seismic evidence for widespread possible gas hydrate horizons on continental slopes and rises. *AAPG bulletin*, 63(12):2204–2213, 1979.

S. Sorrell, J. Speirs, R. Bentley, A. Brandt, and R. Miller. Global oil depletion: A review of the evidence. *Energy Policy*, 38(9):5290–5295, 2010. doi: 10.1016/j.enpol.2010.04.046.

M. v. Stackelberg and H. Müller. On the structure of gas hydrates. *The Journal of Chemical Physics*, 19(10):1319–1320, 1951.

E. Suess, M. Torres, G. Bohrmann, R. Collier, J. Greinert, P. Linke, G. Rehder, A. Trehu, K. Wallmann, G. Winckler, et al. Gas hydrate destabilization: enhanced dewatering, benthic material turnover and large methane plumes at the Cascadia convergent margin. *Earth and Planetary Science Letters*, 170(1-2):1–15, 1999. doi: 10.1016/S0012-821X(99)00092-8.

N. Sultan, P. Cochonat, M. Canals, A. Cattaneo, B. Dennielou, H. Haflidason, J. S. Laberg, D. Long, J. Mienert, F. Trincardi, R. Urgeles, T. O. Vorren, and C. Wilson. Triggering mechanisms of slope instability processes and sediment failures on continental margins: A geotechnical approach. *Marine Geology*, 213(1-4):291–321, 2004a. doi: 10.1016/j.margeo.2004.10.011.

N. Sultan, P. Cochonat, J. P. Foucher, and J. Mienert. Effect of gas hydrates melting on seafloor slope instability. *Marine Geology*, 213(1-4):379–401, 2004b. doi: 10.1016/j.margeo.2004.10.015.

A. K. Sum, R. C. Burruss, and E. D. Sloan. Measurement of clathrate hydrates via raman spectroscopy. *The Journal of Physical Chemistry B*, 101(38):7371–7377, 1997. doi: 10.1021/jp970768e.

B. Tohidi, J. Yang, M. Salehabadi, R. Anderson, and A. Chapoy. CO_2 hydrates could provide secondary safety factor in subsurface sequestration of CO_2. *Environmental science & technology*, 44(4):1509–1514, 2010. doi: 10.1021/es902450j.

B. E. Tucholke, G. M. Bryan, and J. I. Ewing. Gas-hydrate horizons detected in seismic-profiler data from the western north atlantic. *AAPG bulletin*, 61(5):698–707, 1977.

T. Uchida, T. Hirano, T. Ebinuma, H. Narita, K. Gohara, S. Mae, and R. Matsumoto. Raman spectroscopic determination of hydration number of methane hydrates. *AIChE Journal*, 45(12):2641–2645, 1999. doi: 10.1002/aic.690451220.

A. Van Cleeff and G. Diepen. Gas hydrates of nitrogen and oxygen. *Recueil Des Travaux Chimiques Des Pays-Bas*, 79(6):582–586, 1960. doi: 10.1002/recl.19650840815.

J. P. Verdon, J.-M. Kendall, A. L. Stork, R. A. Chadwick, D. J. White, and R. C. Bissell. Comparison of geomechanical deformation induced by megatonne-scale CO2 storage at Sleipner, Weyburn, and In Salah. *Proceedings of the National Academy of Sciences*, 110(30):E2762–E2771, 2013. doi: 10.1073/pnas.1302156110.

K. Wallmann, E. Pinero, E. Burwicz, M. Haeckel, C. Hensen, A. Dale, and L. Ruepke. The global inventory of methane hydrate in marine sediments: A theoretical approach. *Energies*, 5(7):2449–2498, 2012. doi: 10.3390/en5072449.

M. R. Walsh, S. H. Hancock, S. J. Wilson, S. L. Patil, G. J. Moridis, R. Boswell, T. S. Collett, C. A. Koh, and E. D. Sloan. Preliminary report on the commercial viability of gas production from natural gas hydrates. *Energy Economics*, 31(5):815–823, 2009. doi: 10.1016/j.eneco.2009.03.006.

W. Xu and C. Ruppel. Predicting the occurence, distribution, and evolution of methane gas hydrate in porous marine sediments. *Journal of Geophysical Research*, 104(B3):5081–5095, 1999.

K. Yamamoto and S. Dallimore. Aurora-JOGMEC-NRCan Mallik 2006-2008 gas hydrate research project progress. *Natural Gas & Oil*, 304:285–4541, 2008.

K. Yamamoto, Y. Terao, T. Fujii, T. Ikawa, M. Seki, M. Matsuzawa, T. Kanno, et al. Operational overview of the first offshore production test of methane hydrates in the Eastern Nankai Trough. In *Offshore Technology Conference*. Offshore Technology Conference, 2014. doi: 10.4043/25243-MS.

A. Yefremova and B. Zhizhchenko. Gas hydrate occurrences in offshore deposits. *DAN SSSR (Proceedings of the USSR Academy of Sciences)*, 214(5):1179–1181, 1974.

Y.F Makogon. *Hydrates of hydrocarbons*. 1997.

M. Zabel and H. D. Schulz. Importance of submarine landslides for non-steady state conditions in pore water systems - Lower Zaire (Congo) deep-sea fan. *Marine Geology*, 176(1-4):87–99, 2001. doi: 10.1016/S0025-3227(01)00164-5.

M. D. Zoback and S. M. Gorelick. Earthquake triggering and large-scale geologic storage of carbon dioxide. *Proceedings of the National Academy of Sciences*, 109 (26):10164–10168, 2012. doi: 10.1073/pnas.1202473109.

Chapter 2

Phase equilibria of the CH_4-CO_2 binary and the CH_4-CO_2-H_2O ternary mixtures in the presence of a CO_2-rich liquid phase

Article published in *Energies* (2017)
L.N. Legoix, L. Ruffine, J.P. Donval, M. Haeckel
doi: 10.3390/en10122034

Abstract The knowledge of the phase behavior of the carbon dioxide (CO_2)-rich mixtures is a key factor to understand the chemistry and migration of natural volcanic CO_2 seeps in the marine environment, as well as to develop engineering proceses for CO_2 sequestration coupled to methane (CH_4) production from gas hydrate deposits. In both cases, it is important to gain insights into the interactions of the CO_2-rich phase – liquid or gas – with the aqueous medium (H_2O) in the pore space below the seafloor or in the ocean. Thus, the CH_4-CO_2 binary and CH_4-CO_2-H_2O ternary mixtures were investigated at relevant pressure and temperature conditions. The solubility of CH_4 in liquid CO_2 (vapor-liquid equilibrium) was determined in laboratory experiments and then modelled with the Soave-Redlich-Kwong equation of state (EoS) consisting of an optimized binary interaction parameter $k_{ij(CH_4-CO_2)} = 1.32 \times 10^3 \times T - 0.251$ describing the non-ideality of the mixture. The hydrate-liquid-liquid equilibrium (HLLE) was measured in addition to the composition of the CO_2-rich fluid phase in the presence of H_2O. In contrast to the behavior in the presence of vapor, gas hydrates become more stable when increasing the CH_4 content, and the relative proportion of CH_4 to CO_2 decreases in the CO_2-rich phase after gas hydrate formation.

Keywords gas hydrate; CH_4; CO_2-rich mixtures; phase equilibria; Soave-Redlich-Kwong (SRK) cubic equation of state (EoS)

2.1 Introduction

CO_2 is ubiquitous in geological systems, and is encountered in geofluids in multiple phases (e.g., [Lewicki et al., 2007, Boiron et al., 2007]). Generally, it is either

generated by the degradation of organic matter, decomposition of carbonate rock, or post-genetic mantle processes. However, the occurrence of a CO_2-rich gaseous, liquid, and gas hydrate phase is typically limited to volcanic systems [Sakai et al., 1990, Inagaki et al., 2006, Konno et al., 2006, Lupton et al., 2006], where it is often accompanied by admixtures of hydrocarbon gases such as CH_4. Reconstructing the migration pattern of such fluids from their source within the sedimentary column to their discharge and fate into the H_2O column requires a correct understanding of the involved thermodynamic phase equilibria. In addition, as society is increasingly concerned about mitigating CO_2 emissions into the atmosphere, understanding the phase behavior of CO_2-rich mixtures becomes more important for the design and conception of reliable carbon storage processes. Amongst the processes under investigation, the storage of CO_2 in solid gas hydrates by replacing the CH_4 from natural accumulations seems to be very promising, since it helps to meet the global energy demand, while reducing net global carbon emissions. CH_4 production from gas hydrates coupled to CO_2 sequestration has been investigated intensively; e.g., with some laboratory-scale experiments [Ebinuma, 1993, Nakano et al., 1998b, Ota et al., 2005, Schicks et al., 2011, Deusner et al., 2012], and in a field-scale production test [Boswell et al., 2017]. The method involves multiple phase equilibria, where a liquid aqueous and a CO_2-rich phase coexist with vapor and solid gas hydrates, depending on the prevailing temperature and pressure conditions. The present article starts by reviewing the experimental data available for both CH_4-CO_2 (Table 2.1) and CH_4-CO_2-H_2O (Table 2.2) systems at equilibrium conditions involving a CO_2-rich liquid phase. Then, the apparatus and approaches used to generate the new data are briefly described. In the third part of the paper, new experimental data will be presented and discussed. An important requirement for the development of CH_4 hydrate production coupled with CO_2-sequestration is the knowledge of the contents of H_2O and CH_4 lost in the liquid CO_2. Currently, a lack of CH_4 solubility data for the liquid CO_2 phase [Vitu et al., 2007] hinders thermodynamic models to accurately evaluate the amount of CH_4 that is lost in the liquid CO_2 phase for such a production scheme. Few works have measured the phase properties of such mixtures at high pressures and temperatures ranging between 273.15 and 301 K (Table 2.1). Clearly, more measurements are needed in order to develop accurate thermodynamic models to quantitatively assess the CH_4-to-CO_2 hydrate conversion process. Phase equilibria of the CH_4-CO_2 binary mixture have previously been investigated to determine its phase envelopes and phase compositions as a function of temperature and pressure [Duan and Hu, 2004, Vitu et al., 2007]. This binary mixture exhibits a diagram of Type I in the classification of van Konynenburg [Van Konynenburg and Scott, 1980, Al Ghafri et al., 2014]. Thus, in the pressure-composition space, the vapor-liquid equilibrium (VLE) envelopes are characterized by critical points located along a continuous line linking the critical points of CH_4 (190.55 K; 4.60 MPa) and CO_2 (304.21 K; 7.38 MPa) [Poling and Prausnitz, 2001]. However, few data points are available for the CH_4-CO_2 VLE in the temperature range of 273.15 and 301 K (Table 2.1). This range is located between the freezing point of H_2O and the critical temperature of CO_2, and also includes the typical marine conditions favorable for the formation of

gas hydrates. [Arai et al., 1971] performed the VLE in a glass capillary cell. The pressure was then increased while keeping the temperature constant, and the resulting volume change of the mixture was measured with a cathetometer. The bubble point was determined by analyzing the pressure change with respect to the molar volume due to the vanishing of the vapor phase. [Kaminishi and Toriumi, 1966, Kaminishi et al., 1968] investigated the VLE inside a high-pressure-stirred cell, and they were able to sample both phases. [Xu et al., 1991, 1992] used a similar method as the present work, with a gas chromatograph to analyze liquid and gas sampled from a high-pressure cell. [Bian et al., 1993] used a static method to analyze both phases and the critical pressure. The CH_4-CO_2-H_2O ternary system has been studied under multiple phase equilibrium. [Al Ghafri et al., 2014] did a very interesting study of this mixture at VLE, vapor-liquid-liquid equilibrium (VLLE), liquid-liquid equilibrium (LLE), and hydrate-vapor-liquid-liquid equilibrium (HVLLE). Indeed, in the p–T diagram, the VLLE region delimited by the Quadruple curve, the upper-critical end point (UCEP) curve, and the CO_2 vaporization curve has been studied by [Al Ghafri et al., 2014], with composition measurements for all phases. The CH_4-CO_2-H_2O ternary system is able to form a CO_2-rich liquid phase under relatively higher pressure, and this drastically changes the hydrate stability field in comparison with pure CO_2. However, experimental data at hydrate-liquid-liquid equilibrium (HLLE) conditions are scarce (see comprehensive summary in Table 2.2). Considering experimental data from all authors, the temperatures investigated are between 282.92 and 294 K, with pressures ranging from 4.5 to 494 MPa, and the initial load of CO_2 varying from 0.78 to 1 mole fraction. The data below 30 MPa are shown for the HVLLE and the HLLE in Figure 1, together with calculated dissociation curves of gas hydrate for pure CH_4 and pure CO_2 gas hydrate formers, and vapor pressure of pure CO_2 [Kossel et al., 2013]. The occurrence of the CO_2-rich liquid phase is possible for such ternary systems with gas hydrates only for CH_4 mole fractions of 0-0.225 for the initial CH_4-CO_2 gas feed [Bi et al., 2013]. Thus, it is possible to have an upper-quadruple point (Q_2) where gas hydrate (H), liquid H_2O (L_{H_2O}), CO_2-rich liquid (L_{CO_2}), and vapor (V) phases coexist (HVLLE) [Bi et al., 2013]. However, for a given temperature, the CH_4-CO_2-H_2O system is able to form a CO_2-rich liquid phase under higher pressures than for pure CO_2. The quadruple points Q_2 for such mixtures are located at higher pressures, shifting the hydrate stability zone towards the high-pressure region accordingly. The Q_2 for a CH_4 molar fraction of 0.225 has been estimated by [Bi et al., 2013] to be at 287.9 K and 8.4 MPa. Thus, the Q_2 zone is accurately described by several authors [Seo et al., 2000, Seo and Lee, 2001, Bi et al., 2013, Al Ghafri et al., 2014] (Table 2.2) (Figure 2.1, "+" orange symbols). For temperatures below Q_2, or a richer CH_4 mole fraction, the area is well described and several stability points of mixed gas hydrates with vapor and aqueous phase, the hydrate-vapor-liquid equilibrium (HVLE), monitoring have been published as reviewed by [Kastanidis et al., 2017]. The same is true for the gas hydrate stability in the presence of a pure CO_2-rich liquid phase (HLLE) (Table 2.2), whereas data for CH_4 admixtures in the CO_2-rich liquid phase exists only for 5.9 mol % CH_4 (Table 2.2) [Vitu et al., 2007]. These authors measured gas hydrate dissociation

points using an isochoric step-heating method, keeping the H_2O mole fraction between 0.53 and 0.57. The present article will also focus on the HLLE region with mixed CH_4-CO_2-hydrates.

Reference	**Isotherm Studied /K**	**Pressure Range /MPa**	**Number of Data Point** (x_{CH_4}, y_{CH_4})
[Kaminishi et al., 1968]	273.15 283.15	5.20-8.08 6.12-8.08	(3,4) (3,3)
[Arai et al., 1971]	273.15 288.15	4.15-8.41 5.38-8.04	(3,9) (5,7)
[Xu et al., 1992]	288.50 293.40	5.12-8.15 5.73-7.98	(10,10) (13,13)
[Bian et al., 1993]	301.00	6.86-7.70	(6,6) + Critical point
This work	274.15 277.15 283.15 288.15 290.15	3.64-8.33 3.94-8.20 4.60-8.08 5.17-7.63 5.44-7.82	(9,0) (11,0) (4,0) (4,0) (6,0)

Table 2.1: Experimental data for the CH_4-CO_2 binary system at vapour-liquid equilibrium (VLE), between 273.15 and 301 K.

System	**Phases**	T **/K** p **/MPa**	**CH_4 Composition**	**Data**	**Reference**
CO_2-H_2O	H-L_{H_2O}-L_{CO_2}-V Point in $p-T$ space	283.19 ($\pm$ 0.46) 4.49 ($\pm$ 0.20)	-	9	Ref.1
	H-L_{H_2O}-L_{CO_2} Line in $p-T$ space	282.92-294.00 4.5-494	-	61	Ref.2
CH_4-CO_2-H_2O	H-L_{H_2O}-L_{CO_2}-V Line in $p-T$ space	283.86-285.56 4.930-6.720	0.0517-0.1750 (y_{CH_4}, vapor phase)	3	[Seo et al., 2000]
		283.86-285.76 4.930-7.251	0.0596-0.2026 (y_{CH_4}, vapor phase)	4	[Seo and Lee, 2001]
		283.51-287.04 4.74-8.37	0.05-0.22 ($z^*_{CH_4}$, gas load)	18	[Bi et al., 2013]
		283.90-286.19 4.925-7.62	-	5	[Al Ghafri et al., 2014]
		284.15 5.81	0.059 ($z^*_{CH_4}$, gas load)	1	[Chapoy et al., 2015]
	H-L_{H_2O}-L_{CO_2} Surface in $p-T$ space	285.75-286.95 12.25-19.97	0.059 ($z^*_{CH_4}$, gas load)	2	[Chapoy et al., 2015]
		285.11-288.39 7.17-27.71	0.100-0.154 ($z^*_{CH_4}$, gas load)	7	This work

Table 2.2: Available experimental data for the CO_2-H_2O binary and CH_4-CO_2-H_2O ternary mixtures involving a CO_2-rich liquid phase. Ref.1: [Unruh and Katz, 1949, Robinson et al., 1971, Yoon and Lee, 1997, Fan and Guo, 1999, Seo et al., 2000, Seo and Lee, 2001, Mooijer-Van Den Heuvel et al., 2001, Ruffine et al., 2010, Bi et al., 2013], Ref.2: [Takenouchi and Kennedy, 1964, Ng and Robinson, 1985, Ohgaki et al., 1993, Nakano et al., 1998a, Fan and Guo, 1999, Mooijer-Van Den Heuvel et al., 2001, Ruffine et al., 2010, Chapoy et al., 2011, Alsiyabi et al., 2014].

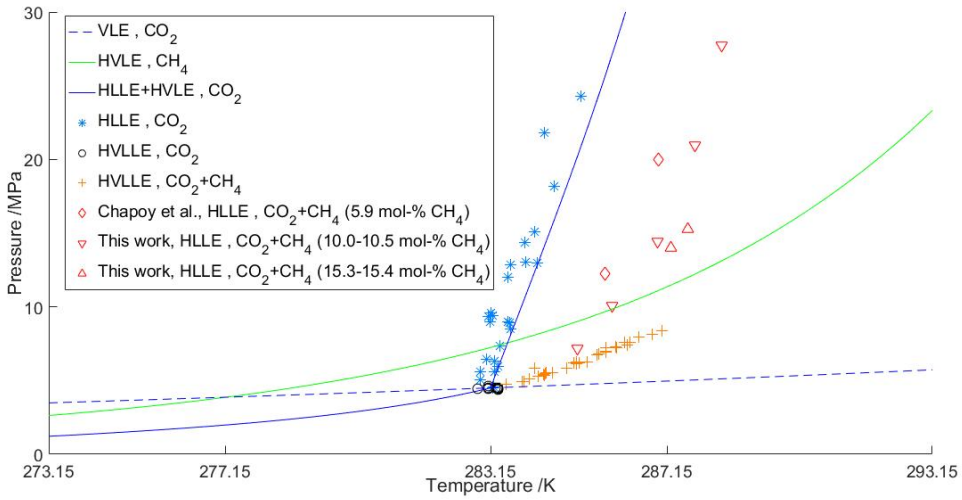

Figure 2.1: Available experimental data describing gas hydrate equilibria for the (CH_4)-CO_2-H_2O system in the presence of H-L_{H_2O}-L_{CO_2}-(V) phases below 30 MPa. HLLE: hydrate-liquid-liquid equilibrium; HVLE: hydrate-vapor-liquid equilibrium; HVLLE: hydrate-vapor-liquid-liquid equilibrium; VLE: vapor-liquid equilibrium. References are the one from Table 2.2, or see original figure in Legoix et al. [2017].

2.2 Experiments

2.2.1 Experimental apparatus

The phase equilibrium experiments were performed with the apparatus described by [Ruffine and Trusler, 2010], which was modified to accomodate a high-pressure stirrer (minimaster, Premex Reactor AG, Lengnau, Switzerland) (Figure 2.2). It consists of a cylindrical 316Ti variable-volume high-pressure cell with a 17-4PH stainless steel moving piston (Hand-Operated Pressure Generator with optical cell, SITEC-Sieber Engineering AG, Maur, Switzerland). The cell can be operated at pressures up to 60 MPa, and temperatures ranging between 253 and 473 K. The volume of the cell varies from 20.8 ($\pm$ 0.6) to 65.4 ($\pm$ 0.3) mL. Both ends of the cell are closed by a sapphire window. At the top of the cell, a ROLSI^{TM} sampler (Rapid On-Line Sampler-Injector, Armines CTP/MINES ParisTech, Fontainebleau, France) [Guilbot et al., 2000] was connected to a TCD-FID (Thermal Conductivity Detector-Flame Ionization Detector)-coupled GC-MS (Gas Chromatography-Mass Spectrometry) (7890A-5975C, Agilent, Santa Clara, CA, USA), allowing the withdrawal of an aliquot of a selected phase for compositional analysis. The GC-MS data were processed with the MSDChem software and the Chemstation integrator (Agilent, Santa Clara, CA, USA). To avoid condensation or partial vaporization of the sample, both the ROLSItm and the transfert line were heated up to 423 K with a thermal resistance controlled by a West 6100+ interface (ISE Inc., Cleveland, OH, USA). A high-pressure stirrer was connected at the bottom port of the cell to improve

the mixing and shorten the time needed to achieve thermodynamic equilibrium. The stirrer speed, set by a 24 V/DC motor, could be varied between 200 and 1500 rpm. A high-pressure metering pump (Optos, Eldex Laboratories Inc., Napa, CA, USA) was used to inject liquids into the cell at pressures of up to 52.5 MPa with an adjustable flow rate of 0.1-10.0 mL min-1. The thermal regulation was achieved using a compact circulator (ministat 230, Huber Kaltemaschinenbau AG, Offenburg, Germany) filled with a mixture of H_2O/EtOH (50/50 vol %).

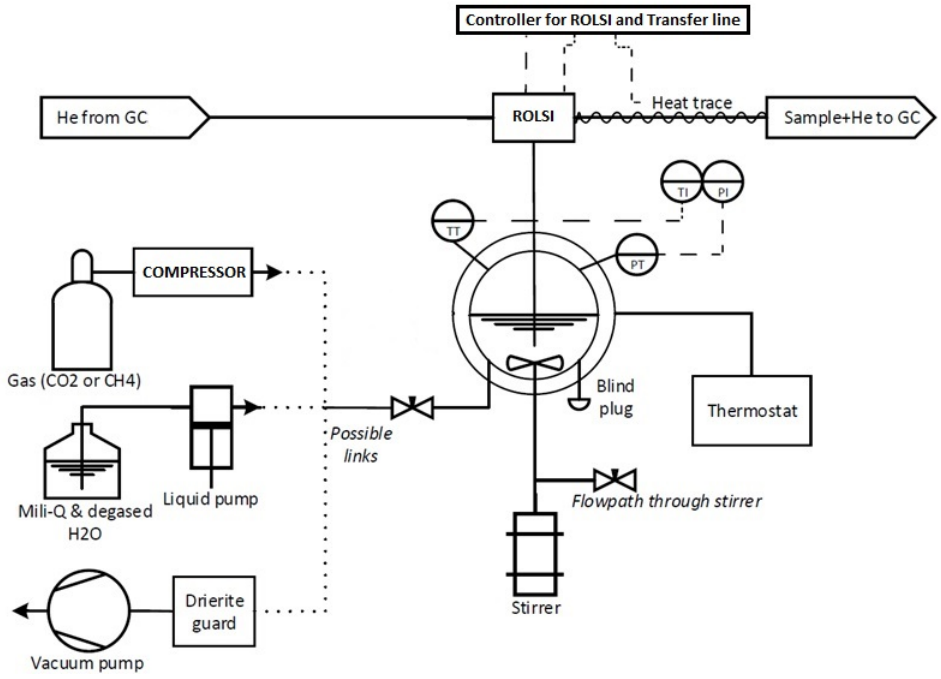

Figure 2.2: Sketch of the experimental set-up including the high-pressure cell, modified from Ruffine and Trusler [2010].

2.2.2 Materials

All gases – pure components or gas mixtures – were supplied by l'Air Liquide. CH_4 and CO_2 had a claimed purity of 99.99 mol %, while the standard mixture of CH_4-CO_2 had a certified composition of 10.04 ($\pm$ 0.20) mol % of CH_4. For all experiments requiring H_2O, MiliQ-H_2O with a resistivity of 18.2 MΩ cm was degassed prior the injection.

2.2.3 Experimental procedure

For VLE, CO_2 was injected first at the desired temperature, followed by the injection of CH_4 step-wise into the cell until reaching the desired final pressure. Equilibrium was reached quickly by using the stirrer. The composition of the liquid phase was analyzed with the GC.

For gas hydrate experiments, the temperature of the cell was set to 288.15 K and its volume to the maximum. A custom made CH_4-CO_2 gas mixture, obtained from pure CH_4 and CO_2, was used for Mixtures 1, 2, 3, 6, 7 and the standard mixture from L'Air Liquide for Mixture 4 and 5. The composition of the custom made mixture was determined by GC. The cell volume was then reduced to form a liquid phase by pressure increase. H_2O was injected afterwards and the temperature was set to 276.85 K to allow the formation of gas hydrates. An isochoric stepwise heating procedure [Tohidi et al., 2000] with a temperature increment of 0.5 K every 5 hours was applied to determine the hydrate dissociation conditions. The composition of the CO_2-rich liquid phase was measured by discrete sampling during gas hydrate formation and dissociation.

2.3 Results and discussion

2.3.1 CH_4-CO_2 binary system

Data at 288.15 and 283.15 K were used to validate the experimental procedure for the VLE study by comparison with those from [Arai et al., 1971] and [Kaminishi et al., 1968] (Table 2.3). Our data agree well with those of both research groups. For the isotherm at 283.15 K, our composition data at 8.08 MPa has a relative deviation from the one of [Kaminishi et al., 1968] by 2.1 %. Finally, the vapor pressures of pure CO_2 for all isotherms were compared to the correlation from [WebBook, 2017, Span and Wagner, 1996] (Table 2.3). Five isotherms were built from experiments performed at a temperature range of 274.15 to 290.15 K (Table 2.4, Figure 2.3) to complete the current database (Table 2.1). When comparing these data points to modelled isotherms [Kossel et al., 2013] based on the established algorithm of [Duan and Hu, 2004] which uses the Soave–Redlich–Kwong (SRK) equation of state (EoS), a good fit is obtained. This binary system has also been studied by [Vitu et al., 2007], using a group contribution approach and the Predictive PR78 EoS model including a temperature-dependent binary interaction parameter of 0.093–0.112.

In this work, a thermodynamic model was developed based on the SRK-EoS and applied to the system CH_4-CO_2. A dependent binary interaction parameter $k_{ij(CH_4-CO_2)} = 1.32 \times 10^3 \times T - 0.251$ was optimized over the temperature interval corresponding to the experimental bubble points between 274.15 and 290.15 K. A good agreement was also obtained for measurements outside of this temperature range (i.e., for the dew points and at 273.15, 293.4, and 301 K; Figure 2.3), demonstrating the predictive capability of the EoS. However, the present model does not reproduce the behavior of the system near the critical point with satisfactory accuracy. Thus, provided that the conditions of interest are not close to the critical point, a simple model based on a cubic EoS allows for a good description of the CH_4-CO_2 mixture at VLE at the temperature and pressure ranges encountered in most of the marine environment of interest for our study (i.e., CO_2-rich seeps and gas hydrate deposits on continental margins). This is convenient to implement, for example, into gas hydrate reservoir models where a more sophisticated EoS would increase computational time too much.

RD %	T /K	p /MPa	x_{CH_4}	Reference
-5.4 (x_{CH_4})	288.15	7.63	0.1097	This work
		7.65	0.1160	[Arai et al., 1971]
-2.1 (x_{CH_4})	283.15	8.08	0.1732	This work
		8.08	0.177	[Kaminishi et al., 1968]
1.7 (p)	274.15	3.64	0	This work
		3.58	0	[WebBook, 2017, Span and Wagner, 1996]
1.8 (p)	277.15	3.94	0	This work
		3.87	0	[WebBook, 2017, Span and Wagner, 1996]
2.2 (p)	283.15	4.60	0	This work
		4.50	0	[WebBook, 2017, Span and Wagner, 1996]
1.6 (p)	288.15	5.17	0	This work
		5.09	0	[WebBook, 2017, Span and Wagner, 1996]
1.9 (p)	290.15	5.44	0	This work
		5.34	0	[WebBook, 2017, Span and Wagner, 1996]

Table 2.3: Relative deviation (RD) of solubility data (mole fractions) and vapor pressures (of pure CO_2 with x_{CH_4}= 0) between this work and literature values.

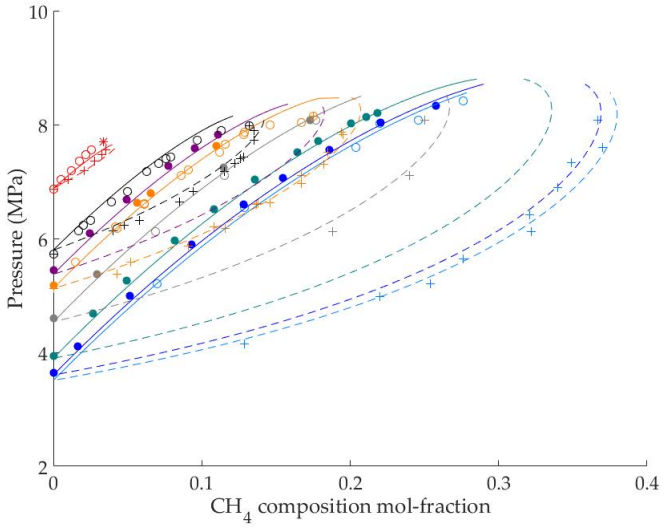

Figure 2.3: Liquid and vapor phase compositions of the CH_4-CO_2 mixture between 273.15 and 301 K along eight isoherms: T = 273.15 K (cyan); T = 274.15 K (blue); T = 277.15K (green); T = 283.15 K (grey); T = 288.15 K (288.5 for Xu et al. [1992] data) (orange); T = 290.15 K (purple); T = 283.4 K (black); T = 301 K (red). Experimental bubble points x_{CH_4} from this work (filled dot), experimental bubble points x_{CH_4} from other authors (empty dot), experimental dew points y_{CH_4} from other authors (cross), critical point (star) [Kaminishi et al., 1968, Arai et al., 1971, Xu et al., 1992]. Modelling of the bubble lines (solid-lines) and the dew lines (dotted-lines) is based on the SRK-EoS.

2.3.2 CH_4-CO_2-H_2O ternary system

Seven gas hydrate dissociation points delimiting the HLLE were measured for CH_4 mole fractions of 0.1–0.105 and 0.153–0.154 of the initial gas mixture (Table 2.5).

T /K	p /MPa	x_{CH_4}	T /K	p /MPa	x_{CH_4}
274.15	3.64	0	277.15	8.02	0.2005
274.15	4.11	0.0166	277.15	8.13	0.2107
274.15	4.99	0.0518	277.15	8.20	0.2185
274.15	5.90	0.0929	283.15	4.60	0
274.15	6.60	0.1284	283.15	5.37	0.0293
274.15	7.06	0.1545	283.15	7.24	0.1145
274.15	7.56	0.186	283.15	8.08	0.1732
274.15	8.04	0.2206	288.15	5.17	0
274.15	8.33	0.2577	288.15	6.62	0.0566
277.15	3.94	0	288.15	6.80	0.0654
277.15	4.69	0.0266	288.15	7.63	0.1097
277.15	5.26	0.0495	290.15	5.44	0
277.15	5.97	0.0817	290.15	6.09	0.0243
277.15	6.51	0.1083	290.15	6.69	0.0496
277.15	7.04	0.1358	290.15	7.27	0.0772
277.15	7.51	0.1643	290.15	7.59	0.0951
277.15	7.71	0.1786	290.15	7.82	0.1107

Table 2.4: Relative deviation (RD) of solubility data (mole fractions) and vapor pressures (of pure CO_2 with x_{CH_4}=0) between this work and literature values.

The experimental data were compared with calculations of the CSMGem program [Sloan and Koh, 2008]. The program systematically underestimated the gas hydrate dissociation pressure, with absolute deviations up to 7 MPa compared to our experimental data (Table 2.5). The p–T curve of gas hydrate dissociation of pure CO_2 is strongly dependent on the temperature, showing a very steep slope. Likewise, the CH_4-CO_2 mixed gas hydrate dissociation appears to be strongly dependent on the temperature when no vapor phase is present (Figure 2.1).

		Mix. 1	**Mix. 2**	**Mix. 3**	**Mix. 4**	**Mix. 5**	**Mix. 6**	**Mix. 7**
Composition Mole fraction	$z^*_{CH_4}$	0.105	0.105	0.105	0.100	0.100	0.153	0.154
	z_{CH_4}	0.031	0.043	0.038	0.029	0.052	0.103	0.090
	z_{CO_2}	0.266	0.369	0.328	0.263	0.467	0.572	0.492
	z_{H_2O}	0.703	0.588	0.634	0.708	0.481	0.325	0.418
	$x^*_{CH_4}$ without gas hydrate	0.102 (0.088)	0.110 (0.108)	0.111 (0.108)	0.106 (0.105)	0.106 (0.102)	0.154 (0.154)	0.155 (0.157)
	$x^*_{CH_4}$ with gas hydrate	0.095 (0.060)	0.102 (0.072)	0.106 (0.063)	0.092 (0.097)	0.089 (0.073)	0.152 (0.138)	0.149 (0.133)
Gas hydrate dissociation	T /K	285.11	285.90	286.93	287.77	288.39	287.24	287.61
	p /MPa	7.17 (6.33)	10.07 (7.52)	14.45 (11.73)	20.94 (16.54)	27.71 (20.87)	13.99 (10.72)	15.25 12.08

Table 2.5: Experimental data of H-L_{H_2O}-L_{CO_2} equilibria (HLLE) for the CH_4-CO_2-H_2O ternary system. Values inside brackets are CSMGem [Sloan and Koh, 2008] model values applied on the system.

The CH_4-to-CO_2 concentration ratio (i.e., without considering H_2O composition, $x^*_{CH_4}$) in the CO_2-rich liquid phase decreased when gas hydrate was formed. In order to understand if this change is caused by hydrate formation or simply a p–T effect, the CSMGem program [Sloan and Koh, 2008] is here employed on the data

(Table 2.5). Considering a case study with Mixture 2 at 288.15 K and 10 MPa, CSMGem predicts an aqueous and a CO_2-rich liquid phase, as is visually observed in our experiments (Table 2.5). CSMGem computes that CH_4 amounts to only 2 % of the dissolved gases in the aqueous phase; i.e., $x^*_{CH_4}/(x^*_{CH_4} + x^*_{CO_2})$. Indeed, the CO_2 is more soluble than CH_4 in liquid H_2O, and hence CH_4 is enriched in the CO_2-rich liquid phase when H_2O is pumped into the CH_4-CO_2 mixture (Table 2.5, $x^*_{CH_4}$ without gas hydrate). When the temperature is decreased from 288.15 to 276.85 K, mixed gas hydrates containing a CH_4/CO_2 ratio of 21/79 should form (CSMGem), thereby reducing the CH_4-to-CO_2 ratio in the CO_2-rich liquid phase, as it was observed in the experiments.

The formation of gas hydrate was visually observed, relatively rapidly after the start of the stirring. Gas hydrates accumulated rapidly in the cell, and the stirrer was then switched off to prevent any damage (Figure 2.4). It was visually observed that the gas hydrate formed first at the H_2O phase interface and then grew in the H_2O phase before spreading across the entire surface of the sapphire window, blocking the view (Figure 2.4).

The time of incipient gas hydrate formation and the stirring conditions are summarized in Table 2.6 with no evident correlation between time of gas hydrate formation start and initial setup (composition, pressure, stirring speed).

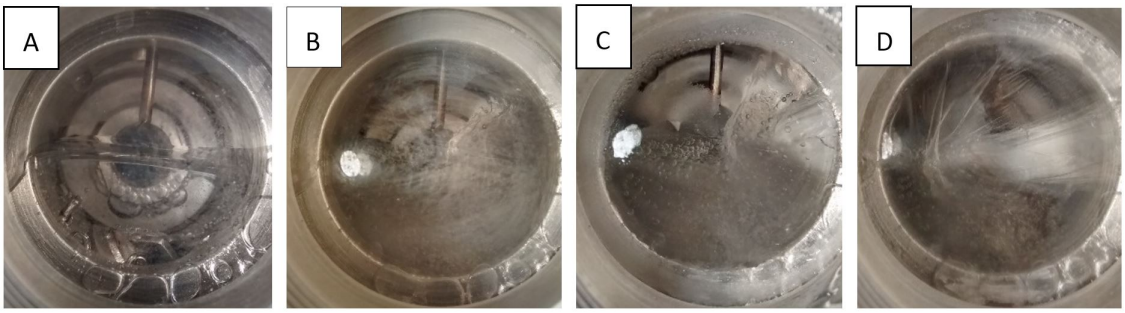

Figure 2.4: Photos showing different steps during gas hydrate formation and dissociation with Mixture 2. From left to right: (A) after H_2O injection (L_{H_2O}); (B) just after incipent formation start (H-L_{H_2O}); (C) ca. 40 min after formation start (H-L_{H_2O}-L_{CO_2}); (D) ca. 170 min after formation start (H-L_{H_2O}-L_{CO_2}).

	Mix. 1	**Mix. 2**	**Mix. 3**	**Mix. 4**	**Mix. 5**	**Mix. 6**	**Mix. 7**
Stirrer rotation speed /rpm	1000	1000	1000	100	100	700	700
Time of incipient formation /min	18	14	33	18	10	10	56

Table 2.6: Incipient gas hydrate time of formation on the CH_4-CO_2-H_2O ternary system.

2.4 Conclusions

Mixtures of CH_4-CO_2 and CH_4-CO_2-H_2O involving a CO_2-rich liquid phase are investigated under $p-T$ conditions typical for marine environments, such as CO_2-rich

seeps of volcanic origin and gas hydrate deposits suitable for gas production via CO_2 injection.

VLE data were measured and modelled with a simple Soave-Redlich-Kwong EoS for the CH_4-CO_2 system, at conditions between the freezing point of H_2O and the critical point of CO_2. This model enables, for example, the accurate prediction of how much CH_4 is retained in the CO_2-rich liquid phase. Subseqently, a set of data on gas hydrate dissociation was measured to evaluate the phase behavior of the CH_4-CO_2 hydrate containing a CO_2-rich liquid phase without any vapor phase. The measurements collected in this newly explored phase region (CH_4-CO_2-H_2O HLLE) indicate that the added CH_4 increases the stability of the resulting gas hydrates, which is the opposite trend compared to the region where a vapor phase is stable. Moreover, the formation of gas hydrates in this system consequently reduces the CH_4 in the coexisting CO_2-rich liquid phase. For a CH_4 production scenario under the investigated $p-T$ conditions, this study indicates that mixed CH_4-CO_2 hydrates are more stable than pure CO_2 hydrates, thus allowing the storage of CO_2 in mixed gas hydrates under an extended temperature range for a given pressure. In addition, a more accurate model for calculating the CH_4 content in the dense CO_2 liquid phase is under development, which will improve the mass balancing of reservoir simulations of CH_4 hydrate production via CO_2 injection and also improve our understanding of the phase behavior of natural liquid CO_2 seeps, where CH_4 is a common admixture.

The CH_4-CO_2-H_2O system still needs to be further investigated in the phase region presented here, particularly in the HLLE domain at the lower and upper end of CH_4 concentrations allowing for a CO_2-rich liquid phase. Indeed, already small additions of CH_4 drastically affect the gas hydrate stability pressure, whereas high concentrations would provide more insights into the border of the HLLE region.

Acknowledgements

This work was supported by the SUGAR project, funded by the German Ministry of Research (Grant No. 03G0856A), and the “Hydrate as Geohazards” project from the Unité des Geosciences Marines (IFREMER).

Bibliography

S. Z. S. Al Ghafri, E. Forte, G. C. Maitland, J. J. Rodriguez-Henríquez, and J. P. M. Trusler. Experimental and Modeling Study of the Phase Behavior of (Methane + CO_2 + Water) Mixtures. *The Journal of Physical Chemistry B*, 118(49):14461–14478, 2014. doi: 10.1021/jp509678g.

I. Alsiyabi, A. Chapoy, and B. Tohidi. Effect of common impurities on the hydrate stability of carbon dioxide rich systems. *Proceedings of the 8th International Conference on gas Hydrates (ICGH8-2014)*, 2014.

Y. Arai, G. ichi Kaminishi, and S. Saito. The experimental determination of the P-V-T-X relations for the carbon dioxide-nitrogen and the carbon dioxide-methane systems. *Journal of Chemical Engineering of Japan*, 4(2):113–122, 1971. doi: 10.1252/jcej.4.113.

Y. Bi, T. Yang, and K. Guo. Determination of the upper-quadruple-phase equilibrium region for carbon dioxide and methane mixed gas hydrates. *Journal of Petroleum Science and Engineering*, 101:62–67, 2013. doi: 10.1016/j.petrol.2012.11.019.

B. Bian, Y. Wang, J. Shi, E. Zhao, and B. C. Lu. Simultaneous determination of vapor-liquid equilibrium and molar volumes for coexisting phases up to the critical temperature with a static method. *Fluid Phase Equilibria*, 90(1):177–187, 1993. doi: 10.1016/0378-3812(93)85012-B.

M. C. Boiron, M. Cathelineau, G. Ruggieri, A. Jeanningros, G. Gianelli, and D. A. Banks. Active contact metamorphism and CO_2-CH_4 fluid production in the Larderello geothermal field (Italy) at depths between 2.3 and 4 km. *Chemical Geology*, 237(3-4):303–328, 2007. doi: 10.1016/j.chemgeo.2006.06.028.

R. Boswell, D. Schoderbek, T. S. Collett, S. Ohtsuki, M. White, and B. J. Anderson. The Ignik Sikumi field experiment, Alaska North Slope: Design, operations, and implications for CO_2-CH_4 exchange in gas hydrate reservoirs. *Energy and Fuels*, 31(1):140–153, 2017. doi: 10.1021/acs.energyfuels.6b01909.

A. Chapoy, R. Burgass, B. Tohidi, J. M. Austell, and C. Eickhoff. Effect of Common Impurities on the Phase Behavior of Carbon-Dioxide-Rich Systems: Minimizing the Risk of Hydrate Formation and Two-Phase Flow. *SPE Journal*, 16(04):921–930, 2011. doi: 10.2118/123778-PA.

A. Chapoy, R. Burgass, B. Tohidi, and I. Alsiyabi. Hydrate and phase behavior modeling in CO_2-rich pipelines. *Journal of Chemical and Engineering Data*, 60(2): 447–463, 2015. doi: 10.1021/je500834t.

C. Deusner, N. Bigalke, E. Kossel, and M. Haeckel. Methane production from gas hydrate deposits through injection of supercritical CO_2. *Energies*, 5(7):2112–2140, 2012. doi: 10.3390/en5072112.

Z. Duan and J. Hu. A new cubic equation of state and its applications to the modeling of vapor-liquid equilibria and volumetric properties of natural fluids. *Geochimica et Cosmochimica Acta*, 68(14):2997–3009, 2004. doi: 10.1016/j.gca.2003.11.034.

T. Ebinuma. Method for dumping and disposing of carbon dioxide gas and apparatus therefor, Nov. 16 1993. US Patent 5,261,490.

S. S. Fan and T. M. Guo. Hydrate formation of CO_2-rich binary and quaternary gas mixtures in aqueous sodium chloride solutions. *Journal of Chemical and Engineering Data*, 44(4):829–832, 1999. doi: 10.1021/je990011b.

P. Guilbot, A. Valtz, H. Legendre, and D. Richon. Rapid on-line sampler-injector: A reliable tool for HT-HP sampling and on-line GC analysis. *Analusis*, 28(5): 426–431, 2000. doi: 10.1051/analusis:2000128.

F. Inagaki, M. M. M. Kuypers, U. Tsunogai, J.-i. Ishibashi, K.-i. Nakamura, T. Treude, S. Ohkubo, M. Nakaseama, K. Gena, H. Chiba, H. Hirayama, T. Nunoura, K. Takai, B. B. Jorgensen, K. Horikoshi, and A. Boetius. Microbial community in a sediment-hosted CO_2 lake of the southern Okinawa Trough hydrothermal system. *Proceedings of the National Academy of Sciences*, 103(38): 14164–14169, 2006. doi: 10.1073/pnas.0606083103.

G. Kaminishi and T. Toriumi. Gas-liquid equilibrium under high pressures. VI. Vapor-liquid phase equilibrium in the CO_2-H_2, CO_2-N_2, and CO_2-O_2 systems. *Kogyo Kagaku Zasshi*, 69(2):175–178, 1966.

G.-I. Kaminishi, Y. Arai, S. Saito, and S. Maeda. Vapor-liquid equilibria for binary and ternary systems containing carbon dioxide. *Journal of Chemical Engineering of Japan*, 1(2):109–116, 1968. doi: 10.1252/jcej.1.109.

P. Kastanidis, G. E. Romanos, A. K. Stubos, I. G. Economou, and I. N. Tsimpanogiannis. Two-and three-phase equilibrium experimental measurements for the ternary CH_4+ CO_2+ H_2O mixture. *Fluid Phase Equilibria*, 451:96–105, 2017. doi: 10.1016/j.fluid.2017.08.0020378-3812.

U. Konno, U. Tsunogai, F. Nakagawa, M. Nakaseama, J.-i. Ishibashi, T. Nunoura, and K.-i. Nakamura. Liquid CO_2 venting on the seafloor: Yonaguni Knoll IV hydrothermal system, Okinawa Trough. *Geophysical Research Letters*, 33(16), 2006. doi: 10.1029/2006GL026115.

E. Kossel, N. K. Bigalke, E. Pinero, and M. Haeckel. The SUGAR Toolbox: a library of numerical algorithms and data for modelling of gas hydrate systems and marine environments. 2013.

L. N. Legoix, L. Ruffine, J.-P. Donval, and M. Haeckel. Phase Equilibria of the CH_4-CO_2 Binary and the CH_4-CO_2-H_2O Ternary Mixtures in the Presence of a CO_2-Rich Liquid Phase. *Energies*, 10(12):2034, 2017. doi: 10.3390/en10122034.

J. L. Lewicki, J. Birkholzer, and C.-F. Tsang. Natural and industrial analogues for leakage of CO_2 from storage reservoirs: Identification of features, events, and processes and lessons learned. *Environmental Geology*, 52(3):457–467, 2007. doi: 10.1007/s00254-006-0479-7.

J. Lupton, D. Butterfield, M. Lilley, L. Evans, K. I. Nakamura, W. Chadwick, J. Resing, R. Embley, E. Olson, G. Proskurowski, E. Baker, C. De Ronde, K. Roe, R. Greene, G. Lebon, and C. Young. Submarine venting of liquid carbon dioxide on a Mariana Arc volcano. *Geochemistry, Geophysics, Geosystems*, 7(8), 2006. doi: 10.1029/2005GC001152.

M. M. Mooijer-Van Den Heuvel, R. Witteman, and C. J. Peters. Phase behaviour of gas hydrates of carbon dioxide in the presence of tetrahydropyran, cyclobutanone, cyclohexane and methylcyclohexane. In *Fluid Phase Equilibria*, volume 182, pages 97–110, 2001. doi: 10.1016/S0378-3812(01)00384-3.

S. Nakano, M. Moritoki, and K. Ohgaki. High-Pressure Phase Equilibrium and Raman Microprobe Spectroscopic Studies on the CO_2 Hydrate System. *Journal of Chemical & Engineering Data*, 43(5):807–810, 1998a. doi: 10.1021/je9800555.

S. Nakano, K. Yamamoto, and K. Ohgaki. Natural gas exploitation by carbon dioxide from gas hydrate fields—high-pressure phase equilibrium for an ethane hydrate system. *Proceedings of the Institution of Mechanical Engineers, Part A: Journal of Power and Energy*, 212(3):159–163, 1998b. doi: 10.1243/0957650981536826.

H.-J. Ng and D. B. Robinson. Hydrate formation in systems containing methane, ethane, propane, carbon dioxide or hydrogen sulfide in the presence of methanol. *Fluid Phase Equilibria*, 21(1-2):145–155, 1985. doi: 10.1016/0378-3812(85)90065-2.

K. Ohgaki, Y. Makihara, and K. Takano. Formation of CO_2 hydrate in pure and sea waters. *Journal of chemical engineering of Japan*, 26(5):558–564, 1993. doi: 10.1252/jcej.26.558.

M. Ota, K. Morohashi, Y. Abe, M. Watanabe, R. Lee Smith, and H. Inomata. Replacement of CH_4 in the hydrate by use of liquid CO_2. *Energy Conversion and Management*, 46(11-12):1680–1691, 2005. doi: 10.1016/j.enconman.2004.10.002.

B. E. Poling and J. M. Prausnitz. *The Properties of Gases and Liquids*, volume 5. 2001. doi: 10.1021/ja0048634.

D. Robinson, B. Metha, et al. Hydrates in the propane carbon dioxide-water system. *Journal of Canadian Petroleum Technology*, 10(01), 1971. doi: 10.2118/71-01-04.

L. Ruffine and J. Trusler. Phase behaviour of mixed-gas hydrate systems containing carbon dioxide. *The Journal of Chemical Thermodynamics*, 42(5):605–611, 2010. doi: 10.1016/j.jct.2009.11.019.

L. Ruffine, J. P. Donval, J. L. Charlou, A. Cremière, and B. H. Zehnder. Experimental study of gas hydrate formation and destabilisation using a novel high-pressure apparatus. *Marine and Petroleum Geology*, 27(6):1157–1165, 2010. doi: 10.1016/j.marpetgeo.2010.03.002.

H. Sakai, T. Gamo, E. Kim, M. Tsutsumi, T. Tanaka, J. Ishibashi, H. Wakita, M. Yamano, and T. Oomori. Venting of Carbon Dioxide-Rich Fluid and Hydrate Formation in Mid-Okinawa Trough Backarc Basin. *Science*, 248(4959):1093–1096, 1990. doi: 10.1126/science.248.4959.1093.

J. M. Schicks, E. Spangenberg, R. Giese, B. Steinhauer, J. Klump, and M. Luzi. New approaches for the production of hydrocarbons from hydrate bearing sediments. *Energies*, 4(1):151–172, 2011. doi: 10.3390/en4010151.

Y. T. Seo and H. Lee. Multiple-phase hydrate equilibria of the ternary carbon dioxide, methane, and water mixtures. *Journal of Physical Chemistry B*, 105(41): 10084–10090, 2001. doi: 10.1021/jp011095+.

Y.-T. Seo, S.-P. Kang, H. Lee, C.-S. Lee, and W.-M. Sung. Hydrate phase equilibria for gas mixtures containing carbon dioxide: A proof-of-concept to carbon dioxide recovery from multicomponent gas stream. *Korean Journal of Chemical Engineering*, 17(6):659–667, 2000. doi: 10.1007/BF02699114.

E. D. Sloan and C. A. Koh. Clathrate Hydrates of Natural Gases,. *AIChE Journal*, 47(3):693–704, 2008.

R. Span and W. Wagner. A new equation of state for carbon dioxide covering the fluid region from the triple-point temperature to 1100 K at pressures up to 800 MPa. *Journal of Physical and Chemical Reference Data*, 25(6):1509–1596, 1996. doi: 10.1063/1.555991.

S. Takenouchi and G. C. Kennedy. The binary system H_2O-CO_2 at high temperatures and pressures. *American Journal of Science*, 262(9):1055–1074, 1964. doi: 10.2475/ajs.262.9.1055.

B. Tohidi, R. W. Burgass, A. Danesh, K. K. Ostergaard, and A. C. Todd. Improving the accuracy of gas hydrate dissociation point measurements. *Gas Hydrates: Challenges for the Future*, 912:924–931, 2000. doi: 10.1111/j.1749-6632.2000.tb06846.x.

C. H. Unruh and D. L. Katz. Gas Hydrates of Carbon Dioxide-Methane Mixtures. *Journal of Petroleum Technology*, 1(4):83–86, 1949. doi: 10.2118/949983-G.

P. H. Van Konynenburg and R. L. Scott. Critical Lines and Phase Equilibria in Binary Van Der Waals Mixtures. *Philosophical Transactions of the Royal Society A: Mathematical, Physical and Engineering Sciences*, 298(1442):495–540, 1980. doi: 10.1098/rsta.1980.0266.

S. Vitu, J. N. Jaubert, J. Pauly, J. L. Daridon, and D. Barth. Bubble and dew points of carbon dioxide + a five-component synthetic mixture: Experimental data and modeling with the PPR78 model. *Journal of Chemical and Engineering Data*, 52 (5):1851–1855, 2007. doi: 10.1021/je7001978.

N. C. WebBook. Available online: Webbook.nist.gov / chemistry / fluid (accessed on 10 september 2017). SRD 69, 2017.

N. Xu, J. Yao, Y. Wang, J. Shi, and B. C. Lu. Vapor-liquid equilibria of five binary systems containing R-22. *Fluid Phase Equilibria*, 69(C):261–270, 1991. doi: 10.1016/0378-3812(91)90038-9.

N. Xu, J. Dong, Y. Wang, and J. Shi. High pressure vapor liquid equilibria at 293 K for systems containing nitrogen, methane and carbon dioxide. *Fluid Phase Equilibria*, 81(C):175–186, 1992. doi: 10.1016/0378-3812(92)85150-7.

J. H. Yoon and H. Lee. Clathrate Phase Equilibria for the Water-Phenol-Carbon Dioxide System. *AIChE Journal*, 43(7):1884–1893, 1997. doi: 10.1002/aic.690430723.

Chapter 3

Experimental study of mixed gas hydrates from gas feed containing CH_4, CO_2 and N_2: phase equilibrium in presence of excess water and gas exchange

Article published in *Energies* (2018)
L.N. Legoix, L. Ruffine, C. Deusner, M. Haeckel
doi: 10.3390/en11081984

Abstract This article presents gas hydrate experimental measurements for mixtures containing methane (CH_4), carbon dioxide (CO_2) and nitrogen (N_2) with the aim to better understand the impact of water (H_2O) on the phase equilibrium. Some of these phase equilibrium experiments were carried out with a very high water-to-gas ratio that shifts the gas hydrate dissociation points to higher pressures. This is due to the significantly different solubilities of the different guest molecules in liquid H_2O. A second experiment focused on CH_4-CO_2 exchange between the hydrate and the vapor phases at moderate pressures. The results show a high retention of CO_2 in the gas hydrate phase with small pressure variations within first hours. However, for our system containing 10.2 g of H_2O full conversion of the CH_4 hydrate grains to CO_2 hydrate is estimated to require 40 days. This delay is attributed to the shrinking core effect, where initially an outer layer of CO_2-rich hydrate is formed that effectively slows down the further gas exchange between the vapor phase and the inner core of the CH_4-rich hydrate grain.

Keywords gas hydrates, CH_4, CO_2, N_2, high-pressure experiments, phase equilibrium, gas exchange

3.1 Introduction

Clathrate hydrates are crystallographic structures made up of cage-forming water molecules containing small guest molecules (e.g., [Sloan Jr and Koh, 2007]). In the environment, these are typically natural gas compounds and as a consequence gas hydrates are encountered below the permafrost in polar regions, and in marine sediments of all active and passive continental margins (e.g., [Claypool and Kvenvolden,

1983, Kvenvolden, 1988, Pinero et al., 2013]). While CH_4 is the most notorious gas molecule being the dominant natural gas, also larger natural gas compounds with specific steric hindrance like ethane, propane and isobutane can be enclathrated into the water lattice (e.g., [Kida et al., 2006, Lu et al., 2007, Bourry et al., 2009]). Amongst the notable physicochemical properties of gas hydrates are their high selectivity in enclathrating guest molecules and the high storage capacity of those gases (e.g., [Gudmundsson et al., Sloan Jr, 2003, Sloan Jr and Koh, 2007, Eslamimanesh et al., 2012]).

In the first part of the presented work, mixed gas hydrates formed from CO_2, N_2 and CH_4 gases are studied, providing thermodynamic data on systems relevant to CO_2 storage in the gas hydrate phase, potentially coupled to CH_4 production from natural CH_4 hydrates. In the marine environment depleted oil and gas reservoirs, saline aquifers or deep-sea sediments are foreseen as geological units for the storage of the anthropogenic CO_2 emitted at industrial point sources [Lackner, 2003]. In this context, the formation of CO_2 hydrates has been discussed as natural seal that may form under suitable ambient pressure and temperature ($p-T$) conditions at the interface between the stored liquid CO_2 and the ocean water [Ohgaki et al., 1993] or sedimentary porewater [House et al., 2006]. Meanwhile, interest in using natural CH_4 hydrates as an energy resource is growing and several production field tests have been conducted in recent years. Both processes, sub-surface carbon storage and gas hydrate exploitation, can be combined. For example, the exposure of CH_4 hydrates to a CO_2:N_2 (23:77 mol/mol) gas mixture has been studied in laboratory experiments by Park et al. [2006], and this mixture was also used in the Ignik Sikumi CH_4 production field test below the Alaskan permafrost [Schoderbek et al., 2013, Boswell et al., 2016]. N_2 acts as a carrier gas and its admixture to CO_2 avoids technical and safety problems involved in using a dense liquid CO_2 phase. This mixture is also representative for flue gas emitted by power plants: exhaust gases produced by oxy-fuel and partial oxidation processes exceeds 40 mol-% CO_2, but flue gas from combustion power plants or industrial furnaces usually contains only 4-27 mol-% CO_2 [Car et al., 2008], mixed with trace of other gases, such as (O_2, H_2S, NO_X), while the dominant component is N_2 [Linga et al., 2007].

CO_2-N_2-CH_4 gas streams injected in water can lead to the occurrence of a large variety of phase equilibria depending on the $p-T$ conditions and the molar composition of the system, such as Vapor-Liquid Equilibrium (VLE), Hydrate-Vapor-Liquid Equilibrium (HVLE), Hydrate-Liquid-Liquid-Vapor Equilibrium (HLLVE). Accordingly, it is clearly important to investigate phase equilibrium thermodynamics of gas mixtures made of CH_4, CO_2 and N_2 at $p-T$ conditions relevant to gas hydrate formation. The N_2-CH_4 system was already reviewed and studied by Duan and Hu [2004] and the vapor-liquid equilibrium on the binary CO_2-N_2 has already been investigated and recently reviewed with addition of new data [Fandiño et al., 2015, Westman et al., 2016]. Moreover, CO_2 is more soluble in an aqueous phase than CH_4 and N_2 under ambient temperature conditions, which shows the importance to consider the water phase proportion in the system.

In our work, a set of experiments provides HVLE thermodynamic data of the

CH_4-CO_2-H_2O, CO_2-N_2-H_2O and CH_4-CO_2-N_2-H_2O systems. While the CO_2-CH_4-H_2O system has been investigated and summarized by Kastanidis et al. [2017], data collected for the two other systems are presented here in Tables 3.1 and 3.2. The collected data are in accordance and the injected water proportion from other works is always considered as low, with no impact on gas composition due to dissolution differences between gases. Sun et al. [2017] flushed the gas several times at equilibrium with liquid H_2O before starting the gas hydrate formation, in order to have the vapor phase at the dissolution point similar to the gas feed. Thus, in this work the feed gas is systematically considered as the gas composition at the gas hydrate dissociation point, as in the work from other authors (Table 3.1 and 3.2). The second part of our work presents experimental results of gas exchange between the vapor and the gas hydrate phase, with CH_4 and CO_2 gases. Several laboratory studies of gas exchange within a gas hydrate phase were performed, especially for CH_4-CO_2 exchange using different fluid phases, porous media and additives, reviewed by Deusner et al. [2012], Komatsu et al. [2013]. Here, the aim was to investigate the phenomena that occurs when a CH_4 hydrate is coexisting with a CO_2 vapor phase outside its initial stability zone, taking in consideration the slow evolution of gas exchange due to solid-state diffusion.

3.2 Experiments

3.2.1 Experimental setups

The experimental apparatus consists of a compact high-pressure cell (designed by the Service Ingénierie et Instrumentation Marine (SIIM), IFREMER, Plouzané, France) (Figure 3.1) made of Titanium TA6V, operating at temperatures between 263 and 373 K, and for pressure up to 30 MPa. A three-port valve allows connecting the cell to a pressure transducer ($\pm$ 0.01 MPa) Serie 23 SY (Keller, Winterthur, Switzerland), together with either a vacuum pump or a fluid injection system. To quickly establish equilibrium conditions, a magnetic stirrer is mixing the solution. The cell is immerged in a thermal bath regulated by a temperature controller ECO Silver RE 12 (Lauda, Lauda-Königshofen, Germany) and monitored by a K-Type thermocouple ($\pm$ 0.4 K). A high-pressure liquid metering pump Optos (Eldex Laboratories Inc., Napa, CA, USA) is used to inject precise amounts of water into the cell. The total volume of the cell, including the magnetic stirrer and the connected pressure transducer, is 51.8 ($\pm$ 0.1) mL. This volume was determined by three injections of 2-propanol pressurized up to 9.8 MPa at a fixed temperature of 313.35 K following the procedure described by Ruffine and Trusler [2010]. The mass of the injected liquid was measured by weighing; dividing by the fluid density applying the model of Zúñiga-Moreno and Galicia-Luna [2002] gave the volume of the cell. The apparatus employed for the gas replacement experiment is a high-pressure variable-volume view cell, with a volume set to 26.9 mL. A detailed description of this apparatus can be found elsewhere [Ruffine et al., 2010, Legoix et al., 2017].

Reference	T /K p /MPa	CO_2 mole fraction	Number of data points
[Fan and Guo, 1999]	273.1-280.2 1.22-3.09	$z^*_{CO_2}$ = 0.9099-0.9652	9
[Olseni et al., 1999]	273.4-281.9 1.986-9.550	$y^*_{CO_2}$ = 0.1620-0.7189	15
[Seo et al., 2000, Kang et al., 2001]	272.85-284.25 1.565-24.12	$z^*_{CO_2}$ = 0.0663-0.9659	28
[Linga et al., 2007]	273.7 7.7	$z^*_{CO_2}$ = 0.169 $y^*_{CO_2}$ = 0.139	1
[Bruusgaard et al., 2008]	275.3-283.1 1.6-22.4	$z^*_{CO_2}$ = 0.21-0.80 $y^*_{CO_2}$ = 0.162-0.787	24
[Herri et al., 2011]	273.4-281.1 5.30-6.60	$y^*_{CO_2}$ = 0.16-0.59	16
[Kim et al., 2011]	276.88-285.41 5.0-20.0	$z^*_{CO_2}$ = 0.841-0.906	16
[Belandria et al.]	273.6-281.7 2.032-17.628	y_{CO_2} = 0.127-0.747	35
[Sfaxi et al., 2012]	278.1-285.3 4.16-29.92	$z^*_{CO_2}$ = 0.271-0.812	9
[Lee et al., 2014]	275.0-280.8 8.23-24.51	$z^*_{CO_2}$ = 0.1-0.2	17
[Sun et al., 2015]	273.4-278.4 5.28-17.53	$z^*_{CO_2}$ = 0.101-0.251	17
[Sadeq et al., 2017]	275.75-284.45 5-20	$z^*_{CO_2}$ = 0.26-0.36	10
[Chazallon and Pirim, 2018]	270.5-278.3 -	$z^*_{CO_2}$ = 0.01-0.47	9
This work	276.06-280.97 9.762-20.583	$z^*_{CO_2}$ = 0.2317	4

Table 3.1: Overview of HVLE experimental data for the ternary system CO_2-N_2-H_2O

3.2.2 Materials

All gases were supplied by L'Air Liquide. When used as single gas, CH_4, CO_2 and N_2 had a claimed purity of 0.99995 by mole content. Two binary gas mixtures, CO_2-N_2 and CO_2-CH_4, were used in this study with a reported composition of 0.2317 ($\pm$ 0.46) and 0.8996 ($\pm$ 0.10) mol-% of CO_2, respectively. Deionized water with a resistivity of 18.2 MΩ cm was degassed by boiling before using it.

3.2.3 Experimental Procedures

For the measurements of dissociation points, the gas composition was analyzed with a gas chromatograph GC-MS 7890A-5975C (Agilent Technology, Santa Clara, CA, USA) before injecting the deionized water. A Flame Ionization Detector (FID) was used to quantify CH_4, whereas N_2 and CO_2 were measured with a Thermal Conductivity Detector (TCD). When needed, a gas booster DLE 5-15 (Maximator GmbH, Nordhausen, Germany) was used to inject at higher pressures than gas bottle pres-

Reference	T /K p /MPa	CH_4 mol fraction	CO_2 mol fraction	N_2 mol fraction	Number of data points
[Nixdorf and Oellrich, 1997]	276.85-293.41 3.454-23.979	$z^*_{CH_4}$ = 0.9497	$z^*_{CO_2}$ = 0.05	$z^*_{N_2}$ = 0.003	6
[Lee et al., 2012]	ca. 274-282 ca. 2-5	$z^*_{CH_4}$ = 0.41-0.55	$z^*_{CO_2}$ = 0.29-0.40	$z^*_{N_2}$ = 0.05-0.30	26
[Kakati et al., 2015]	284.50-289.34 8.75-11.29	$z^*_{CH_4}$ 0.8989	$z^*_{CO_2}$ = 0.05	$z^*_{N_2}$ = 0.0511	5
[Lim et al., 2017]	279.6-293.0 4.81-30.66	$z^*_{CH_4}$ = 0.5-0.9	$z^*_{CO_2}$ = 0.02-1	$z^*_{N_2}$ = 0.08-0.4	30
[Sun et al., 2017]	274.9-283.9 2.29-14.97	$z^*_{CH_4}$ = 0.203-0.826	$z^*_{CO_2}$ = 0.052-0.604	$z^*_{N_2}$ = 0.05-0.577	45
[Zang and Liang, 2017]	276.2-286.3 2.59-8.84	$z^*_{CH_4}$ = 0.4995-0.7005	$z^*_{CO_2}$ = 0.1998-0.4503	$z^*_{N_2}$ = 0.0490-0.1093	34
This work	282.46-288.62 9.679-15.645	$z^*_{CH_4}$ = 0.46-0.941	$z^*_{CO_2}$ = 0.015-0.14	$z^*_{N_2}$ = 0.044-0.40	5

Table 3.2: Overview of HVLE experimental data for the quaternary system CH_4-CO_2-N_2-H_2O.

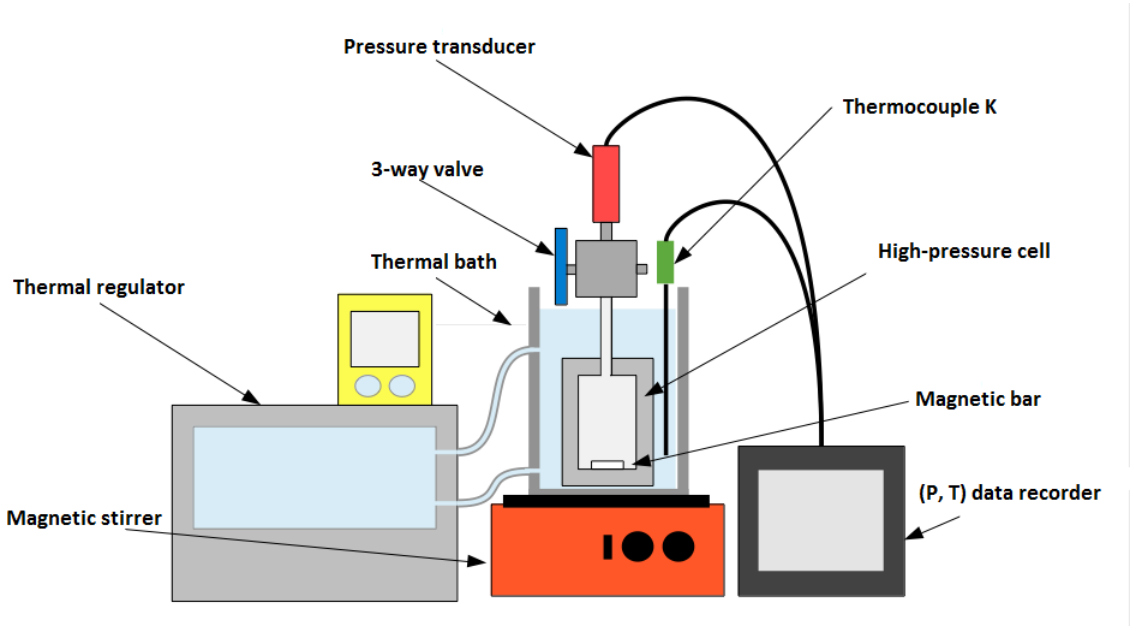

Figure 3.1: Sketch of the high-pressure cell designed to collect thermodynamic data of mixed gas hydrates.

sure. Then water was injected with the metering pump, the temperature was decreased and the stirrer was switched on to form gas hydrates. The pressure drop indicates the formation of gas hydrates. A heating procedure [Tohidi et al., 2000], with step-wise temperature increments of 0.5 K every 2 hours was used to monitor the $p-T$ of dissociation of mixed gas hydrates. This experimental setup and procedure employed to measure phase equilibrium with the Titanium pressure cell was validated by measuring HVLE data of pure CH_4 and pure H_2O. A $p-T$ dissociation

point of (9.459 MPa, 285.79 K) is measured, which is in good agreement with the average value of (9.441 MPa, 285.74 K) from other experiments [McLeod Jr et al., Adisasmito et al., 1991, Yang et al., 2000, Mohammadi et al., 2005].

The gas exchange experiment was carried out in the high-pressure view cell. It consisted in the formation of pure CH_4 hydrates with 10.2 g of H_2O, followed by a depressurization under self-preservation temperature at 265.7 K. When the pressure reached almost 1 bar, the gaseous CO_2 is pressurized into the cell, in order to replace CH_4 molecules in the gas hydrate lattices. The temperature is set to 277.8 K for the rest of the experiment and the evolution of the pressure and of the vapor phase composition were monitored over time.

3.3 Results and discussion

3.3.1 Phase equilibrium of mixed gas hydrates

A series of experiments were carried out to measure HVLE for the ternary mixtures N_2-CO_2-H_2O and CH_4-CO_2-H_2O, and the quaternary mixture CH_4-CO_2-N_2-H_2O (Table 3.3). At 270 K, a minimum of 57 mol-% of CO_2 (more for higher temperature) is required to form a CO_2-rich liquid phase from a CO_2-N_2 mixture [Somait and Kidnay, 1978]. For the CO_2-CH_4 mixture at 273.15 K, clearly more than 60 mol-% of CO_2 is required to form a CO_2-rich liquid phase [Nasir et al., 2015, Legoix et al., 2017]. Thus, no CO_2-rich liquid phase is possible to form since the CO_2 composition of our gas mixtures is always low enough and the temperatures high enough.

T /K	p /MPa Experiment	p /MPa CSMGem (Deviation %) [Sloan Jr and Koh, 2007]	$z^*_{N_2}$	$z^*_{CO_2}$	$z^*_{CH_4}$	H_2O:Gas Feed Molar Ratio	H_2O Saturation vol. %
276.06	9.762	11.165 (14.4)	0.7683	0.2317	0	19.45	58.3
277.63	12.584	14.504 (15.3)	0.7683	0.2317	0	21.52	66.8
279.09	16.373	18.539 (13.2)	0.7683	0.2317	0	24.32	74.9
280.97	20.583	23.873 (16.0)	0.7683	0.2317	0	24.25	78.2
280.92	3.410	3.5798 (5.0)	0	0.8996	0.1004	44.66	83.2
282.61	4.291	4.3982 (2.5)	0	0.8996	0.1004	37.46	83.2
284.97	6.206	6.3211 (1.9)	0	0.8996	0.1004	42.47	91.9
282.46	9.679	No convergence	0.40	0.14	0.46	5.31	41.5
283.37	10.964	10.419 (-5.0)	0.38	0.14	0.48	6.32	39.4
284.11	13.102	10.901 (-16.8)	0.34	0.12	0.54	5.49	40.3
285.70	15.055	13.860 (-7.9)	0.37	0.13	0.50	4.67	39.6
288.62	15.645	14.068 (-10.1)	0.044	0.015	0.941	3.90	38.4

Table 3.3: HVLE data for the systems CO_2-N_2-H_2O, CH_4-CO_2-N_2-H_2O and CH_4-CO_2-H_2O.

Moreover, a very recent study based on Raman spectroscopic measurements highlighted that a CO_2-N_2 gas mixture needs to contain a minimum of 98 mol-% N_2 to coexist with a structure II gas hydrate [Chazallon and Pirim, 2018]. Thus, all gas hydrates are considered as structure I gas hydrate when the CO_2-N_2-CH_4 gas mixture was used. In our work, the water proportion was very high (Table 3.3), thus in the vapor phase at HVLE, the composition of the more soluble gas compound must decrease (but was not measured here). In Figure **??** our data are plotted to-

gether with some data of Kang et al. [2001] and Lee et al. [2014] who measured phase equilibria with gas feed compositions close to ours. Their data with 10 mol-% of CO_2 are also plotted, showing that a decrease of the CO_2:N_2 ratio in the system leads to an increase of the dissociation pressure. For a given N_2-CO_2 gas feed and a given temperature, the equilibrium pressure increases with water content compared to a system with a lower water-to-gas ratio (Figure 3.2). This implies that the gas hydrate stability domain for a flue gas injected into a large water-rich system will likely be shifted to higher pressures. This pressure shift is also noticeable if the feed gas is richer in CO_2 (84.1–90.6 mol-%) with a high H_2O water content [Kim et al., 2011]. This finding is in agreement with Beltran et al. [2012] who highlighted the importance of correctly defining either the initial gas feed and water amount or the composition of the vapor when determining the gas hydrate point of dissociation.

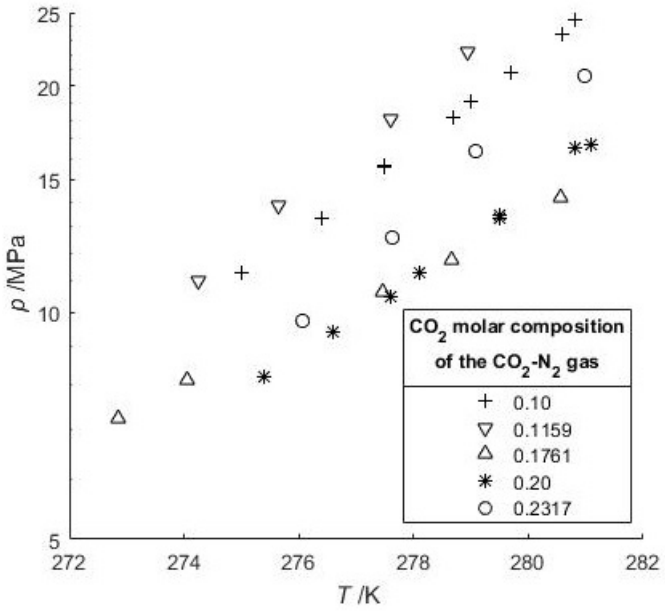

Figure 3.2: Hydrate-Vapor-Liquid Equilibrium (HVLE) data of the CO_2-N_2-H_2O system. Our study provides data for 23.17 mol % CO_2 and high H_2O content. The datasets at low and high pressure correspond to 20 and 10 mol-% of CO_2 in the gas phase [Lee et al., 2014], and 17.61 and 11.59 mol-% of CO_2 [Kang et al., 2001], respectively.

In the following paragraphs, the CSMGem program [Sloan Jr and Koh, 2007] has been used to predict the composition of the vapor and hydrate phases at the dissociation point. CSMGem is a thermodynamic model that computes the $p-T$ conditions of dissociation of gas hydrates and its corresponding phase compositions for a given global composition including H_2O and different gases. With a CO_2-N_2 gas feed, at 276.06 K and 11.165 MPa (Table 3.3) the CSMGem program [Sloan Jr and Koh, 2007] gives a composition of 49.1 mol-% of CO_2 in the gas hydrate phase, and 10.7 mol-% in the vapor (23.17 mol-% in the feed gas). However, if the water content in a system with the same initial gas composition is increased, the CO_2 content in

the vapor phase decreases due to its high solubility in liquid water at ambient temperature conditions. The solubility of different gases, i.e. distribution between the vapor and aqueous phase, affects the gas hydrate composition. Generally, most of studies investigate gas hydrate equilibria by measuring the vapor phase composition at equilibrium or using only very small amounts of water so that the vapor composition stays almost unchanged during the experiments. At a defined temperature, increasing the content of N_2 in the vapor phase increases the composition of the gas hydrate in N_2 and increases its pressure of dissociation.

Our three HVLE data points at gas hydrate dissociation conditions with 10 mol-% CH_4 (Table 3.3) represents complementary data to the HLLE data monitored in a previous study under higher pressures, when no vapor is present [Legoix et al., 2017]. For a CO_2-CH_4 gas feed with 89.96 mol-% CO_2, at 280.92 K and 3.5798 MPa (Table 3.3) the CSMGem program gives a composition of 73.9 mol-% of CO_2 in the gas hydrate phase, and 63.1 mol-% in the vapor phase. However, for a negligible amount of water the calculated pressure does not change significantly (3.3049 MPa) because the HVLE $p-T$ curves of CO_2 and CH_4 are relatively close to each other compared to the curves of CO_2 and N_2. Finally, a series of HVLE data measured with a lower water content and a CO_2-N_2-CH_4 gas feed are in accordance with recent literature data (Figure 3.3).

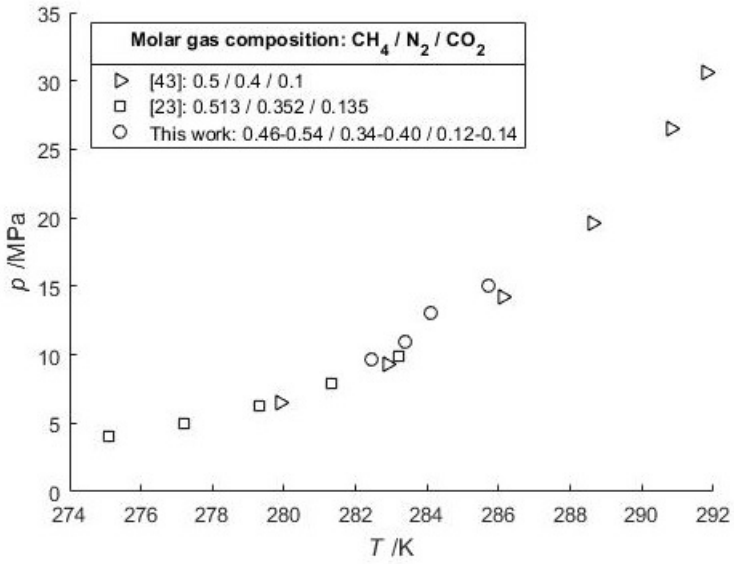

Figure 3.3: Comparison of HVLE data of typical pretreated CO_2-N_2 flue gas compositions that are diluted by CH_4 gas (ca. 50 mol-%) in natural gas hydrate settings.

3.3.2 CH_4-CO_2 exchange between a vapor phase and a bulk gas hydrate phase

The objective of this experiment was to study the gas exchange mechanism between an initial bulk CH_4 hydrate phase and after exposure to a surrounding CO_2 vapor

phase (Figure 3.4). In the experiment CH_4 hydrate is formed from pure CH_4 and pure H_2O, and subsequently the gas feed is changed to CO_2. The temperature is held constant during the reaction, while pressure and vapor composition are monitored. After injecting CO_2 the pressure is kept below the stability pressure of pure CH_4 hydrate, but still above the stability pressure of pure CO_2 hydrate during the entire gas hydrate exchange experiment. After 6 days the vapor phase contains 60.3 mol-% of CH_4, while the pressure has approached 2.90 MPa at a temperature of 277.7 K. For these input parameters, CSMGem [Sloan Jr and Koh, 2007] predicts a gas hydrate containing 43.2 mol-% of CH_4 that has a dissociation pressure of 2.79 MPa. However, after 6 day when the experiment was stopped, the curves of pressure and vapor phase composition still show a very gentle slope (Figure 3.5) indicating that complete thermodynamic equilibrium has not yet been achieved and the exchange reaction is still slowly progressing. The following paragraph discusses the possible processes occurring in the batch experiment.

The observed change in gas composition and pressure evolution indicate that the experiment can be split in two parts (Figure 3.5). At the beginning the CH_4 vapor content increases very quickly to ca 40 mol-%, while the overall pressure drops by 0.6 MPa, indicating CH_4 hydrate dissociation being decoupled from CO_2 hydrate formation. In addition, an overall pressure drop can only result from CO_2 consumption by excess water in the cell. In the second phase the pressure in the cell is slowly increasing again, complemented by a parallel further, gentle CH_4 increase in the vapor phase, indicating that a coupled gas exchange of CH_4 by CO_2 in the hydrate phase becomes the dominant process. This direct gas hydrate conversion has been described previously by the shrinking-core process [Falenty et al., 2016]. Here, CO_2 replaces the CH_4 in the hydrate grain forming an outer CO_2-rich hydrate shell around an inner CH_4 hydrate core. Consequently, gas exchange is controlled by the percolation of gas molecules through the CO_2-rich hydrate shell, i.e. CH_4 is transported to the vapor phase surrounding the hydrate grains and CO_2 is transported from the outside to the inner hydrate core. Thus, the kinetics of the coupled hydrate conversion is generally slow and depends on the size of the CH_4 hydrate grains.

In the following mass balance we attempt to discriminate the three processes, CH_4 hydrate dissociation, CO_2-rich hydrate formation from excess water and shrinking-core hydrate conversion, from each other. The total CO_2 amount is the one found in the initial vapor phase, just after the removal of CH_4 and injection of CO_2 in the vapor phase. The initial H_2O mass is 10.2 g given by a balance during the injection of H_2O. Then, the initial CH_4 amount is considered to be 1 atm of CH_4 that remained in the vapor phase plus the CH_4 found in gas hydrate formed from 10.2 g of H_2O, using a constant hydration number fixed to 5.75 (i.e., $h_{H_2O} = 0.852$). The aim is to find from this initial assumption, the proportion of the CH_4 hydrate that were effectively formed with the corresponding excess H_2O, and the end time of the gas exchange between the CH_4 hydrate and the CO_2-rich vapor phase. For the rate of the gas exchange, here is considered a linear increase of CH_4 coming from the gas hydrate phase, enriching the vapor phase. This linear increase for our system is measured from the slope of the last two data points of our experiment (Figure 3.5):

Figure 3.4: Top panel: Visual observation of the evolution of the different phases during gas hydrate crystallization (from left to right: directly after water injection; after stirrer has been set to 400 rpm; 1 min after the gas hydrate formation incipient; 48 min after the gas hydrate formation incipient). Bottom panel: Visual state of the system during the gas exchange process (from left to right: t= 0h; t= 1.47h; t= 18.90h; t= 89.73h; t= 118.90h; t= 145.73h).

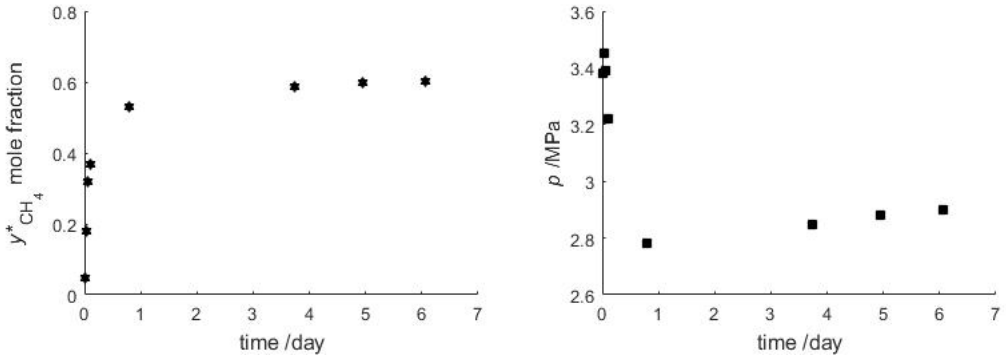

Figure 3.5: Evolution of the composition of the vapor phase (Left) and evolution of the pressure (Right) during the replacement of CH_4 by CO_2. see Table 3.4 for the list of measured values.

$$y*_{CH_4}[molefraction] = 2.236 * 10^{-4} * t[/hour] + 0.570$$
$$p[/MPa] = 7.454 * 10^{-4} * t[/hour] + 2.791$$

The total amounts of each component (CH_4, CO_2, H_2O) in the system and the observed average temperature of 277.8 K are used as inputs for the CSMGem program that returns the corresponding composition of phases at thermodynamic equilibrium and the pressure of the mixed gas hydrate dissociation (HVLE). The resulting $y^*_{CH_4}$ and $h^*_{CH_4}$ (i.e., molar fraction of CH_4 within gas hydrate compared to CO_2) together with the phase fraction calculated at the end of the gas exchange, give a new value of the total amount of CH_4. For each iteration, the total fraction of each component is changed leading each time to a lower proportion of initial CH_4 hydrate formed.

The calculation is finished when the mass balance is reached. The result shows that 86.2 % of H_2O was consumed initially to form the pure CH_4 hydrate, i.e. 13.8 % remained as liquid excess water in the cell. The gas exchange between CH_4 and CO_2 in the hydrate is finished supposedly within 39.7 days, resulting in a mixed gas hydrate containing 62.7 mol-% of CH_4 ($h^*_{CH_4}$) and a vapor phase containing 78.4 mol-% of CH_4 ($y^*_{CH_4}$). This means that 1.4 g of H_2O would not have been bound in CH_4 hydrate at the beginning (i.e., being excess water), which is in agreement with the pressure decrease initially observed. This pressure decrease is due to the formation of CO_2-rich hydrate consuming 0.7 g of excess water (dissolution of CO_2 in liquid H_2O would require using 7.7 g of H_2O to achieve the same pressure drop).

3.4 Conclusion

A series of phase equilibrium (HVLE) experiments with different gas mixtures of CH_4-CO_2, CO_2-N_2 and CH_4-CO_2-N_2 were conducted. Compared to previous work in the literature the data shows that the disparity of solubility in the aqueous phase between gases strongly affects the dissociation pressure of mixed gas hydrates at a given temperature, especially for flue-gas type containing CO_2 and N_2. Since CO_2-N_2 gas mixtures are considered for a CH_4 production from gas hydrate reservoirs, or the storage of a flue gas in a natural setup (below the permafrost or within the sediments on continental margins), the water saturation level of the sediment will then systematically affect the stability of the gas hydrate formed from CO_2-N_2-(CH_4) mixtures. These gas hydrates could have a thermodynamic stability affected by the complex evolution of the environment during and after the injection. Thus, the CO_2-N_2-containing mixed hydrate formed in the vicinity of the well may become unstable, if surrounding formation water flows towards the well. The gas exchange experiment performed outside pure CH_4 hydrate stability pressure confirms that several processes are competing during the gas hydrate exchange: direct CO_2-CH_4 exchange within the initial CH_4 hydrate, dissociation of the initial CH_4 hydrate, and formation of CO_2-rich hydrate with excess water. Complete conversion of CH_4 hydrate to CO_2 hydrate will typically take several weeks to months, depending on the CH_4 hydrate grain size. As a perspective, there is a need of thermodynamic and kinetic data of phase evolutions (i.e., gas hydrate growth and dissociation) of the CH_4-CO_2-N_2-H_2O system in presence of gas hydrates. Moreover, further studies on hydrate kinetics need to be done to evaluate better the competition between gas hydrate dissociation and direct gas exchange in a closed system, and during a depressurization process.

3.5 Appendix

t /h	T /K	p /MPa	$y^*_{CH_4}$ /mol %
0.53	277.0	3.38	4.9
0.97	277.8	3.45	17.8
1.47	277.8	3.39	31.8
2.65	277.8	3.22	36.8
18.9	277.7	2.78	53.0
89.73	277.7	2.85	58.6
118.9	277.8	2.88	59.7
145.73	277.7	2.90	60.3

Table 3.4: Evolution of the gas phase with a CO_2-CH_4 gas exchange on an initial CH_4 hydrate.

Acknowledgements

This research was supported by the SUGAR project, funded by the German Ministry of Research (grant no. 03G0856A), and the "Fluid migration within sedimentary environments", a research focus of the Geochemical Laboratory (LCG-GM-REM-IFREMER).

Bibliography

S. Adisasmito, R. J. Frank III, and E. D. Sloan Jr. Hydrates of carbon dioxide and methane mixtures. *Journal of Chemical and Engineering Data*, 36(1):68–71, 1991. doi: 10.1021/je00001a020.

V. Belandria, A. Eslamimanesh, A. H. Mohammadi, and D. Richon. Gas hydrate formation in carbon dioxide + nitrogen + water system: Compositional analysis of equilibrium phases. doi: 10.1021/ie101635k.

J. G. Beltran, H. Bruusgaard, and P. Servio. Gas hydrate phase equilibria measurement techniques and phase rule considerations. *The Journal of Chemical Thermodynamics*, 44(1):1–4, 2012. doi: 10.1016/j.jct.2011.08.026.

R. Boswell, D. Schoderbek, T. S. Collett, S. Ohtsuki, M. White, and B. J. Anderson. The Ignik Sikumi Field Experiment, Alaska North Slope: Design, Operations, and Implications for CO_2–CH_4 Exchange in Gas Hydrate Reservoirs. *Energy and Fuels*, 31(1):140–153, 2016. doi: 10.1021/acs.energyfuels.6b01909.

C. Bourry, B. Chazallon, J. L. Charlou, J. P. Donval, L. Ruffine, P. Henry, L. Geli, M. N. Çagatay, S. İnan, and M. Moreau. Free gas and gas hydrates from the Sea of Marmara, Turkey: Chemical and structural characterization. *Chemical Geology*, 264(1-4):197–206, 2009. doi: 10.1016/j.chemgeo.2009.03.007.

H. Bruusgaard, J. G. Beltrán, and P. Servio. Vapor- liquid water- hydrate equilibrium data for the system N_2 + CO_2 + H_2O. *Journal of Chemical and Engineering Data*, 53(11):2594–2597, 2008. doi: 10.1021/je800445x.

A. Car, C. Stropnik, W. Yave, and K.-V. Peinemann. Pebax®/polyethylene glycol blend thin film composite membranes for CO_2 separation: Performance with mixed gases. *Separation and Purification Technology*, 62(1):110–117, 2008. doi: 10.1016/j.seppur.2008.01.001.

B. Chazallon and C. Pirim. Selectivity and CO_2 capture efficiency in CO_2-N_2 clathrate hydrates investigated by in-situ Raman spectroscopy. *Chemical Engineering Journal*, 342:171–183, 2018. doi: 10.1016/j.cej.2018.01.116.

G. E. Claypool and K. A. Kvenvolden. Methane and other hydrocarbon gases in marine sediment. *Annual Review of Earth and Planetary Sciences*, 11(1):299–327, 1983.

C. Deusner, N. Bigalke, E. Kossel, and M. Haeckel. Methane production from gas hydrate deposits through injection of supercritical CO_2. *Energies*, 5(7):2112–2140, 2012. doi: 10.3390/en5072112.

Z. Duan and J. Hu. A new cubic equation of state and its applications to the modeling of vapor-liquid equilibria and volumetric properties of natural fluids. *Geochimica et Cosmochimica Acta*, 68(14):2997–3009, 2004. doi: 10.1016/j.gca.2003.11.034.

A. Eslamimanesh, A. H. Mohammadi, D. Richon, P. Naidoo, and D. Ramjugernath. Application of gas hydrate formation in separation processes: A review of experimental studies. *The Journal of Chemical Thermodynamics*, 46:62–71, 2012. doi: 10.1016/j.jct.2011.10.006.

A. Falenty, J. Qin, A. Salamatin, L. Yang, and W. Kuhs. Fluid composition and kinetics of the in situ replacement in CH_4–CO_2 hydrate system. *The Journal of Physical Chemistry C*, 120(48):27159–27172, 2016. doi: 10.1021/acs.jpcc.6b09460.

S.-S. Fan and T.-M. Guo. Hydrate formation of CO_2-rich binary and quaternary gas mixtures in aqueous sodium chloride solutions. *Journal of Chemical and Engineering Data*, 44(4):829–832, 1999. doi: 10.1021/je990011b.

O. Fandiño, J. P. Trusler, and D. Vega-Maza. Phase behavior of (CO_2+H_2) and (CO_2+N_2) at temperatures between (218.15 and 303.15) K at pressures up to 15 MPa. *International Journal of Greenhouse Gas Control*, 36:78–92, 2015. doi: 10.1016/j.ijggc.2015.02.018.

J. S. Gudmundsson, M. Parlaktuna, A. Khokhar, et al. Storage of natural gas as frozen hydrate. doi: 10.2118/24924-PA.

J.-M. Herri, A. Bouchemoua, M. Kwaterski, A. Fezoua, Y. Ouabbas, and A. Cameirão. Gas hydrate equilibria for CO_2–N_2 and CO_2–CH_4 gas mixtures—Experimental studies and thermodynamic modelling. *Fluid Phase Equilibria*, 301(2):171–190, 2011. doi: 10.1016/j.fluid.2010.09.041.

K. Z. House, D. P. Schrag, C. F. Harvey, and K. S. Lackner. Permanent carbon dioxide storage in deep-sea sediments. *Proceedings of the National Academy of Sciences*, 103(33):12291–12295, 2006. doi: 10.1073/pnas.0605318103.

H. Kakati, A. Mandal, and S. Laik. Phase stability and kinetics of CH_4 + CO_2 + N_2 hydrates in synthetic seawater and aqueous electrolyte solutions of NaCl and $CaCl_2$. *Journal of Chemical and Engineering Data*, 60(6):1835–1843, 2015. doi: 10.1021/acs.jced.5b00042.

S.-P. Kang, H. Lee, C.-S. Lee, and W.-M. Sung. Hydrate phase equilibria of the guest mixtures containing CO_2, N_2 and tetrahydrofuran. *Fluid Phase Equilibria*, 185(1-2):101–109, 2001. doi: 10.1016/S0378-3812(01)00460-5.

P. Kastanidis, G. E. Romanos, A. K. Stubos, I. G. Economou, and I. N. Tsimpanogiannis. Two-and three-phase equilibrium experimental measurements for the

ternary CH_4 + CO_2 + H_2O mixture. *Fluid Phase Equilibria*, 451:96–105, 2017. doi: 10.1016/j.fluid.2017.08.0020378-3812.

M. Kida, O. Khlystov, T. Zemskaya, N. Takahashi, H. Minami, H. Sakagami, A. Krylov, A. Hachikubo, S. Yamashita, H. Shoji, et al. Coexistence of structure I and II gas hydrates in Lake Baikal suggesting gas sources from microbial and thermogenic origin. *Geophysical Research Letters*, 33(24), 2006. doi: 10.1029/2006GL028296.

S. H. Kim, M. Do Seo, J. W. Kang, and C. S. Lee. Hydrate-containing phase equilibria for mixed guests of carbon dioxide and nitrogen. *Fluid Phase Equilibria*, 306(2):229–233, 2011. doi: 10.1016/j.fluid.2011.04.011.

H. Komatsu, M. Ota, R. L. Smith Jr, and H. Inomata. Review of CO_2–CH_4 clathrate hydrate replacement reaction laboratory studies–properties and kinetics. *Journal of the Taiwan Institute of Chemical Engineers*, 44(4):517–537, 2013. doi: 10.1016/j.jtice.2013.03.010.

K. A. Kvenvolden. Methane hydrate—a major reservoir of carbon in the shallow geosphere? *Chemical geology*, 71(1-3):41–51, 1988. doi: 10.1016/0009-2541(88)90104-0.

K. S. Lackner. A guide to CO_2 sequestration. *Science*, 300(5626):1677–1678, 2003. doi: 10.1126/science.1079033.

H.-H. Lee, S.-H. Ahn, B.-U. Nam, B.-S. Kim, G.-W. Lee, D. Moon, H. J. Shin, K. W. Han, and J.-H. Yoon. Thermodynamic stability, spectroscopic identification, and gas storage capacity of CO_2-CH_4-N_2 mixture gas hydrates: Implications for landfill gas hydrates. *Environmental Science and Technology*, 46(7):4184–4190, 2012. doi: 10.1021/es203389k.

Y. Lee, S. Lee, J. Lee, and Y. Seo. Structure identification and dissociation enthalpy measurements of the CO_2 + N_2 hydrates for their application to CO_2 capture and storage. *Chemical Engineering Journal*, 246:20–26, 2014. doi: 10.1016/j.cej.2014.02.0451385-8947.

L. N. Legoix, L. Ruffine, J.-P. Donval, and M. Haeckel. Phase Equilibria of the CH_4-CO_2 Binary and the CH_4-CO_2-H_2O Ternary Mixtures in the Presence of a CO_2-Rich Liquid Phase. *Energies*, 10(12):2034, 2017. doi: 10.3390/en10122034.

D. Lim, H. Ro, Y. Seo, Y. ju Seo, J. Y. Lee, S. J. Kim, J. Lee, and H. Lee. Thermodynamic stability and guest distribution of CH_4/N_2/CO_2 mixed hydrates for methane hydrate production using N_2/CO_2 injection. *Journal of Chemical Thermodynamics*, 106:16–21, 2017. doi: 10.1016/j.jct.2016.11.012.

P. Linga, A. Adeyemo, and P. Englezos. Medium-pressure clathrate hydrate/membrane hybrid process for postcombustion capture of carbon dioxide. *Environmental Science and Technology*, 42(1):315–320, 2007. doi: 10.1021/es071824k.

H. Lu, Y.-t. Seo, J.-w. Lee, I. Moudrakovski, J. A. Ripmeester, N. R. Chapman, R. B. Coffin, G. Gardner, and J. Pohlman. Complex gas hydrate from the cascadia margin. *Nature*, 445(7125):303, 2007. doi: 10.1038/nature05463.

H. O. McLeod Jr, J. M. Campbell, et al. Natural gas hydrates at pressures to 10,000 psia. doi: 10.2118/1566-G-PA.

A. H. Mohammadi, R. Anderson, and B. Tohidi. Carbon monoxide clathrate hydrates: equilibrium data and thermodynamic modeling. *AIChE journal*, 51(10): 2825–2833, 2005. doi: 10.1002/aic.10526.

Q. Nasir, K. M. Sabil, and K. Lau. Measurement of isothermal (vapor + liquid) equilibria, (VLE) for binary (CH_4+ CO_2) from T=(240.35 to 293.15) K and CO_2 rich synthetic natural gas systems from T=(248.15 to 279.15) K. *Journal of Natural Gas Science and Engineering*, 27:158–167, 2015. doi: 10.1016/j.jngse.2015.08.045.

J. Nixdorf and L. R. Oellrich. Experimental determination of hydrate equilibrium conditions for pure gases, binary and ternary mixtures and natural gases. *Fluid Phase Equilibria*, 139(1-2):325–333, 1997. doi: 10.1016/S0378-3812(97)00141-6.

K. Ohgaki, Y. Makihara, and K. Takano. Formation of CO_2 hydrate in pure and sea waters. *Journal of chemical engineering of Japan*, 26(5):558–564, 1993. doi: 10.1252/jcej.26.558.

M. B. Olseni, A. Majumdar, and P. R. Bishnoi. Experimental studies on hydrate equilibrium-carbon dioxide and its systems. *International Journal of the Society of Materials Engineering for Resources*, 7(1):17–23, 1999. doi: 10.5188/ijsmer.7.17.

Y. Park, D.-Y. Kim, J.-W. Lee, D.-G. Huh, K.-P. Park, J. Lee, and H. Lee. Sequestering carbon dioxide into complex structures of naturally occurring gas hydrates. *Proceedings of the National Academy of Sciences*, 103(34):12690–12694, 2006. doi: 10.1073/pnas.0602251103.

E. Pinero, M. Marquardt, C. Hensen, M. Haeckel, and K. Wallmann. Estimation of the global inventory of methane hydrates in marine sediments using transfer functions. *Biogeosciences (BG)*, 10(2):959–975, 2013. doi: 10.5194/bg-10-959-2013.

L. Ruffine and J. Trusler. Phase behaviour of mixed-gas hydrate systems containing carbon dioxide. *The Journal of Chemical Thermodynamics*, 42(5):605–611, 2010. doi: 10.1016/j.jct.2009.11.019.

L. Ruffine, J.-P. Donval, J.-L. Charlou, A. Cremière, and B. Zehnder. Experimental study of gas hydrate formation and destabilisation using a novel high-pressure apparatus. *Marine and Petroleum Geology*, 27(6):1157–1165, 2010. doi: 10.1016/j.marpetgeo.2010.03.002.

D. Sadeq, S. Iglauer, M. Lebedev, C. Smith, and A. Barifcani. Experimental determination of hydrate phase equilibrium for different gas mixtures containing methane, carbon dioxide and nitrogen with motor current measurements. *Journal of Natural Gas Science and Engineering*, 38:59–73, 2017. doi: 10.1016/j.jngse.2016.12.025.

D. Schoderbek, H. Farrell, J. Howard, K. Raterman, S. Silpngarmlert, K. Martin, B. Smith, and P. Klein. ConocoPhillips gas hydrate production test. Technical report, ConocoPhillips Co., Houston, TX (United States), 2013.

Y.-T. Seo, S.-P. Kang, H. Lee, C.-S. Lee, and W.-M. Sung. Hydrate phase equilibria for gas mixtures containing carbon dioxide: a proof-of-concept to carbon dioxide recovery from multicomponent gas stream. *Korean Journal of Chemical Engineering*, 17(6):659–667, 2000. doi: 10.1007/BF02699114.

I. B. A. Sfaxi, V. Belandria, A. H. Mohammadi, R. Lugo, and D. Richon. Phase equilibria of $CO_2 + N_2$ and $CO_2 + CH4$ clathrate hydrates: Experimental measurements and thermodynamic modelling. *Chemical Engineering Science*, 84:602–611, 2012. doi: 10.1016/j.ces.2012.08.041.

E. D. Sloan Jr. Fundamental principles and applications of natural gas hydrates. *Nature*, 426(6964):353, 2003. doi: 10.1038/nature02135.

E. D. Sloan Jr and C. Koh. *Clathrate hydrates of natural gases*. CRC press, 2007.

F. A. Somait and A. J. Kidnay. Liquid-vapor equilibriums at 270.00 K for systems containing nitrogen, methane, and carbon dioxide. *Journal of Chemical and Engineering Data*, 23(4):301–305, 1978. doi: 10.1021/je60079a019.

S.-C. Sun, C.-L. Liu, and Q.-G. Meng. Hydrate phase equilibrium of binary guest-mixtures containing CO_2 and N_2 in various systems. *The Journal of Chemical Thermodynamics*, 84:1–6, 2015. doi: 10.1016/j.jct.2014.12.018.

Y.-H. Sun, S.-L. Li, G.-B. Zhang, W. Guo, and Y.-H. Zhu. Hydrate phase equilibrium of $CH_4 + N_2 + CO_2$ gas mixtures and cage occupancy behaviors. *Industrial and Engineering Chemistry Research*, 56(28):8133–8142, 2017. doi: 10.1021/acs.iecr.7b01093.

B. Tohidi, R. Burgass, A. Danesh, K. Østergaard, and A. Todd. Improving the accuracy of gas hydrate dissociation point measurements. *Annals of the New York Academy of Sciences*, 912(1):924–931, 2000. doi: 10.1111/j.1749-6632.2000.tb06846.x.

S. F. Westman, H. G. Stang, S. W. Løvseth, A. Austegard, I. Snustad, S. T. Størset, and I. S. Ertesvåg. Vapor-liquid equilibrium data for the carbon dioxide and nitrogen ($CO_2 + N_2$) system at the temperatures 223, 270, 298 and 303 K and pressures up to 18 MPa. *Fluid Phase Equilibria*, 409:207–241, 2016. doi: 10.1016/j.fluid.2015.09.034.

S. Yang, I. Yang, Y. Kim, and C. Lee. Measurement and prediction of phase equilibria for water+ CO_2 in hydrate forming conditions. *Fluid Phase Equilibria*, 175(1-2):75–89, 2000. doi: 10.1016/S0378-3812(00)00467-2.

X. Zang and D. Liang. Phase Equilibrium Data for the Hydrates of Synthesized Ternary $CH_4/CO_2/N_2$ Biogas Mixtures. *Journal of Chemical & Engineering Data*, 63(1):197–201, 2017. doi: 10.1021/acs.jced.7b00823.

A. Zúñiga-Moreno and L. A. Galicia-Luna. Densities of 1-propanol and 2-propanol via a vibrating tube densimeter from 313 to 363 K and up to 25 MPa. *Journal of Chemical and Engineering Data*, 47(2):155–160, 2002. doi: 10.1021/je0100138.

Chapter 4

Flow-through experiments in gas hydrate bearing sediments with CH_4-CO_2-N_2 gas mixtures

Article in preparation for *Marine & Petroleum Geology*
L.N. Legoix, C. Deusner, L. Ruffine, E. Kossel, M. Haeckel

Abstract Four laboratory experiments with injection of different gas mixtures into methane hydrate-bearing sandy matrix followed by stepwise depressurizations were carried out to analyze the efficiencies and rates of both methane (CH_4) production and carbon dioxide (CO_2) retention, and better understand key process parameters. The initial flue gas contained CO_2 and nitrogen (N_2) at a ratio of 19.4:80.6. Methane was added to this binary mixture in subsequent experiments to evaluate the influence of enhanced CH_4 concentrations on the exchange process. The increase of CH_4 content in the injected gas mixture leads to a faster formation of secondary gas hydrates resulting in plugging the injection ports and accumulating gas in the reactor. Thus, the increase in CH_4 concentration could result in permeability issues in some distance of the injection well rather than in its direct vicinity. However, even at increased CH_4 concentrations this process reveals a better retention of CO_2 compared to N_2 and CH_4, especially at the early stage of each injection. This is due to preferential retention of CO_2 in both the hydrate and water phases. Over the experimental period of two weeks which included both gas injection and depressurization steps a high proportion of CH_4 is still retained in the gas hydrate phase. Our results allowed us to further interpret the Ignik Sikumi field test, and elements of response were proposed regarding the technical problems which were reported by Boswell et al. [2017].

Keywords gas hydrate-bearing sediment, CH_4, CO_2, N_2, flow-through, high-pressure experiment

4.1 Introduction

Gas hydrate is an ice-like solid material, with a crystalline structure in which water (H_2O) molecules form cages. These cages could host various guest molecules such as CH_4 and specific heavier hydrocarbons (C_2+), hydrogen sulfide (H_2S), as well as

carbon dioxide (CO_2), nitrogen (N_2), helium (He). Gas hydrates can be characterized by single or multiple guest occupation. Although various crystalline structures exist, three are very common. They are called structure SI, SII [Stackelberg and Müller, 1951] and SH [Ripmeester et al., 1987] and differ from each other by the enclathrated guest molecule and pressure-temperature, p-T, conditions. A gas hydrate with a single guest, *e.g.* CH_4, could also have structural transitions depending on p-T conditions [Shimizu et al., 2002].

Numerous potential industrial applications on gas hydrate-based technologies have been raised, such as the gas separation, reviewed by Eslamimanesh et al. [2012], Babu et al. [2015], natural gas transport and storage, as well as desalination. Gas hydrates are also present in nature, in specific locations on Earth where the temperature and pressure are favorable for its existence. Thus, they are mainly located below the seafloor of continental margins and below permafrost. Although there is evidence of natural gas hydrates containing hydrocarbons produced from thermal degradation of organic matter at depth (e.g., [Davidson et al., 1986]), microbial CH_4 remains the main molecule stored in natural gas hydrate-bearing sediments [Y.F Makogon, 1997]. Considering the rates of particular carbon degradation, a huge proportion of 100-2000 Gt of methane carbon is estimated to be stored within natural gas hydrate deposits offshore [Archer et al., 2009, Burwicz et al., 2011, Wallmann et al., 2012, Pinero et al., 2013].

Besides, modern societies will face energy and environmental challenges due to the increase of both, the projected future global energy demand combined with the scarcity of conventional fossil resources [Mohr et al., 2015], and anthropogenic greenhouse gas emissions [Le Quéré et al., 2016]. In this context, the production of natural gas from conventional reservoirs is increasing [BritishPetroleum, 2018] and the exploitation of unconventional reservoirs like shale gas and gas hydrate deposits are considered as serious options to contribute to the energy transition schemes. Nowadays, the economical production of shale gas is viable whereas it is not the case for gas hydrates. Therefore, a breakthrough technology is needed. Ideally, natural gas production from hydrate deposits should be coupled to a carbon dioxide sequestration [Ohgaki et al., 1996], as it could lower both the production costs and our carbon fingerprint.

In this context, a methane production test coupled to flue gas sequestration has been conducted at the Ignik Sikumi test site (Alaskan permafrost) in 2012 [Schoderbek et al., 2013, Boswell et al., 2017]. A CO_2:N_2 (23:77 mol:mol) gas mixture was injected prior to depressurization steps at temperature and pressure in the hydrate-bearing sediments of around 278.15 K and 6.9 MPa. Indeed, this mixture represents a typical composition of flue gas emitted by power plant, and Park et al. [2006] previously investigated the use of such a gas mixture for gas swapping inside hydrate at the microscale using spectroscopic techniques. The use of this CO_2-N_2 mixture could avoid any CO_2 purification process from power plant industries and improve the CH_4 recovery rate [Park et al., 2006]. Furthermore, the density of liquid CO_2 could also produce unwanted downhole fractures [Boswell et al., 2017] and technical problems on pumps.

Several laboratory experiments of CH_4 recovery using a CO_2-N_2 flue gas injection have been performed very recently [Yang et al., 2017a, Li et al., 2018, Hassanpouryouzband et al., 2018a,b, Schicks et al., 2018, Mu and von Solms, 2018]. Hassanpouryouzband et al. [2018a] measured the pressures corresponding to the optimum partitioning ratio of CO_2 between the vapor and hydrate phase at different temperatures from bulk phase experiments. Li et al. [2018] investigated the CO_2-(N_2) exchange with fracture filling CH_4 hydrate. Mu and von Solms [2018] have performed a set of experiment to evaluate the effect of hydrate saturation and mass transfer properties of hydrate bearing sandstones on the CH_4-CO_2 exchange. Besides, the influence of water saturation in gas hydrate reservoirs has been studied with different setups [Yang et al., 2017b, Wang et al., 2018].

The aforementioned studies provide insights into the mechanisms of CO_2-CH_4 replacement in hydrate. However, there are still phenomena poorly understood like multiple phase behavior with the involvement of multiple components within the gas hydrate deposits. This lack of knowledge partly explains the major technical problems encountered during the production tests, such as the dissociation-induced cooling of the reservoir and the risks of sand production.

Flow-through experiments permits to investigate the combination of fluid flow and gas hydrate dynamics, and to analyze key process parameters such as efficiencies and rates of CH_4 production and CO_2 retention. One particular focus of our experimental study was to characterize the downstream reservoir behavior, in contrast to the near-injection well region. Therefore, the CH_4 load of the injection fluid (0-50 mol %) has been varied here, thus mimicking scenarios in which the injected fluid (CO_2-N_2) becomes gradually enriched with CH_4 because of gas hydrate exchange and hydrate dissociation. The CH_4 production yields and rates were monitored, and the CO_2 retention efficiencies were assessed at high temporal resolution. The results from our flow-through experiments show substantial differences with regard to injection fluid hold-up and replacement of pore water, and secondary gas hydrate formation had a strong influence on sediment permeability.

The present work is an attempt to provide elements of response for some technical problems identified during the Ignik Sikumi field test. This test aimed to produce natural gas by performing CO_2-N_2 injection followed by the depressurization of the deposit.

4.2 Experiment

4.2.1 Apparatus

The experimental setup is the Natural Environment Simulator for Sub-seafloor Interactions (NESSI) modified from Deusner et al. [2012] (Figure 4.1). It consists of a cylindrical high-pressure reactor capable of holding a 1L-scale sample (ParrInst, USA) placed vertically with multiple connecting ports at both its top and bottom. The temperature is controlled with a thermostat (Huber, Offenburg, Germany) which allows the circulation of a fluid through the double casing of the reactor. Different injection systems are connected to the reactor for injection of liquids and gases. A

1 L vessel (ParrInst, USA) with a dip tube is used to inject quickly seawater into the reactor, by pushing from the top of the vessel with CH_4, and then a HPLC pump S1122 (SYKAM, Fürstenfeldbruck, Germany) is used to complete the seawater injection until steady pressure is reached. For the gases, the desired gas mixture is prepared in a separated mixing vessel of 1 L volume and injected through the gas hydrate-bearing sediment with two metering piston pump of 250 mL (Teledyne ISCO, Lincoln NE, USA). These pumps are used to inject a controlled volume of gas at constant pressure and flow, and to avoid large time period between gas charging and injection. Thus, while one pump is filling in gas mixture, the other one is pushing in parallel the already charged gas mixture into the reactor. The water salinity is measured from sample of produced seawater with a conductivity meter 340i (WTW, Weilheim, Germany) with an accuracy of 0.1 g kg^{-1}. The salinity is measured to remove by calculation the amount of pure water used to clean and pressurize the outlet lines between different steps in the same experiment. The outlet pressure is regulated with a back-pressure regulator (BPR) (TESCOM Europe, Selmsdorf, Germany), which later is replaced by a metering-needle valve during depressurization steps. For the on-line gas analysis, a Raman spectrometer (Figure 4.6) from Horiba Jovin Yvon is used, and allows the collection of signals from four probes. In these experiments, only two probes were used and placed between the reactor and the back-pressure regulator to analyze the outflow (Figure 4.1 and 4.6). These probes are located upstream the liquid-gas separator, in different positions since a trickle flow formed of liquid water and gas could appear in these lines during the experiments. Thus, the discharged trickle flow (gas + liquid) pass through a 5 L glass bottle acting as a separator at constant pressure and temperature. The water is collected in the bottle and further weighted and subsampled for salinity measurements, and the gas phase flowrate is measured by a mass flow meter (MFM) F111B (Bronkhorst, Ruurlo, Netherlands). The gas is finally collected in Tedlar bags and subsampled afterwards for compositional analysis by Gas Chromatograph (GC).

4.2.2 Material

Methane, carbon dioxide and nitrogen are supplied by Air Liquide with a claimed purity of 99.995, 99.995 and 99.999 mol %, respectively. Ice particles are made from deionized water and the sediment used here is dry quartz sand with a grain size of 0.1-0.6 mm, a mean diameter of 0.29 mm and a grain density of 2.65 g cm^{-3} (G20TEAS, Schlingmeier, Schwülper, Germany). Synthetic seawater medium was prepared according to Dickson [1993].

4.2.3 Experimental Procedure

First, a homogenous gas hydrate-bearing sediment containing pure CH_4 hydrates finely distributed in a coarse sand matrix was initially prepared similarly to Deusner et al. [2012]. Thus, ice particles are sorted out with 0.3-1.0 mm sieves and then mixed to the sand using a freezer and liquid nitrogen to keep the resulting mixture frozen. A section of the high-pressure reactor is filled with the ice-sand matrix (1044 mL), and two p-T data loggers are placed within the sediment at 265 K. Then, the reactor

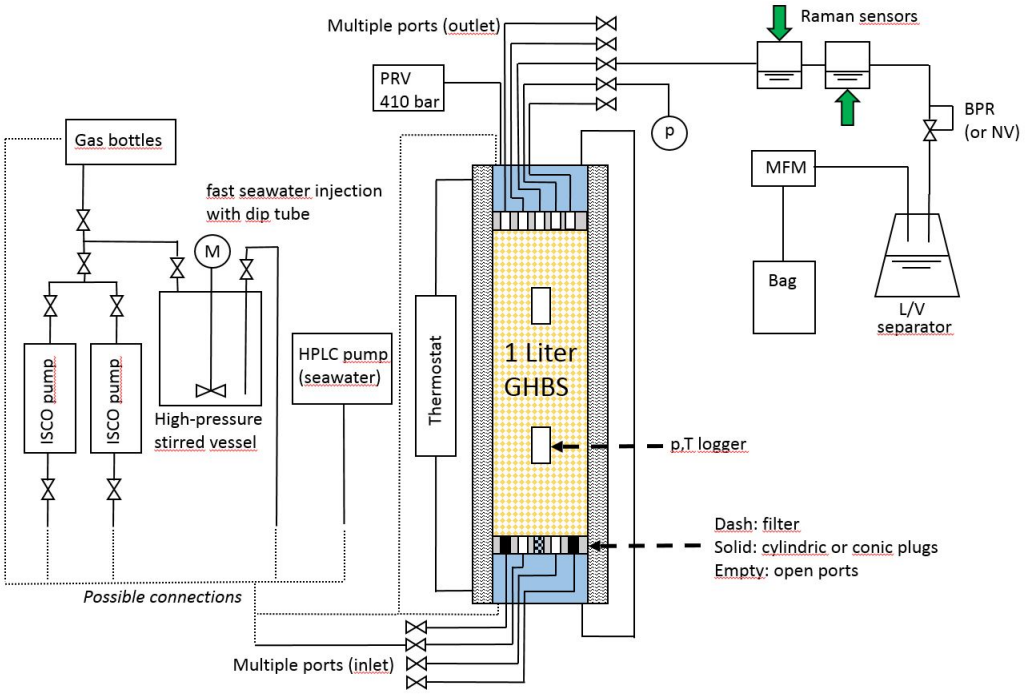

Figure 4.1: Sketch of the experimental apparatus NESSI to perform flow-through experiments with gas hydrate-bearing sediments, modified from Deusner et al. [2012]. Initial CH_4 and H_2O injections are done using a tube connected to inlet and outlet for pressurizing uniformly the reactor.

is pressurized-depressurized three times at 2 MPa with CH_4 to evacuate the present air, and then it is pressurized and left closed with 14 MPa of CH_4. The temperature is alternatively set below and above the freezing point of water every 2 days, at 265 and 274 K, respectively, to speed up and complete gas hydrate formation within particles [Chen et al., 2010]. After a minimum 10 days of equilibration between CH_4 vapor and CH_4 hydrate formed from ice, the vapor phase is evacuated by quick depressurization under self-preservation temperature of 267 K, in order to preserve at best the hydrate phase from dissociation [Stern et al., 2001, 2003]. Then, seawater is quickly pressurized in the system at 13.5 MPa and 274 K. At these p-T conditions, the solubility of CH_4 in seawater in the presence of hydrates is of around 0.05 mol per kg of water [Kossel et al., 2013]. In total about 800 mL of seawater were injected. This means that a maximum amount of 0.04 mol of CH_4 could be dissolved. However, the CH_4 amount retained in hydrates is around 1.8 mol, considering full cage occupation within structure I hydrates. Thus, when cold seawater is pressurized in the reactor, a negligible proportion of hydrates will dissociate until the aqueous phase is saturated in CH_4 (Table 1). The HPLC pump connected to the reactor was flushing seawater for 2 days to fill the dead volumes and let the system reach pressure and temperature stabilization. The synthetic gas hydrate-bearing sediment (GHBS) is then ready for the next steps and contains an aqueous and a CH_4 hydrate phases distributed in coarse sand (Table 4.1).

	Experiment 1	Experiment 2	Experiment 3	Experiment 4
GHBS /mL	1044.2	1044.2	1044.2	1044.2
Sand (in GHBS) /mL	411.9	387.8	387.5	467.6
Ice (in GHBS) /mL	210.0	197.8	197.6	132.0
CH_4 hydrate /mL	209.1*	197.0*	196.6*	131.1*
Hydrate saturation Sh /vol %	33.1	30.0	30.0	22.8
Porosity vol-%	60.6	62.9	62.9	55.2
Seawater (outside pore volume) /mL	386.3	337.8	349.5	414.5

Table 4.1: Initial composition in the high-pressure reactor before the first injection, considering the mass of initial components employed. (*): value after consideration of CH_4 dissolution from hydrate and 1 atm of remaining vapor into water after the CH_4 evacuation.

Afterwards, two constant-pressure flow-through gas injections are done. Flow-through injection means that the replacement gas mixture is injected from the bottom (inlet) of the reactor and passes through the GHBS while the top (outlet) is open, with the pressure kept constant by the back-pressure regulator (BPR) (Figure 4.1). A first injection is done by flushing ca. 1 L of gas mixture (at 13.5 MPa and 273 K) at 5 mL min^{-1}. The reactor is left closed for a week, and then a second injection is done under the same conditions. In the course of four experiments, the proportion of CH_4 admixture is increased in the replacement fluid initially consisting of an average of 80.6:19.4 mol-% of N_2:CO_2, resulting in four different compositions of 0,12.6,25.4 and 50.0 mol-% of CH_4 in the injected gas for each experiment (see Table 4.2). The gas collected downstream the MFM in Tedlar bags is analyzed by gas chromatography. The MFM signal is calibrated for pure CH_4 and corrected for the gas composition measured by the GC using the conversion table of Bronkhorst [Bronkhorst, 2018]. This is done since the high proportion of N_2 affects the thermal properties (compared to CH_4 or CO_2) of the gas measured by the MFM (Table 4.3, outflow calculation).

Finally, after the second injection, the pressure is reduced stepwise. The day after the second injection, the outlet metering-needle valve is carefully opened to produce a fast pressure drop of 2 MPa, and then closed. This fast pressure drop procedure is repeated every days until the reactor is fully depressurized. The produced gas and seawater were collected and analyzed.

Deviations were observed between the mass balance based on the inflow and on the outflow calculations (Table 4.3). The inflow mostly relies on the accuracy of the volumetric pump (ISCO Pump) pressure measurement, the accuracy of the GC measurements and the accuracy of the gas density computed by the SUGAR Toolbox (Peng-Robison based equation) [Kossel et al., 2013]. The outflow calculation depends on the accuracy of MFM and GC measurements. Moreover, during the gas injections, any clogging and problems that forces to change the injection port is accompanied with a small amount of gas loss, that could also affect the accuracy of the injected gas calculated. Some trace of O_2 (from air) initially present in the outlet part or in the sampling devices were also measured in GC samples. Thus, the corresponding N_2 coming from air is also subtracted to obtain the correct gas composition (CH_4-N_2-CO_2) coming from the reactor.

	Experiment 1	**Experiment 2**	**Experiment 3**	**Experiment 4**
CH_4	0	12.6	25.4	50.0
CO_2	16.7	18.4	15.1	9.4
N_2	83.3	69.0	59.5	40.6

Table 4.2: Average composition (1st and 2nd injections) of the gas (mol-%) for each experiment.

	Experiment 1	**Experiment 2**	**Experiment 3**	**Experiment 4**
CH_4	-3.8	-0.1	-14.8	-1.2
CO_2	-23.0	-15.6	-26.9	0.0
N_2	-14.2	-8.8	-21.2	8.0
Mass balance 'value [unit] {measurement method}				
Inflow calculation for the replacement gas mixture: for molecule i n_i [mol] = n_{total} [mol] * y_i [mol-fraction] {GC} with n_{total} [mol] = V_{total} [L] {ISCO Pump} * density [mol.L^{-1}] {SUGAR Toolbox} The 'density [mol.L^{-1}] {SUGAR Toolbox}' is calculated from 'y [mol-fraction] {GC}', 'T [degC] {ISCO Pump chiller}' and 'p [MPa] {ISCO Pump}				
Calculation of the outflow gas: n_i [mol] = n_{total} [mol] {MFM} * y_i [mol-fraction] {GC} The 'n_{total} [mol] {MFM}' is calibrated from 'y [mol-fraction] {GC}', and 'Bronkhorst conversion tables'				

Table 4.3: Mass balance (molar) deviation (%) between gas outflow and inflow.

4.3 Results and discussion

4.3.1 Experimental results

Figure 4.2 shows the evolution of the gas composition after the two injections. In this work, the initial hydrates that contains pure CH_4 is called primary gas hydrates while the secondary gas hydrates refer to the hydrates formed afterward from the gas mixture in the reactor.

During the first experiment, the CH_4 produced comes only from primary gas hydrate since the injected gas mixture does not contain CH_4. Thus, the CH_4 produced is only coming from the gas exchange process, hydrate dissociation or exsolution from seawater. As mentioned above, the amount of methane dissolved in the seawater is small compared to the total injected. Therefore, it is considered as negligible. At the end of the first injection, 5.23 % of CH_4 contained in primary hydrates were produced, and 8.17 % after the second injection. Thus, 13.40 % CH_4 coming from primary gas hydrates were produced after two injections, with one week of induction time in between (Figure 4.4, experiment 1, CH_4 curve). The CH_4 is mostly produced at the beginning of the injections (Figure 4.2, experiment 1), and the induction time between two injections favors this CH_4 production. Due to the adding of CH_4 in the injection fluid for the other experiments, such quantitative measurement of CH_4 produced from primary hydrates is not possible to establish here. For this first experiment, the mass balance on CH_4 is the most accurate. Table 4.3 shows that the amount of CH_4 measured by the MFM is similar to what was retained within the initial primary hydrates. For the second injection of experiment 2, Raman measurements of the gas show that CH_4 is preferentially produced over CO_2 during the first 30 min of the injection. Then the produced gas composition become constant and similar to the injected gas. However the solubility of CO_2 at such experimental pressure conditions is high compared to CH_4 and N_2 of one more order of magnitude [Kossel et al., 2013]. The total amount of CO_2 produced is between 1.20 and 2.27 mol depending on the experiment. The solubility of CO_2 in presence of (pure) CO_2 hydrates is 0.82 mol per kg of seawater [Wong et al., 2005, Kossel et al., 2013]. Thus, contrasting to N_2 and CH_4 (see section 4.2.3.), the CO_2 retention in the aqueous phase is here non-negligible. Thus, even if CO_2 is known to form kinetically faster hydrates [Englezos et al., 1987, Clarke and Bishnoi, 2005], the amount of CO_2 needed to saturate the seawater before forming hydrates is high compared to CH_4. As the aqueous phase is already saturated in CH_4, fast secondary hydrate formation can occurs when more CH_4 is added in the injection fluid, increasing the likelihood to have clogging.

Furthermore, if an early CH_4 production is noticeable on the first two experiments at 0 and 12.5 mol % of CH_4 in influent, the composition of the gas remains always close to the injected gas composition for the last two experiments (25 and 50 mol % of CH_4 in influent). This behavior may be due to the limited transfer of CH_4 from the primary gas hydrates to vapor phase already enriched in CH_4. The mixed hydrates (CH_4-CO_2-N_2) become more stable (thermodynamically) with increasing CH_4 proportion [Sun et al., 2017]. Here CO_2 is still much more retained in the

hydrates and aqueous phases compared to N_2. This reflects the faster kinetics of CO_2 to form secondary hydrates compared to N_2 and CH_4 at 13.5 MPa and 274.15 K. Thus, the CO_2 has an opposite evolution to CH_4 during the injections: a lower proportion of CO_2 is produced at the beginning of each injection. The replacement rate is limited in this case when a lot of N_2 is present in the injected fluid. This is in agreemet with the statement made from multi-scale experiments by Schicks et al. [2018].

The change in vapor phase composition upon gas injection is more visible in Figure 4.5, where the production of CH_4 and CO_2 are normalized with the production of N_2. N_2 in this process is the molecule that has neither production nor storage interests.

Indeed, the objectives of doing gas replacement and depressurizations is to store a maximum amount of CO_2 and recover a maximum amount of CH_4. The N_2 is considered in these processes as a carrier gas, to avoid any fast secondary CO_2 hydrate formation that could rapidly plug the well by reacting with the pore water. The CO_2:N_2 curve reflects the efficiency of the CO_2 storage (Figure 4.5). N_2 and CO_2 are injected together, thus a low CO_2:N_2 ratio in the produced gas reflects an enhancement of the CO_2 retention in the reactor. In Figure 6, the CO_2:N_2 ratio increases during injection 1 as the gas pass through the reactor with limited exchange during the course of the injection. During injection 2, the CO_2:N_2 ratio reaches a minimum that indicates that CO_2 is preferentially stored compared to N_2, and then this ratio increases with decreasing pressure, mostly due to dissociation of secondary gas hydrates. The change in CO_2 solubility in seawater with pressure is not enough to explain the amount of CO_2 produced during the last depressurizations. The pressure where CO_2:N_2 ratio starts to increase again represents the lower boundary pressure that should be reached during depressurizations to optimize CO_2 retention, this is in accordance with recent batch and bulk phase experiments [Hassanpouryouzband et al., 2018a].

The ability of the gas to flow through the GHBS is dependent on the composition of the injected gas. In this study, injection blockage were observed when the gas is enriched in CH_4, especially during the injection 2 of experiment 3, and injection 1 of experiment 4. The blockage during experiment 3 occurred at the top of the reactor, since the excess pressure reached by the pumps were monitored by the two data loggers (located in the GHBS). This was not the case for the blockage during the experiment 4 since the pressure of the data loggers did not increase when the gas pump pressures reached high values. A blockage forced to switch the injection port to another to allow flowing the gas again. This could have resulted in some loss of gas downstream the reactor and explains partially the negative deviation of mass balance between outlet and inlet. Thus, this blockage during experiment 4 occurred at the bottom of the reactor (injection point) and a huge gas retention (in GHBS and/or at the bottom free space of the reactor filled in seawater) was observed. Indeed, a sudden gas production was monitored later during depressurization at high pressure (Figure 4.4, experiment 4, early stage of depressurization), suggesting that this excess gas produced is not due to any hydrate dissociation.

The formation of secondary gas hydrate acts as a double-edged sword, as it en-

hances the storage of CO_2 in the reservoir as well as the mechanical stability, but the creation of solid channels could also avoid a good gas distribution in space and decreases contact of the vapor with the primary CH_4 hydrate in the vicinity of the borehole.

The production of methane and water increases in the course of depressurization steps due to hydrate dissociation. For all experiments, the CH_4 composition in the end is very high, and that means this compound is largely present in the hydrate phase (Figure 4.3).

Even with a deviation calculated between the inflow and outflow (Table 4.3), an attempt to describe better the evolution of phases inside the reactor is done (Figures 4.7,4.8,4.9 and 4.10). The start and the end of each injection and depressurization (Tables 4.5,4.6,4.7 and 4.8) defined the steps for the calculations mentionned hereafter. The amount of water available in the entire reactor (GHBS and free space outside porous media) was calculated from the injected amount at the beginning minus the cumulative water collected. The solubility of CO_2 and N_2 in water was calculated from Henry law and the one for CH_4 is calculated in presence of pure CH_4 hydrate [Duan and Sun, 2006, Kossel et al., 2013] (blue on Figures 4.7,4.8,4.9 and 4.10). The latter is employed since CH_4 hydrate is dominantly present in the system for all experiments. When the temperature is slightly below 273.15 K due to Joule-Thomson effect during the gas hydrate dissociation, the temperature to calculate the vapor density is set to 273.15 K to stay in the range of the program [Kossel et al., 2013]. The volume of the vapor phase is considered equal to the volume of cumulative water produced, and its composition equal to the one measured by GC at the corresponding step (red on Figures 4.7,4.8,4.9 and 4.10). Finally the global molar amount is calculated with the gas injected minus the gas produced. The molar amounts calculated in the aqueous and vapor phase are then substracted to the total amount calculated from the global molar amount. This new amount gather the composition of the primary hydrate, the secondary hydrate and also the molar difference coming from the deviation of mass balance (green on Figures 4.7,4.8,4.9 and 4.10). This calculation is simple and each phase is calculated using the experimental measurements. Thus no recalculation of phase distribution was done here, for example the water phase is not re-calculated according to any hydrate formation or dissolution.

The water proportion in the reactor decreased gradually from no CH_4 added in the inflow (experiment 1, Figure 4.7) to high CH_4 contents (experiment 4, Figure 4.10). Indeed the enrichement in CH_4 of the vapor phase produced different effects in the reactor. The density of the fluid decreases (also if CO_2 proportion decreases) and then less water is replaced during the gas injection. Moreover, secondary gas hydrates would form faster and retain easier the gas in the reactor. Indeed the chemical potential of CH_4 in gas hydrate and aqueous phase are already the same since the reactor is already saturated in CH_4, thus secondary gas hydrate is supposed to be formed faster with a vapor phase rich in CH_4 [Kvamme, 2016].

Then, this vapor enrichment in CH_4 occurs also during gas exchange between two injections, when the reactor was left close for one week. Thus, the observed pressure

drop between the injections could be due to several combined processes including secondary gas hydrate formation and gas dissolution into the aqueous phase.

For all experiments, the amount of CO_2 retained in the water phase is very high and of the same order of magnitude compared to the CO_2 amounts found in the vapor phase. During depressurization, the CO_2 in hydrate phase reach a local maximum (CO_2 content, green curves on Figures 4.7,4.8,4.9 and 4.10). This maximum of CO_2 contained in hydrate fits with a very low amounts of CO_2 in vapor phase and relative amount in water phase that still high. This could reflect that the secondary hydrate is still forming with CO_2 coming from the aqueous phase, which is not so visible for CH_4 and N_2.

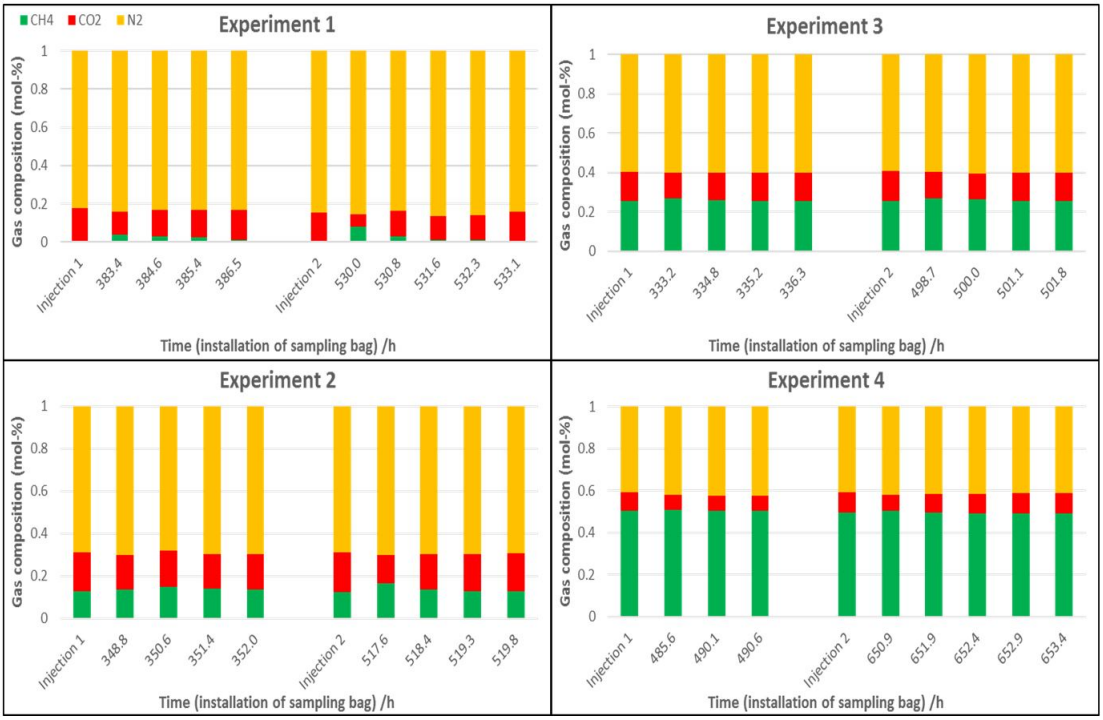

Figure 4.2: Gas composition evolution during injection steps. 'Injection 1' and 'Injection 2' are the composition of the injected gas and following histogram rectangles correspond to the composition of the outflow gas during the injection step.

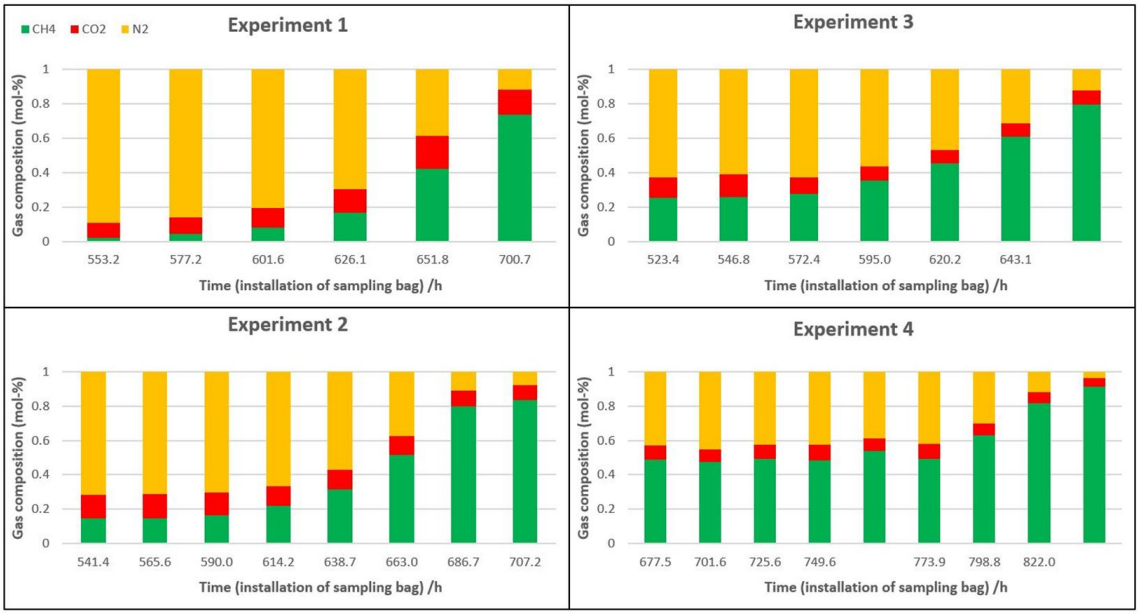

Figure 4.3: Gas composition evolution during depressurization steps. Each histogram rectangle represents the composition of the outflow gas during a fast depressurization, and no abscisses values indicated that gas were collected in a different bag during the same depressurization.

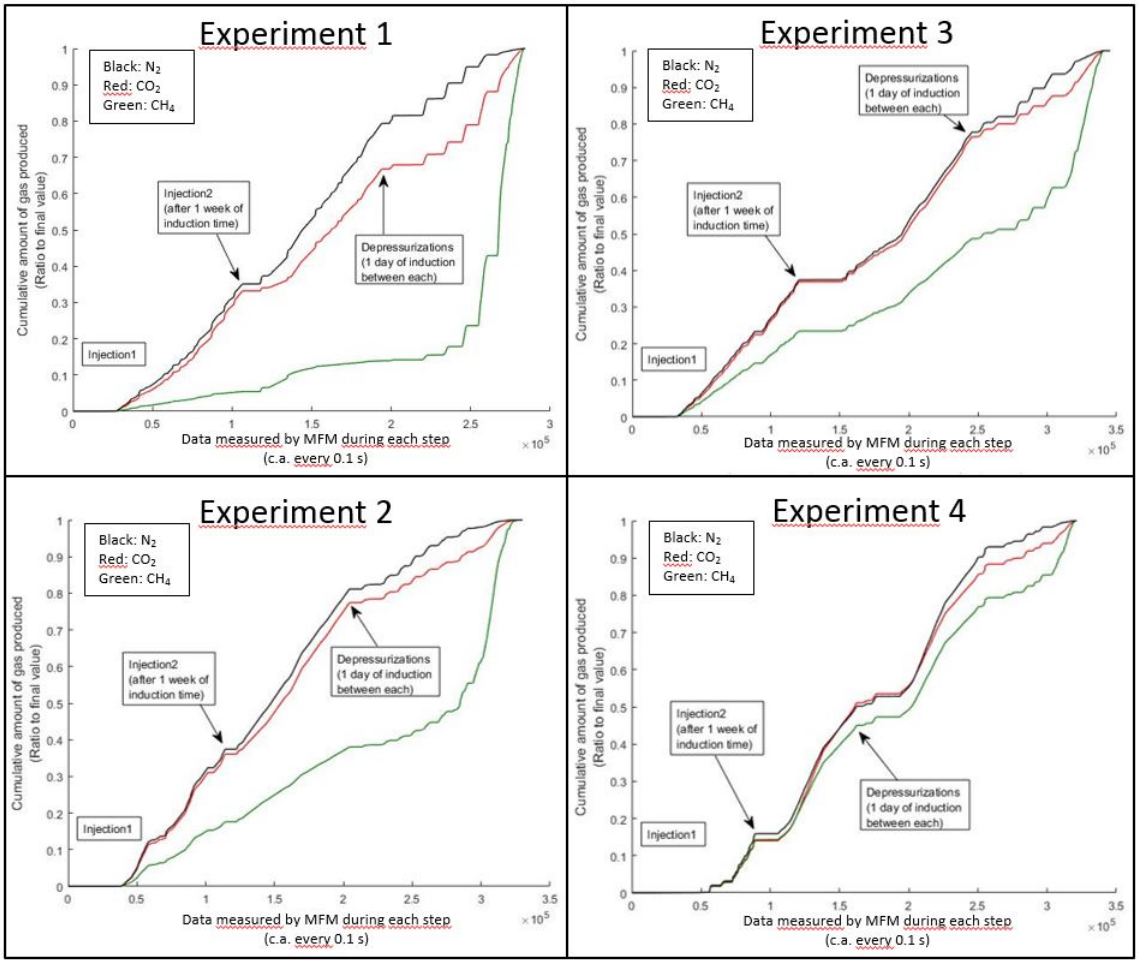

Figure 4.4: Cumulative gas production for each component during the injections and stepwise depressurization. The waiting time between each step, when no gas is produced, are not plotted here.

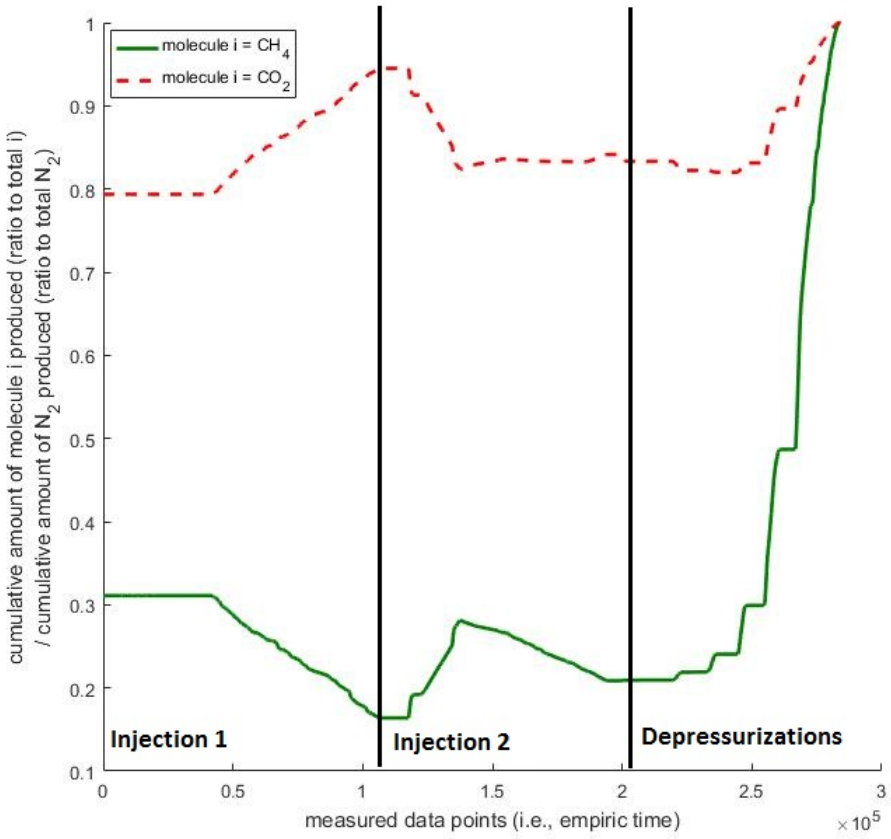

Figure 4.5: Ratio of CO_2:N_2 and CH_4:N_2 produced during the experiment 1 (i.e., the red dotted curve represents the ratio of the CO_2 curve to N_2 curve of Figure 4.4, experiment 1).

4.3.2 Insights on a field scale production scheme

In this section, the results from our experiments are used to analyze better what happened during the Ignik Sikumi field Test in 2012 [Schoderbek et al., 2013, Boswell et al., 2017]. During this field Test, 24,410 standard-m^3 (Sm^3) of CH_4 were produced (Table 4.4). All of this CH_4 comes from gas hydrates. Then, considering that no vapor phase was initially present in the GHBS, and that the dissolved CH_4 in porewater is negligible, a simple calculation is done to estimate the minimum size of the reservoir exploited. Here, the CH_4 is supposed to be produced from fully dissociated pure CH_4 gas hydrate crystallized in structure I. Here is assumed that all hydrate cage is filled with one molecule. This leads to a total volume of 172 Sm^3 of CH_4 released per 1 m^3 of hydrate. The hydrate saturation considered here is the highest measured (with Archie law), i.e. 72 vol-%, and the porosity of the initial GHBS is 40 vol-%. This means that the volume of gas hydrate is 24410/172 = 142 m^3, the pore volume (seawater + gas hydrate) is 142/0.72 = 197 m^3, and the volume of GHBS is 197/0.4 = 493 m^3. If we consider a spherical dissociation around the well downstream, this represents a sphere of 9.8 m diameter of GHBS. For comparison, this represents a volume 4.93 x 10^5 more important than our 1 L GHBS synthesized in the laboratory. The thickness of the "C-1 sand" exploited in the Ignik Sikumi field is only 9.1 m thick [Boswell et al., 2017]. However the circulating fluids move along the hydrate-rich layer since it is surrounded by clay-rich sediments with a lower permeability. The high amount of CH_4 produced compared to other gases (Table 4.4) indicates that the pressure drop went further in the well than the injected flue gas. From these calculations, about 55 m^3 of free water and about 142*0.8 = 114 m^3 of water bounded in hydrates are mobilized in the reservoir. This represents a total of 169 m^3 of water that should be produced. It is lower than the 180.7 m^3 effectiveley collected but the same order of magnitude. This means that the reservoir size touched by the depressurization is larger than the minimum one just calculated above (493 m^3), with CH_4 hydrate only partially dissociated.

At the end of the test 60 % of the injected CO_2 and only 30 % of N_2 remained in the reservoir. About 62 kmol of CO_2 were injected during the field test, meaning that about 93 m^3 of water are needed to dissolve this gas under pressure and temperature conditions in the reservoir and only 8 m^3 of CO_2 hydrates are also enough to sequester the gas. Moreover, the mixed hydrate is forming close to the well compared to the far distance reached by the depressurization [Schicks et al., 2018]. Since a lot of water was produced, this means that the CO_2 not recovered is likely stored into rich-CO_2 hydrates formed kinetically from pore water and hydrate gas exchange.

The gas production during the Ignik Sikumi field test could be splitted into three different parts to study better different processes occuring in the reservoir. During the first 10 days of the CH_4 production rate decreased while sand and water were produced with a steady rate. The water collected is more important than the pore water corresponding to the CH_4 produced from hydrate. Then the second part, during the 5 following days, the water and sand are produced with a very high rate. The CH_4 also is produced at a high rate with little N_2 and CO_2 production. This may be due to a mobilisation of hydrate and sand particles together and a direct

	V_{CH_4} /$\mathbf{Sm^3}$	V_{CO_2} /$\mathbf{Sm^3}$	V_{N_2} /$\mathbf{Sm^3}$	V_{H_2O} /$\mathbf{m^3}$	V_{sand} /$\mathbf{m^3}$
Injection	0	1376.2	4737.4	0	0
Production	24410	550.48	3316.18	180.70	10.65

Table 4.4: Summary of injection and production during the Ignik Sikumi field test [Boswell et al., 2017].

dissociation of primary methane hydrate in the pipeline. Finally during the last part of the test, the pressure is kept below the dissociation pressure of CH_4 hydrate and above the one of CO_2 hydrate. The gas and water were produced at the same rate, and no sand were produced anymore. However the rate of CH_4 production increased permanently while the CO_2 and N_2 remains relatively low. An explaination could be that the pressure decrease reached further distances from the well and dissociate more and more hydrates.

A lower hydrate saturation was used in our experiments (22-33 vol-%) compared to the one in hydrate deposits of Ignik Sikumi (72 vol-%), and most of the primary CH_4 hydrate was still present after the second depressurization during our experiments (more than 86 %). Also our temperature was 4 K lower in average and the pressure up to 13.5 MPa. Thus the conditions to form secondary hydrates were better in our experiments. This suggest that most of the CH_4 produced during the site test was due to a direct dissociation between the CH_4-poor vapor phase and secondly to the depressurization. In our experiments, being below the CH_4 hydrate dissociation pressure produces also a fast relief of CH_4.

4.4 Conclusion

Flow-through experiments in gas hydrate-bearing sediments were performed to get insights into the exchange process between CH_4 hydrate and (CH_4)-CO_2-N_2 gas mixtures. A focus was done on the influence of the methane enrichement of the vapor on the exchange process. Thus, several gas injections and depressurizations were done in laboratory to further study the results of the Ignik Sikumi field test done in 2012 [Schoderbek et al., 2013, Boswell et al., 2017].

It appeared that the exchange followed by the retention of CO_2 in the hydrate is optimal at the early stage of the second injection, which was done after an induction time of one week. In the course of this injection the composition of the produced gas tends to match that of the injected gases. This indicates that the gas is passing through the hydrate without noticeable gas exchange. In the present experiment, the minimum of CO_2:N_2 ratio in the gas outflow shows a better CO_2 storage. Then CH_4 is produced by depressurizations due to secondary hydrate formation and gas exchange. However, most of the CH_4 were produced from primary hydrates when the pressure reached values below its stability point.

After two weeks of gas exchange and depressurization, a larger amount of CO_2 is stored within hydrates compared to N_2. The process observed was also occuring during the field test in Ignik Sikumi. This is due to the higher solubility of CO_2 in

the aqueous phase and to the ability of this molecule to form faster gas hydrates.

Data about the energy efficiency of CH_4 to CO_2-N_2 exchange and the optimization of the time between two injections must be considered such as waiting time before gas production is started. There is a real need to collect data showing explicitly the interactions and kinetic compotitions between the primary and the secondary gas hydrates during both the gas injection and depressurization, either with a direct (i.e., computerized tomography, electrical resistivity) or indirect method (i.e., accurate evaluation of water coming from gas hydrate phases).

4.5 Appendix

Figure 4.6: Raman spectrometer connected to the apparatus for fluid analysis. Analytical section (Left), and high-pressure windowed side and optical head (Right).

Step	t **/h**	T **/K** (1)	p **/MPa** (2)
Injection1	383.41	274.15	12.49
	387.49	274.15	11.15
Injection2	529.98	274.15	9.01
	533.49	274.15	11.10
Depressurization 1	553.21	274.15	10.20
	553.78	274.15	8.15
Depressurization 2	577.18	274.15	8.53
	577.54	274.15	6.68
Depressurization 3	601.63	274.15	6.82
	602.06	274.15	4.09
Depressurization 4	626.14	274.15	4.96
	626.43	274.15	2.10
Depressurization 5	651.83	274.15	3.35
	652.19	274.15	1.09
Depressurization 6	700.74	274.15	2.54
	701.33	274.15	0.10

Table 4.5: p-T conditions inside the reactor during the experiment 1. (1): temperature considered as 274.15 K (no data from logger). (2): Pressure from sensor at outlet (no data from logger).

Step	t **/h**	T **/K**	p **/MPa**
Injection1	348.76	273.79	14.43
	352.79	273.91	13.75
Injection2	517.56	273.83	12.39
	520.49	273.83	13.83
Depressurization 1	541.43	273.75	13.48
	542.25	273.71	11.49
Depressurization 2	565.60	273.75	11.77
	565.87	273.63	9.25
Depressurization 3	589.96	273.71	8.20
	590.16	273.51	7.13
Depressurization 4	614.23	273.71	7.32
	614.55	273.23	5.29
Depressurization 5	638.73	273.67	5.60
	639.13	272.53	3.59
Depressurization 6	662.95	273.71	4.05
	663.30	270.75	2.25
Depressurization 7	686.70	273.55	2.96
	687.56	270.79	0.33
Depressurization 8	707.21	290.99	0.47
	707.49	290.93	0.26

Table 4.6: p-T conditions inside the reactor during the experiment 2.

Step	t **/h**	T **/K**	p **/MPa**
Injection1	333.17	274.43	13.40
	336.95	274.58	13.79
Injection2	498.76	274.39	10.57
	502.56	274.54	14.09
Depressurization 1	523.36	274.31	12.55
	523.85	274.19	10.17
Depressurization 2	546.75	274.27	10.05
	546.86	273.55	7.99
Depressurization 3	572.38	274.27	8.25
	573.00	273.10	5.68
Depressurization 4	594.99	274.27	6.47
	595.12	272.65	4.24
Depressurization 5	620.18	274.31	5.15
	620.37	271.14	2.94
Depressurization 6	643.10	274.23	3.85
	644.00	270.45	0.30

Table 4.7: p-T conditions inside the reactor during the experiment 3.

Step	t **/h**	T **/K**	p **/MPa**
Injection1	486.49	274.15	14.74
	490.97	274.15	13.47
Injection2	650.84	274.15	12.02
	653.75	274.15	13.93
Depressurization 1	677.32	274.11	13.59
	677.56	274.07	11.51
Depressurization 2	701.39	274.03	11.23
	701.49	274.03	9.50
Depressurization 3	725.30	274.03	9.45
	725.39	273.99	7.49
Depressurization 4	749.51	274.03	7.81
	749.99	273.99	5.16
Depressurization 5	773.60	273.99	5.50
	773.74	273.75	3.46
Depressurization 6	273.99	273.99	4.17
	798.72	272.61	2.33
Depressurization 7	821.72	274.03	3.34
	822.48	270.88	0.25

Table 4.8: p-T conditions inside the reactor during the experiment 4.

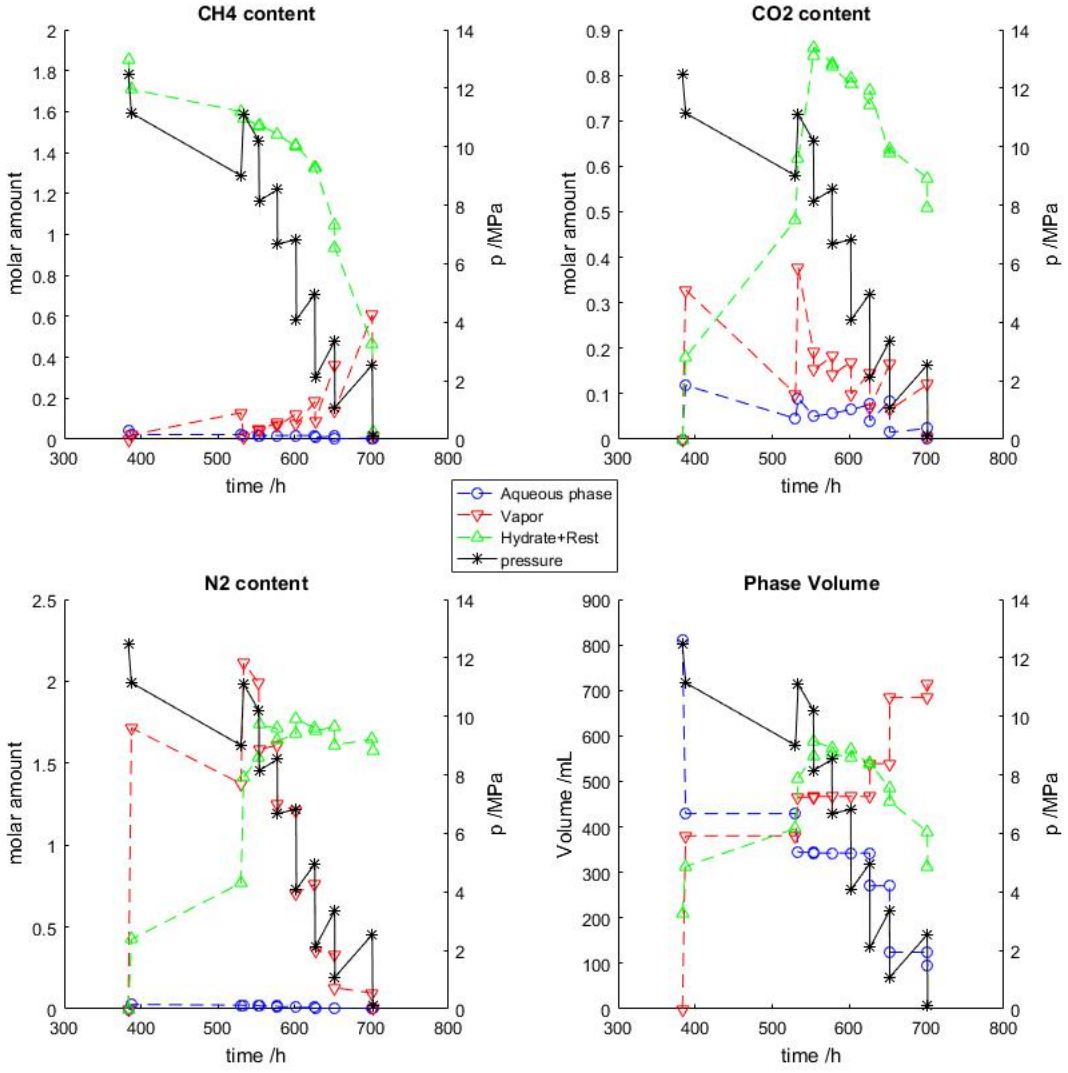

Figure 4.7: CH_4, CO_2 and N_2 content, and proportion of each phase in the reactor during the experiment 1.

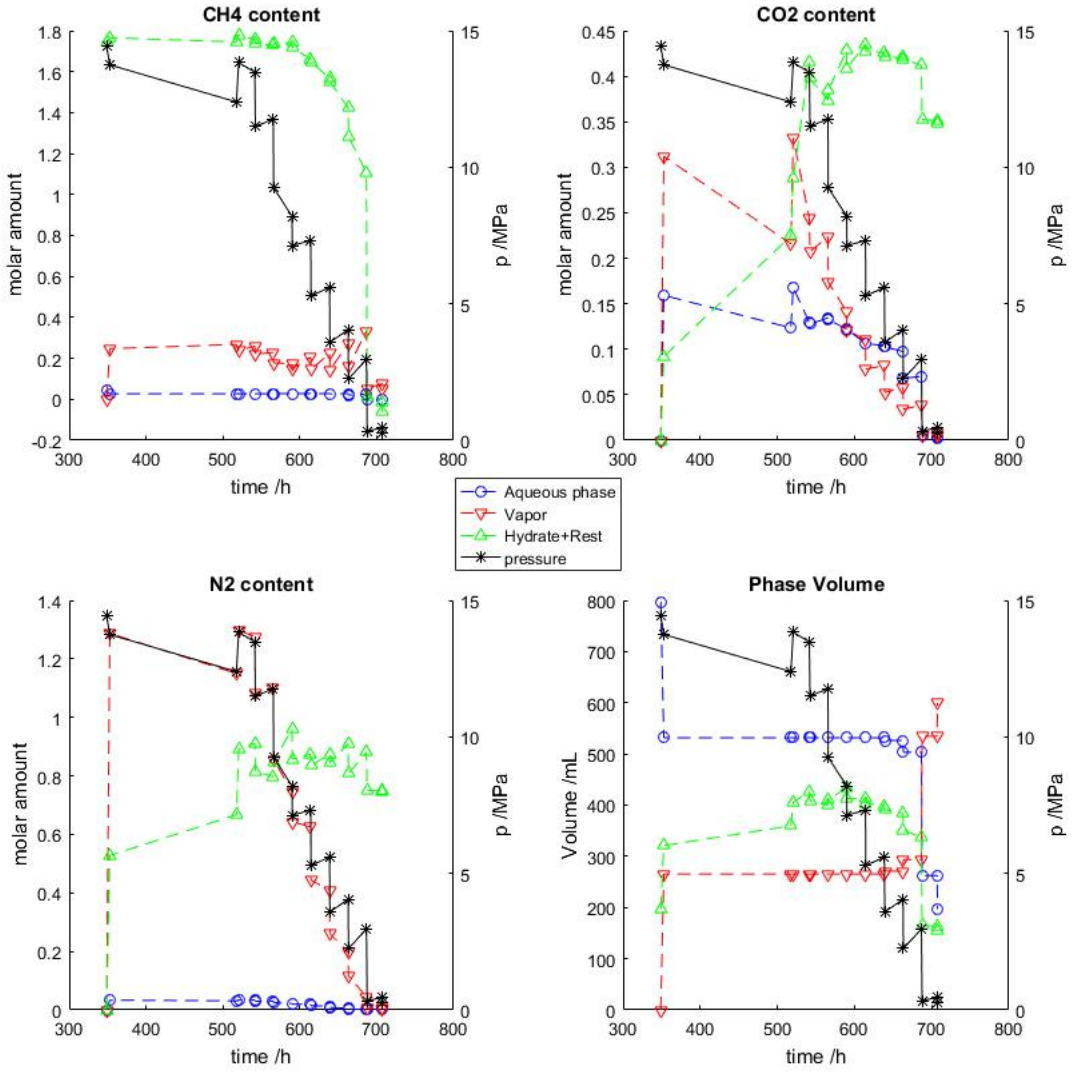

Figure 4.8: CH_4, CO_2 and N_2 content, and proportion of each phase in the reactor during the experiment 2.

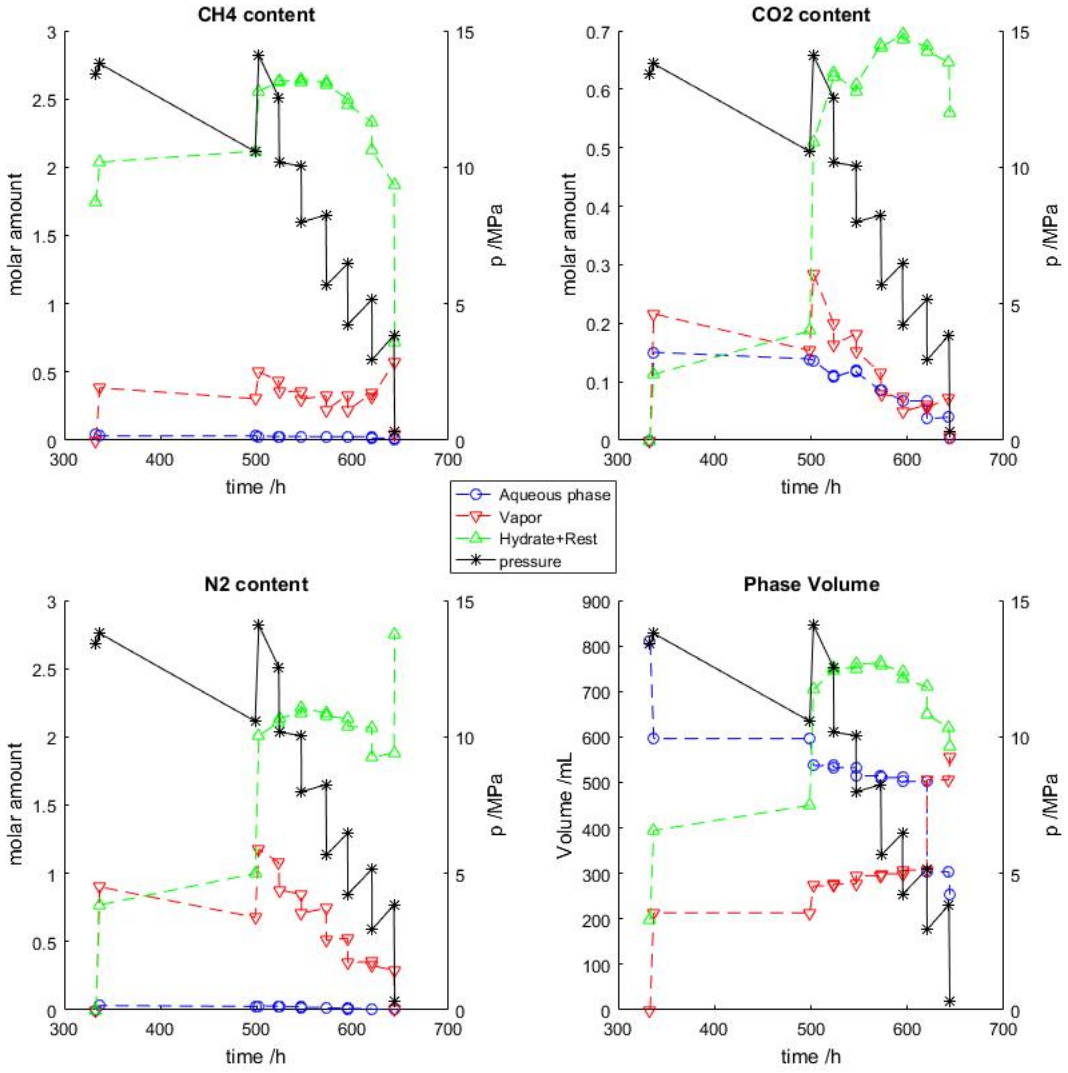

Figure 4.9: CH_4, CO_2 and N_2 content, and proportion of each phase in the reactor during the experiment 3.

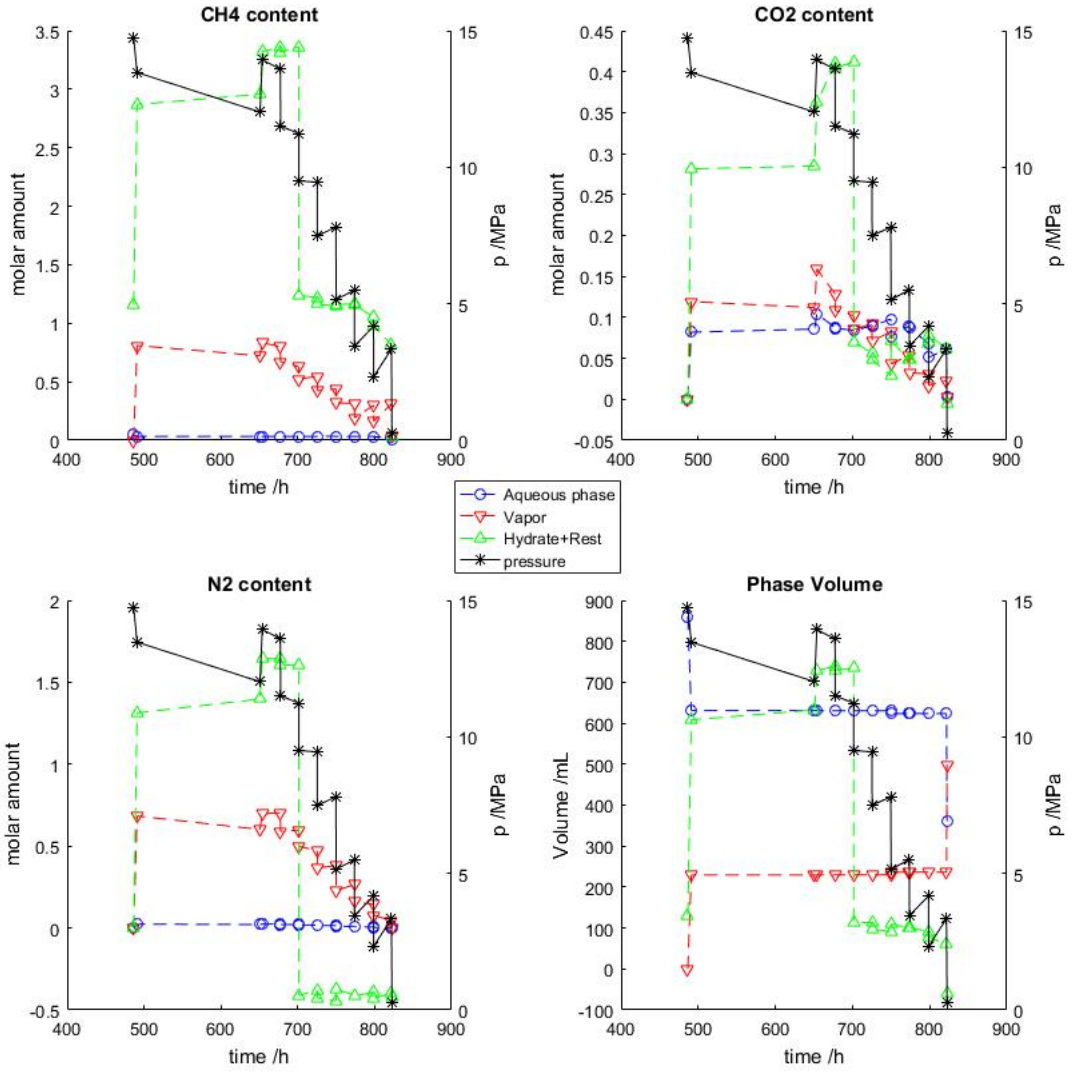

Figure 4.10: CH_4, CO_2 and N_2 content, and proportion of each phase in the reactor during the experiment 4.

Acknowledgements

This work was supported by the SUGAR project, funded by the German Ministry of Research (grant no. 03G0856A), and the research theme "Fluid migration within sedimentary environments" of the Geochemical Laboratory (LCG-GM-REM-IFREMER). The author wants to thank Meike Dibbern, Andrea Bodenbinder and Mark Schmidt for their help in technical analysis.

Bibliography

D. Archer, B. Buffett, and V. Brovkin. Ocean methane hydrates as a slow tipping point in the global carbon cycle. *Proceedings of the National Academy of Sciences*, 106(49):20596–20601, 2009. doi: 10.1073/pnas.0800885105.

P. Babu, P. Linga, R. Kumar, and P. Englezos. A review of the hydrate based gas separation (HBGS) process for carbon dioxide pre-combustion capture. *Energy*, 85:261–279, 2015. doi: 10.1016/j.energy.2015.03.103.

R. Boswell, D. Schoderbek, T. S. Collett, S. Ohtsuki, M. White, and B. J. Anderson. The Iġnik Sikumi field experiment, Alaska North Slope: Design, operations, and implications for CO_2-CH_4 exchange in gas hydrate reservoirs. *Energy and Fuels*, 31(1):140–153, 2017. doi: 10.1021/acs.energyfuels.6b01909.

BritishPetroleum. Bp statistical review of world energy 2017. british petroleum (66), 2018.

Bronkhorst. Instruction Manual - General intructions digital Mass Flow, Pressure instruments laboratory style, IN-FLOW. *Bronkhorst UK*, 2018.

E. B. Burwicz, L. H. Rüpke, and K. Wallmann. Estimation of the global amount of submarine gas hydrates formed via microbial methane formation based on numerical reaction-transport modeling and a novel parameterization of Holocene sedimentation. *Geochimica et Cosmochimica Acta*, 75(16):4562–4576, 2011. doi: 10.1016/j.gca.2011.05.029.

P. C. Chen, W. L. Huang, and L. A. Stern. Methane hydrate synthesis from ice: Influence of pressurization and ethanol on optimizing formation rates and hydrate yield. In *Energy and Fuels*, volume 24, pages 2390–2403, 2010. doi: 10.1021/ef901403r.

M. A. Clarke and P. Bishnoi. Determination of the intrinsic kinetics of CO_2 gas hydrate formation using in situ particle size analysis. *Chemical Engineering Science*, 60(3):695–709, 2005. doi: 10.1016/j.ces.2004.08.040.

D. Davidson, S. Garg, S. Gough, Y. Handa, C. Ratcliffe, J. Ripmeester, J. Tse, and W. Lawson. Laboratory analysis of a naturally occurring gas hydrate from sediment of the gulf of mexico. *Geochimica et Cosmochimica Acta*, 50(4):619–623, 1986. doi: 0.1016/0016-7037(86)90110-9.

C. Deusner, N. Bigalke, E. Kossel, and M. Haeckel. Methane production from gas hydrate deposits through injection of supercritical CO_2. *Energies*, 5(7):2112–2140, 2012. doi: 10.3390/en5072112.

A. G. Dickson. ph buffers for sea water media based on the total hydrogen ion concentration scale. *Deep Sea Research Part I: Oceanographic Research Papers*, 40 (1):107–118, 1993. doi: 10.1016/0967-0637(93)90055-8.

Z. Duan and R. Sun. A model to predict phase equilibrium of CH_4 and CO_2 clathrate hydrate in aqueous electrolyte solutions. *American Mineralogist*, 91(8-9):1346–1354, 2006. doi: 10.2138/am.2006.2017.

P. Englezos, N. Kalogerakis, P. Dholabhai, and P. Bishnoi. Kinetics of formation of methane and ethane gas hydrates. *Chemical Engineering Science*, 42(11):2647–2658, 1987. doi: 10.1016/0009-2509(87)87015-X.

A. Eslamimanesh, A. H. Mohammadi, D. Richon, P. Naidoo, and D. Ramjugernath. Application of gas hydrate formation in separation processes: A review of experimental studies. *The Journal of Chemical Thermodynamics*, 46:62–71, 2012. doi: 10.1016/j.jct.2011.10.006.

A. Hassanpouryouzband, J. Yang, B. Tohidi, E. Chuvilin, V. Istomin, B. Bukhanov, and A. Cheremisin. CO_2 Capture by Injection of Flue Gas or CO_2–N_2 Mixtures into Hydrate Reservoirs: Dependence of CO_2 Capture Efficiency on Gas Hydrate Reservoir Conditions. *Environmental science & technology*, 52(7):4324–4330, 2018a. doi: 10.1021/acs.est.7b05784.

A. Hassanpouryouzband, J. Yang, B. Tohidi, E. Chuvilin, V. Istomin, B. Bukhanov, and A. Cheremisin. Insights into CO_2 Capture by Flue Gas Hydrate Formation: Gas Composition Evolution in Systems Containing Gas Hydrates and Gas Mixtures at Stable Pressures. *ACS Sustainable Chemistry & Engineering*, 6(5):5732–5736, 2018b. doi: 10.1021/acssuschemeng.8b00409.

E. Kossel, N. K. Bigalke, E. Pinero, and M. Haeckel. The sugar toolbox: a library of numerical algorithms and data for modelling of gas hydrate systems and marine environments. 2013.

B. Kvamme. Thermodynamic Limitations of the CO_2/N_2 Mixture Injected into CH_4 Hydrate in the Ignik Sikumi Field Trial. *Journal of Chemical and Engineering Data*, 61(3):1280–1295, 2016. doi: 10.1021/acs.jced.5b00930.

C. Le Quéré, R. M. Andrew, J. G. Canadell, S. Sitch, J. Ivar Korsbakken, G. P. Peters, A. C. Manning, T. A. Boden, P. P. Tans, R. A. Houghton, R. F. Keeling, S. Alin, O. D. Andrews, P. Anthoni, L. Barbero, L. Bopp, F. Chevallier, L. P. Chini, P. Ciais, K. Currie, C. Delire, S. C. Doney, P. Friedlingstein, T. Gkritzalis, I. Harris, J. Hauck, V. Haverd, M. Hoppema, K. Klein Goldewijk, A. K. Jain, E. Kato, A. Körtzinger, P. Landschützer, N. Lefèvre, A. Lenton, S. Lienert, D. Lombardozzi, J. R. Melton, N. Metzl, F. Millero, P. M. Monteiro, D. R. Munro, J. E. Nabel, S. I. Nakaoka, K. O'Brien, A. Olsen, A. M. Omar, T. Ono, D. Pierrot, B. Poulter,

C. Rödenbeck, J. Salisbury, U. Schuster, J. Schwinger, R. Séférian, I. Skjelvan, B. D. Stocker, A. J. Sutton, T. Takahashi, H. Tian, B. Tilbrook, I. T. Van Der Laan-Luijkx, G. R. Van Der Werf, N. Viovy, A. P. Walker, A. J. Wiltshire, and S. Zaehle. Global Carbon Budget 2016. *Earth System Science Data*, 8(2):605–649, 2016. doi: 10.5194/essd-8-605-2016.

B. Li, T. Xu, G. Zhang, W. Guo, H. Liu, Q. Wang, L. Qu, and Y. Sun. An experimental study on gas production from fracture-filled hydrate by CO_2 and CO_2/N_2 replacement. *Energy Conversion and Management*, 165:738–747, 2018.

S. H. Mohr, J. Wang, G. Ellem, J. Ward, and D. Giurco. Projection of world fossil fuels by country. *Fuel*, 141:120–135, 2015. doi: 10.1016/j.fuel.2014.10.030.

L. Mu and N. von Solms. Experimental study on methane production from hydrate-bearing sandstone by flue gas swapping. *Energy & fuels*, 32(8):8167–8174, 2018.

K. Ohgaki, K. Takano, H. Sangawa, T. Matsubara, and S. Nakano. Methane exploitation by carbon dioxide from gas hydrates—phase equilibria for co2-ch4 mixed hydrate system—. *Journal of chemical engineering of Japan*, 29(3):478–483, 1996. doi: 10.1252/jcej.29.478.

Y. Park, D.-Y. Kim, J.-W. Lee, D.-G. Huh, K.-P. Park, J. Lee, and H. Lee. Sequestering carbon dioxide into complex structures of naturally occurring gas hydrates. *Proceedings of the National Academy of Sciences*, 103(34):12690–12694, 2006. doi: 10.1073/pnas.0602251103.

E. Pinero, M. Marquardt, C. Hensen, M. Haeckel, and K. Wallmann. Estimation of the global inventory of methane hydrates in marine sediments using transfer functions. *Biogeosciences (BG)*, 10(2):959–975, 2013. doi: 10.5194/bg-10-959-2013.

J. A. Ripmeester, S. T. John, C. I. Ratcliffe, and B. M. Powell. A new clathrate hydrate structure. *Nature*, 325(6100):135–136, 1987.

J. Schicks, B. Strauch, K. Heeschen, E. Spangenberg, and M. Luzi-Helbing. From Microscale (400 μl) to Macroscale (425 L): Experimental Investigations of the CO_2/N_2-CH_4 Exchange in Gas Hydrates Simulating the Iġnik Sikumi Field Trial. *Journal of Geophysical Research: Solid Earth*, 123(5):3608–3620, 2018. doi: 10.1029/2017JB015315.

D. Schoderbek, H. Farrell, J. Howard, K. Raterman, S. Silpngarmlert, K. Martin, B. Smith, and P. Klein. Conocophillips gas hydrate production test. Technical report, ConocoPhillips Co., Houston, TX (United States), 2013.

H. Shimizu, T. Kumazaki, T. Kume, and S. Sasaki. In situ observations of high-pressure phase transformations in a synthetic methane hydrate. *The Journal of Physical Chemistry B*, 106(1):30–33, 2002. doi: 10.1021/jp013010a.

M. v. Stackelberg and H. Müller. On the structure of gas hydrates. *The Journal of Chemical Physics*, 19(10):1319–1320, 1951.

L. A. Stern, S. Circone, S. H. Kirby, and W. B. Durham. Anomalous preservation of pure methane hydrate at 1 atm. *The Journal of Physical Chemistry B*, 105(9): 1756–1762, 2001. doi: 10.1021/jp003061s.

L. A. Stern, S. Circone, S. H. Kirby, and W. B. Durham. Temperature, pressure, and compositional effects on anomalous or" self" preservation of gas hydrates. *Canadian Journal of Physics*, 81(1-2):271–283, 2003. doi: 10.1139/p03-018.

Y.-H. Sun, S.-L. Li, G.-B. Zhang, W. Guo, and Y.-H. Zhu. Hydrate phase equilibrium of CH_4 + N_2 + CO_2 gas mixtures and cage occupancy behaviors. *Industrial and Engineering Chemistry Research*, 56(28):8133–8142, 2017. doi: 10.1021/acs.iecr.7b01093.

K. Wallmann, E. Pinero, E. Burwicz, M. Haeckel, C. Hensen, A. Dale, and L. Ruepke. The global inventory of methane hydrate in marine sediments: A theoretical approach, 2012.

Y. Wang, J.-C. Feng, X.-S. Li, Y. Zhang, and Z.-Y. Chen. Fluid flow mechanisms and heat transfer characteristics of gas recovery from gas-saturated and water-saturated hydrate reservoirs. *International Journal of Heat and Mass Transfer*, 118:1115–1127, 2018. doi: 10.1016/j.ijheatmasstransfer.2017.11.081.

C. S. Wong, P. Y. Tishchenko, and W. K. Johnson. Effects of high CO_2 molality on the carbon dioxide equilibrium of seawater. *Journal of Chemical & Engineering Data*, 50(3):822–831, 2005. doi: 10.1021/je049717i.

J. Yang, A. Okwananke, B. Tohidi, E. Chuvilin, K. Maerle, V. Istomin, B. Bukhanov, and A. Cheremisin. Flue gas injection into gas hydrate reservoirs for methane recovery and carbon dioxide sequestration. *Energy conversion and management*, 136:431–438, 2017a. doi: 10.1016/j.enconman.2017.01.043.

M. Yang, Z. Fu, L. Jiang, and Y. Song. Gas recovery from depressurized methane hydrate deposits with different water saturations. *Applied Energy*, 187:180–188, 2017b. doi: 10.1016/j.apenergy.2016.10.029.

Y.F Makogon. *Hydrates of hydrocarbons*. 1997.

Chapter 5

Synthesis

In this work, mixed gas hydrate were studied to understand better the processes occuring during CH_4 production coupled to CO_2 sequestration. Three different high-pressure apparatuses were employed to study the thermodynamic stability of different mixed gas hydrates and the gas exchange process.

In a first set of experiment, the vapor-liquid equilibria of the system CH_4-CO_2 was measured with a high-pressure cell at common temperatures and pressures conditions of natural hydrate deposits. The interaction parameter $k_{ij(CH_4-CO_2)} = 1.32 \times 10^3 \times T - 0.251$ representing the non-ideality of the mixture was employed to build phase envelopes using the Soave-Redlich-Kwong equation of state. Then, the hydrate-liquid-liquid equilibria (HLLE) of the system CH_4-CO_2-H_2O were measured (Figure 5.1). The HLLE area on the p-T diagram is localized at typical reservoir conditions for offshore CO_2 sequestration and the hydrate stability is strongly affected by the presence or not of a CO_2-rich liquid phase. When no vapor phase is able to form, an increase of CH_4 in the mixture decreases the pressure of dissociation of the mixed hydrate. This makes possible the sequestration of liquid CO_2 under hydrate phase at higher temperatures when some CH_4 is present (below 22.5 mol-%) (Figure 5.1). The collection of more thermodynamic data, especially at CH_4 concentrations very low or close to 22.5 %, will help to define the limit of the HLLE.

With the same apparatus, a CH_4 replacement by CO_2 was done. The analysis of the evolution of pressure and composition shows firstly a fast dissociation of CH_4 hydrate decoupled to a fast formation of CO_2 hydrate, and in a second time a slow CH_4-CO_2 exchange within the hydrate phase, due to the shrinking-core process. Then, (CH_4)-CO_2-N_2-H_2O hydrate-vapor-liquid equilibria (HVLE) with different H_2O and CH_4 proportions were measured with another high-pressure cell. A huge proportion of H_2O shifts the hydrate dissociation point to higher pressure, while the addition of CH_4 to the CO_2-N_2 gas mixture shifts the hydrate dissociation point to lower pressure.

Finally flow-through experiments were performed, by flowing a flue gas (CO_2-N_2 gas) through a pure synthetic CH_4 hydrate distributed in a sand matrix. It was found that an addition of CH_4 in the flue gas decreased the water produced during the first injection. Furthermore, a consequent amount of CO_2 is retained in the hydrate-bearing sediment compared to N_2. A limited amount of CH_4 were produced from gas exchange and most of hydrates (higher than 86 %) were produced by the

depressurization step. However, more CH_4 were recovered during the second injection compared to the first one, showing that the induction time between gas injection and gas production is important to consider for optimizing the CH_4-CO_2 exchange process.

It will be interesting to further study the process when a mixture with a higher CO_2:N_2 ratio is injected in CH_4 hydrate bearing sediments, since it increases the stability of hydrates and they will be able to form at higher temperatures, except if a CO_2-rich liquid phase is stable. Then, a similar study of the HLLE using (CH_4)-CO_2-N_2 mixtures must be interesting to determine in which p-T area hydrates are thermodynamically stable when a CO_2-rich liquid phase is present.

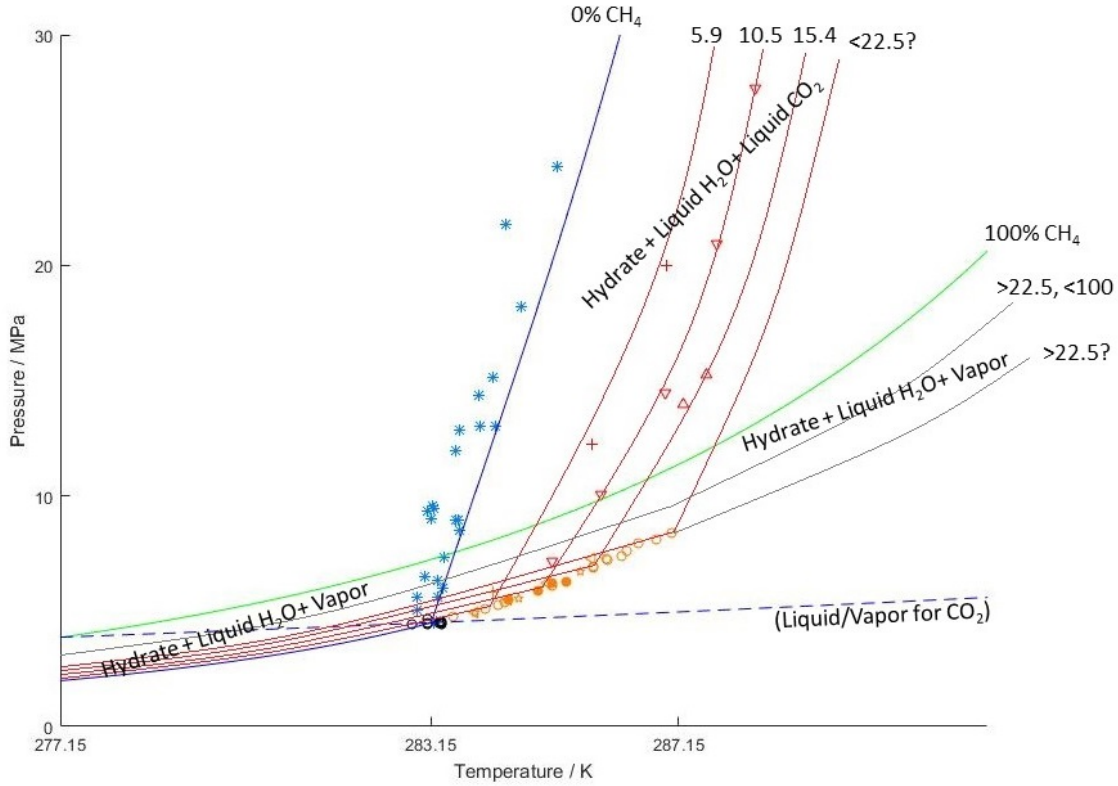

Figure 5.1: Modified from Figure 2.1. Available experimental data describing gas hydrate equilibria for the (CH_4)-CO_2-H_2O system in the presence of H-L_{H_2O}-L_{CO_2}-(V) phases below 30 MPa. Blue (CO_2-H_2O) and green (CH_4-H_2O) lines represents modeling of hydrate equilibria. Grey (high CH_4:CO_2 ratio) and red (low CH_4:CO_2 ratio) lines are drawn to help visualizing hydrate equilibria of CH_4-CO_2-H_2O mixtures.

Chapter 6

Additional work

6.1 Physicochemical properties of gas hydrate-bearing sediments

Chapter published in *Gas Hydrate 2: Geoscience Issues and Potential Industrial Applications, John Wiley & Sons* (2018)
L.N. Legoix, E. Kossel, C. Deusner, L. Ruffine, M. Haeckel
doi: 10.1002/9781119451174.ch8

Abstract This chapter talks about physicochemical properties of gas hydrate-bearing sediments. Lab-based experiments are the most cost-effective and systematic approach to evaluate physicochemical properties and behavior of gas hydrate-bearing sediments in a systematic way. Physicochemical property studies were largely focused on measurements with respect to homogeneous and reproducible gas hydrate distributions. The chapter includes overviews of thermodynamic and kinetic constraints of relevant processes of gas hydrate formation, dissociation and conversion, fluid transport in gas hydrate-bearing sediments, thermal and electrical properties and distribution of gas hydrates. It reviews some flow-through experimental systems and procedures for studying the behavior of gas hydrate-bearing sediments with different research objectives. The chapter provides a brief overview on available systems for high-resolution online fluid monitoring, as well as tools for a destruction-free analysis of the multiphase sample with emphasis on tomographic techniques.

Keywords Natural gas hydrate, Physicochemical properties, Gas hydrate stability zone, Fluid transport in sediments, Porosity, Thermal properties, Electrical properties, Distribution of gas hydrate in sediment, CH_4-CO_2 hydrate conversion, High-pressure experiments, ex-situ and in-situ analysis

6.2 Multidisciplinary investigation on cold seeps with vigorous gas emissions in the Sea of Marmara (Marsite-Cruise): Strategy for site detection and sampling and first scientific outcome

Article published in *Deep-Sea Research Part II: Topical Studies in Oceanography* (2018)
L. Ruffine, H. Ondreas, M.-M. Blanc-Valleron, B.M.A. Teichert, C. Scalabrin, E. Rinnert, D. Birot, C. Croguennec, E. Ponzevera, C. Pierre, J.-P. Donval, A.-S. Alix, Y. Germain, L. Bignon, J. Etoubleau, J.-C Caprais, J. Knoery, F. Lesongeur, B. Thomas, A. Roubi, L.N. Legoix, P. Burnard, N. Chevalier, H. Lu, S. Dupre, C. Fontanier, D. Dissard, N.K. Olgun, H. Yang, H. Strauss, V. Ozaksoy, J. Perchoc, C. Podeur, C. Tarditi, E. Ozbeki, V. Guyader, B. Marty, D. Madre, C. Grall, D. Embriaco, A. Polonia, L. Gasperini, N. Cagatay, P. Henry, L. Géli
doi: 10.1016/j.dsr2.2018.03.006

Abstract MarsiteCruise was undertaken in October/November 2014 in the Sea of Marmara to gain detailed insight into the fate of fluids migrating within the sedimentary column and partially released into the water column. The overall objective is to achieve a more global understanding of cold-seep dynamics in the context of a major active strike-slip fault. Five remotely operated vehicle (ROV) were performed at selecteed areas along the North Anatolian Fault and inherited faults. To efficiently detect, select and sample the gas seeps, we applied an original procedure. It combines sequentially (1) the acquisition of ship-borne multibeam acoustic data from the water column prior to each dive to detect gas emission sites and to design the tracks of the ROV dives, (2) *in situ* and real-time Raman spectroscopy analysis of the gas stream, and (3) onboard determination of molecular and isotopic compositions of the collected gas bubbles. the *in situ* Raman spectroscopy was used as a decision-making tool to evaluate the need for continuing with the sampling of gases from the discovered seep, or to move to another one. Push cores were gathered to study buried carbonates and pore waters at the surficial sediment, while CTD-Rosette allowed collecting samples to measure dissolved-methane concentration within the water column followed by a comparison with measurements from samples collected with the submersible Nautile during the Marnaut cruise in 2007. Overall, the visited sites were characterized by a wide diversity of seeps. CO_2- and oil-rich seeps were found at the westernmost part in the Tekirdag Basin, while amphipods, anemones and coral populated the sites visited at the easternmost part in the Cinarcik Basin. Methane-derived authigenic carbonates and bacterial mats were widespread on the seafloor at all sites with variable size and distributions. The measured methane concentrations in the water column were up to 377 micro-mol, and the dissolved pore-water profiles indicated the occurence of sulfate depleting processes accompanied with carbonate precipitation. The pore-water profiles display evidence of biogeochemical transformations leading to the fast depletion of seawater sulfate

within the first 25-cm depth of the sediment. These results show that the North Anatolian Fault and inherited faults are important migration paths for fluids for which a significant part is discharged into the water column, contributing to the increase of methane concentration at the bottom seawater and favoring the development of specific ecosystems.

Keywords Acoustic survey, Authigenic carbonates, Biogeochemistry, Chemical analyses, Cold seeps, Dissolved major elements, Fluid seepage, Geology, In situ Raman analysis

6.3 Multiple gas reservoirs are responsible for the gas emissions along the Marmara fault network

Article published in *Deep-Sea Research Part II: Topical Studies in Oceanography* (2017)
L. Ruffine, J.-P. Donval, C. Croguennec, P. Burnard, H. Lu, Y. Germain, L.N. Legoix, L. Bignon, M.N. Cagatay, B. Marty, M. Pitel-Roudaut, P. Henry, L. Géli
doi: 10.1016/j.dsr2.2017.11.011

Abstract On continental margins, upward migration of fluids from various sources and various subsurface accumulations, through the sedimentary column to the seafloor, leads to the development of cold seeps where chemical compounds are discharged into the water column. MarsiteCruise was undertaken in November 2014 to investigate the dynamics of cold seeps characterized by vigorous gas emissions in the Sea of Marmara (SoM).
A previous paper published by Bourry et al. (2009) presented the gas geochemistry of three seeps sampled along three different segments in the SoM. Their findings showed that the seeps were sourced by three different reservoirs. In this paper, seventeen seeps were investigated to determine the gas sources, unravel reservoir contributions, and estimate their level of mixing. The molecular and stable isotope compositions of the gas compounds were determined to establish the empirical diagrams that usually allow to delineate source domains. The results provide insights into the complexities of source mixing within the sedimentary column of the SoM before emission of the gases into the water column. the seep gases originate from deep thermogenic or microbial hydrocarbon sources, or from a CO_2-rich source. Microbial sources producing methane from primary methanogenesis have been identified in the Tekirdag and the Cinarcik basins. In addition, six different thermogenic reservoirs or six different pathways of migration are responsible for the supply of gas to the seeps on the highs and in the western basin. Five of them are undergoing biodegradation followed by secondary methanogenesis, thereby providing additional sources of microbial methane to the seeps. Overall, the gases emitted by the seventeen seeps consist of variable mixtures of different components from two or three sources.

Keywords Abiotic CO_2-source, Gas bubbles, molecular and isotopic compositions, Primary and secondary methanogenesis, Sea of Marmara, Seeps, Thermogenic gases

List of Figures

1.1 Structures of gas hydrates I, II and H with corresponding water cages [Ripmeester et al., 1994]. 12

1.2 Example of BSR identified in seismic reflection images (offshore Oregon, U.S.), suggesting gas hydrate occurrence with two high amplitude envelopes (seafloor and BSR) (GEOMAR). 15

1.3 Left: combustion after ignition of muddy thermogenic gas hydrates sampled in the Sea of Marmara with a 12 m gravity core, at a depth around 658 m and a seafloor temperature of 287.15 K (L.N. Legoix, 2014). Right: Methane hydrate lens formed in laboratory with a clay/sand mixture (modified from Ruffine [2015]). 15

1.4 High-pressure cells employed to study gas hydrates (refer to corresponding chapters for complete sketches of each system). Left: Cell equipped with sapphire window (IFREMER-LCG). Middle: Titanium cell for phase equilibria measurements (IFREMER-LCG). Right: Vertical cell for flow-through experiments (GEOMAR-FB2). 20

2.1 Available experimental data describing gas hydrate equilibria for the (CH_4)-CO_2-H_2O system in the presence of H-L_{H_2O}-L_{CO_2}-(V) phases below 30 MPa. HLLE: hydrate-liquid-liquid equilibrium; HVLE: hydrate-vapor-liquid equilibrium; HVLLE: hydrate-vapor-liquid-liquid equilibrium; VLE: vapor-liquid equilibrium. References are the one from Table 2.2, or see original figure in Legoix et al. [2017]. 33

2.2 Sketch of the experimental set-up including the high-pressure cell, modified from Ruffine and Trusler [2010]. 34

2.3 Liquid and vapor phase compositions of the CH_4-CO_2 mixture between 273.15 and 301 K along eight isoherms: T = 273.15 K (cyan); T = 274.15 K (blue); T = 277.15K (green); T = 283.15 K (grey); T = 288.15 K (288.5 for Xu et al. [1992] data) (orange); T = 290.15 K (purple); T = 283.4 K (black); T = 301 K (red). Experimental bubble points x_{CH_4} from this work (filled dot), experimental bubble points x_{CH_4} from other authors (empty dot), experimental dew points y_{CH_4} from other authors (cross), critical point (star) [Kaminishi et al., 1968, Arai et al., 1971, Xu et al., 1992]. Modelling of the bubble lines (solid-lines) and the dew lines (dotted-lines) is based on the SRK-EoS. 36

2.4 Photos showing different steps during gas hydrate formation and dissociation with Mixture 2. From left to right: (A) after H_2O injection (L_{H_2O}); (B) just after incipent formation start (H-L_{H_2O}); (C) ca. 40 min after formation start (H-L_{H_2O}-L_{CO_2}); (D) ca. 170 min after formation start (H-L_{H_2O}-L_{CO_2}). 38

3.1 Sketch of the high-pressure cell designed to collect thermodynamic data of mixed gas hydrates. 51
3.2 Hydrate-Vapor-Liquid Equilibrium (HVLE) data of the CO_2-N_2-H_2O system. Our study provides data for 23.17 mol % CO_2 and high H_2O content. The datasets at low and high pressure correspond to 20 and 10 mol-% of CO_2 in the gas phase [Lee et al., 2014], and 17.61 and 11.59 mol-% of CO_2 [Kang et al., 2001], respectively. 53
3.3 Comparison of HVLE data of typical pretreated CO_2-N_2 flue gas compositions that are diluted by CH_4 gas (ca. 50 mol-%) in natural gas hydrate settings. 54
3.4 Top panel: Visual observation of the evolution of the different phases during gas hydrate crystallization (from left to right: directly after water injection; after stirrer has been set to 400 rpm; 1 min after the gas hydrate formation incipient; 48 min after the gas hydrate formation incipient). Bottom panel: Visual state of the system during the gas exchange process (from left to right: t= 0h; t= 1.47h; t= 18.90h; t= 89.73h; t= 118.90h; t= 145.73h). 56
3.5 Evolution of the composition of the vapor phase (Left) and evolution of the pressure (Right) during the replacement of CH_4 by CO_2. see Table 3.4 for the list of measured values. 56

4.1 Sketch of the experimental apparatus NESSI to perform flow-through experiments with gas hydrate-bearing sediments, modified from Deusner et al. [2012]. Initial CH_4 and H_2O injections are done using a tube connected to inlet and outlet for pressurizing uniformly the reactor. . 69
4.2 Gas composition evolution during injection steps. 'Injection 1' and 'Injection 2' are the composition of the injected gas and following histogram rectangles correspond to the composition of the outflow gas during the injection step. 75
4.3 Gas composition evolution during depressurization steps. Each histogram rectangle represents the composition of the outflow gas during a fast depressurization, and no abscisses values indicated that gas were collected in a different bag during the same depressurization. 76
4.4 Cumulative gas production for each component during the injections and stepwise depressurization. The waiting time between each step, when no gas is produced, are not plotted here. 77
4.5 Ratio of CO_2:N_2 and CH_4:N_2 produced during the experiment 1 (i.e., the red dotted curve represents the ratio of the CO_2 curve to N_2 curve of Figure 4.4, experiment 1). 78

4.6 Raman spectrometer connected to the apparatus for fluid analysis. Analytical section (Left), and high-pressure windowed side and optical head (Right). 81
4.7 CH_4, CO_2 and N_2 content, and proportion of each phase in the reactor during the experiment 1. 84
4.8 CH_4, CO_2 and N_2 content, and proportion of each phase in the reactor during the experiment 2. 85
4.9 CH_4, CO_2 and N_2 content, and proportion of each phase in the reactor during the experiment 3. 86
4.10 CH_4, CO_2 and N_2 content, and proportion of each phase in the reactor during the experiment 4. 87

5.1 Modified from Figure 2.1. Available experimental data describing gas hydrate equilibria for the (CH_4)-CO_2-H_2O system in the presence of H-L_{H_2O}-L_{CO_2}-(V) phases below 30 MPa. Blue (CO_2-H_2O) and green (CH_4-H_2O) lines represents modeling of hydrate equilibria. Grey (high CH_4:CO_2 ratio) and red (low CH_4:CO_2 ratio) lines are drawn to help visualizing hydrate equilibria of CH_4-CO_2-H_2O mixtures. 94

List of Tables

2.1 Experimental data for the CH_4-CO_2 binary system at vapour-liquid equilibrium (VLE), between 273.15 and 301 K. 32

2.2 Available experimental data for the CO_2-H_2O binary and CH_4-CO_2-H_2O ternary mixtures involving a CO_2-rich liquid phase. Ref.1: [Unruh and Katz, 1949, Robinson et al., 1971, Yoon and Lee, 1997, Fan and Guo, 1999, Seo et al., 2000, Seo and Lee, 2001, Mooijer-Van Den Heuvel et al., 2001, Ruffine et al., 2010, Bi et al., 2013], Ref.2: [Takenouchi and Kennedy, 1964, Ng and Robinson, 1985, Ohgaki et al., 1993, Nakano et al., 1998a, Fan and Guo, 1999, Mooijer-Van Den Heuvel et al., 2001, Ruffine et al., 2010, Chapoy et al., 2011, Alsiyabi et al., 2014]. 32

2.3 Relative deviation (RD) of solubility data (mole fractions) and vapor pressures (of pure CO_2 with x_{CH_4}= 0) between this work and literature values. 36

2.4 Relative deviation (RD) of solubility data (mole fractions) and vapor pressures (of pure CO_2 with x_{CH_4}=0) between this work and literature values. 37

2.5 Experimental data of H-L_{H_2O}-L_{CO_2} equilibria (HLLE) for the CH_4-CO_2-H_2O ternary system. Values inside brackets are CSMGem [Sloan and Koh, 2008] model values applied on the system. 37

2.6 Incipient gas hydrate time of formation on the CH_4-CO_2-H_2O ternary system. 38

3.1 Overview of HVLE experimental data for the ternary system CO_2-N_2-H_2O 50

3.2 Overview of HVLE experimental data for the quaternary system CH_4-CO_2-N_2-H_2O. 51

3.3 HVLE data for the systems CO_2-N_2-H_2O, CH_4-CO_2-N_2-H_2O and CH_4-CO_2-H_2O. 52

3.4 Evolution of the gas phase with a CO_2-CH_4 gas exchange on an initial CH_4 hydrate. 58

4.1 Initial composition in the high-pressure reactor before the first injection, considering the mass of initial components employed. (*): value after consideration of CH_4 dissolution from hydrate and 1 atm of remaining vapor into water after the CH_4 evacuation. 70
4.2 Average composition (1^{st} and 2^{nd} injections) of the gas (mol-%) for each experiment. 71
4.3 Mass balance (molar) deviation (%) between gas outflow and inflow. . 71
4.4 Summary of injection and production during the Ignik Sikumi field test [Boswell et al., 2017]. 80
4.5 p-T conditions inside the reactor during the experiment 1. (1): temperature considered as 274.15 K (no data from logger). (2): Pressure from sensor at outlet (no data from logger). 82
4.6 p-T conditions inside the reactor during the experiment 2. 82
4.7 p-T conditions inside the reactor during the experiment 3. 83
4.8 p-T conditions inside the reactor during the experiment 4. 83

Ludovic N. Legoix
Chemist

Saarbruckenstr. 159, 24113 Kiel
llegoix@geomar.de
28 y.o.
Place of birth: Bois-Guillaume, France
Nationality: French

Curriculum Vitae

Since 5/2015	Research associate at the Helmholtz Centre for Ocean Research Kiel, GEOMAR.
10/2013-5/2015	Research associate at the Institut Francais de Recherche pour l'Expoitation de la Mer, IFREMER.
9/2010-9/2013	Sudies of Chemistry and Chemical Engineering at the Ecole Nationale Supérieure d'Ingénieurs de Caen, ENSICAEN.
9/2008-8/2010	Studies of Mathematics, Physics and Chemistry at the preparatory classes Louis-Thuillier.